

Fall 2007

A hyperbolic two -step model based finite difference method for studying thermal deformation in a micro thin film heated by ultrashort -pulsed lasers

Tianchan Niu
Louisiana Tech University

Follow this and additional works at: <https://digitalcommons.latech.edu/dissertations>



Part of the [Applied Mathematics Commons](#), and the [Mathematics Commons](#)

Recommended Citation

Niu, Tianchan, "" (2007). *Dissertation*. 499.
<https://digitalcommons.latech.edu/dissertations/499>

This Dissertation is brought to you for free and open access by the Graduate School at Louisiana Tech Digital Commons. It has been accepted for inclusion in Doctoral Dissertations by an authorized administrator of Louisiana Tech Digital Commons. For more information, please contact digitalcommons@latech.edu.

**A HYPERBOLIC TWO-STEP MODEL BASED FINITE DIFFERENCE
METHOD FOR STUDYING THERMAL DEFORMATION
IN A MICRO THIN FILM HEATED BY
ULTRASHORT-PULSED LASERS**

by

Tianchan Niu, B.S., M.S

A Dissertation Presented in Partial Fulfillment
of the Requirements for the Degree
Doctor of Philosophy

COLLEGE OF ENGINEERING AND SCIENCE
LOUISIANA TECH UNIVERSITY

November 2007

UMI Number: 3283298

INFORMATION TO USERS

The quality of this reproduction is dependent upon the quality of the copy submitted. Broken or indistinct print, colored or poor quality illustrations and photographs, print bleed-through, substandard margins, and improper alignment can adversely affect reproduction.

In the unlikely event that the author did not send a complete manuscript and there are missing pages, these will be noted. Also, if unauthorized copyright material had to be removed, a note will indicate the deletion.

UMI[®]

UMI Microform 3283298

Copyright 2007 by ProQuest Information and Learning Company.

All rights reserved. This microform edition is protected against unauthorized copying under Title 17, United States Code.

ProQuest Information and Learning Company
300 North Zeeb Road
P.O. Box 1346
Ann Arbor, MI 48106-1346

LOUISIANA TECH UNIVERSITY

THE GRADUATE SCHOOL


October 1, 2007

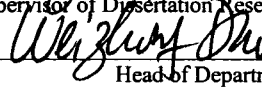
Date

We hereby recommend that the dissertation prepared under our supervision
by Tianchan Niu

entitled A Hyperbolic Two-Step Model Based Finite Difference Method for Studying Thermal
Deformation in a Micro Thin Film Heated by Ultrashort-Pulsed Lasers

be accepted in partial fulfillment of the requirements for the Degree of
Doctor of Philosophy in Computational Analysis and Modeling




Supervisor of Dissertation Research


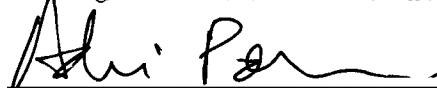
Head of Department

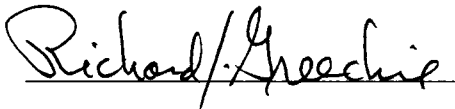
Department

Recommendation concurred in:











Advisory Committee

Approved:


Director of Graduate Studies

Approved:


Dean of the Graduate School



Dean of the College

ABSTRACT

Heat transport through micro thin films plays a very important role in microtechnology applications. Many microelectronic devices have metal thin films as their key components. Microscale heat transfer is also important for the thermal processing of materials, including laser micromachining, laser patterning, laser synthesis and laser surface hardening. Hence, studying the thermal behavior of thin films is essential for predicting the performance of a microelectronic device or for obtaining the desired microstructure. Recently, it has become very popular to use ultrashort-pulsed lasers in thermal processing, which lasers have pulse durations of the order of subpicoseconds to femtoseconds, and these kinds of lasers can limit the undesirable spread of the thermal process zone in the heated sample. However, ultrashort-pulsed lasers can induce ultrafast damage, which occurs after the heating pulse is over. Therefore, in order to apply ultrashort-pulsed lasers successfully, one must study the thermal deformation to prevent the thermal damage.

In the previous research, the parabolic two-step micro heat transport equations have been widely applied in microscale heat transfer. However, when the laser pulse duration is much shorter than the electron-lattice thermal relaxation time for the activation of ballistic behavior in the electron gas, the parabolic two-step model may lose accuracy, as pointed out the in the literature.

It has not been seen in the literature employing the hyperbolic two-step model for studying thermal deformation in a micro thin film exposed to ultrashort-pulsed lasers, which is important for enhancing our understanding of micro heat transfer in a micro thin film exposed to ultrashort-pulsed lasers. Hence, the purpose of this dissertation is to employ the hyperbolic two-step model with temperature-dependent thermal properties for obtaining temperature distribution in a thin film induced by ultrashort-pulsed lasers and to couple with the dynamic equations of motions in order to study thermal deformation in the thin film. To this end, we first develop an implicit finite difference scheme for solving the hyperbolic two-step model with temperature-dependent thermal properties. The scheme is shown to satisfy a discrete analogus of an energy estimate. We then apply it to studying thermal deformations in two-dimensional (2D) thin films exposed to ultrashort-pulsed lasers. In this method, staggered grids are designed, and the coupling effect between lattice temperature and strain rate, as well as the hot electron blast effect in momentum transfer, are considered. As such, this obtained method allows us to avoid non-physical oscillations in the solution.

To demonstrate the applicability of the method, we test three physical cases, (1) 1D double-layered thin film with perfectly contacted interface irradiated by ultrashort-pulsed lasers, (2) 2D single-layered thin film irradiated by ultrashort-pulsed lasers, and (3) 2D double-layered thin film with perfectly contacted interface irradiated by ultrashort-pulsed lasers. Results show that the method is promising and there are some differences between the hyperbolic two-step model and the parabolic model. Particularly, one may see the differences regarding the change in electron temperature ($\Delta T_e / (\Delta T_e)_{\max}$) and the displacement (u) in x direction.

APPROVAL FOR SCHOLARLY DISSEMINATION

The author grants to the Prescott Memorial Library of Louisiana Tech University the right to reproduce, by appropriate methods, upon request, any or all portions of this Dissertation. It is understood that "proper request" consists of the agreement, on the part of the requesting party, that said reproduction is for his personal use and that subsequent reproduction will not occur without written approval of the author of this Dissertation. Further, any portions of the Dissertation used in books, papers, and other works must be appropriately referenced to this Dissertation.

Finally, the author of this Dissertation reserves the right to publish freely, in the literature, at any time, any or all portions of this Dissertation.

Author Trieh Niu
Date 10/22/07

TABLE OF CONTENTS

ABSTRACT	iii
LIST OF TABLES	viii
LIST OF FIGURES	ix
NOMENCLATURE	xiii
ACKNOWLEDGEMENTS	xvii
CHAPTER 1 INTRODUCTION	1
1.1 General Overview	1
1.2 Research Objectives.....	3
1.3 Organization of the Dissertation	4
CHAPTER 2 BACKGROUND AND PREVIOUS WORK	6
2.1 Microscale Heat Transfer Model	6
2.1.1 Microscale Heat Conduction.....	7
2.1.2 Two-Step Model	12
2.1.3 Dual-Phase-Lagging Model	16
2.2 Previous Work	17
2.2.1 One-Dimensional Parabolic Two-Step Model.....	18
2.2.2 Two-Dimensional Parabolic Two-Step Model	19
2.2.3 Other Work	22
CHAPTER 3 ONE-DIMENSIONAL MATHEMATICAL MODEL AND FINITE DIFFERENCE SCHEME	26
3.1 Governing Equations	26
3.1.1 Problem Description	26

3.1.2 Governing Equations	27
3.1.3 Energy Estimate	28
3.2 Finite Difference Scheme	35
3.2.1 Notations	35
3.2.2 Finite Difference Scheme	36
3.2.3 Energy Estimate	37
3.2.4 Algorithm	44
CHAPTER 4 TWO-DIMENSIONAL MATHEMATICAL MODELS AND FINITE DIFFERENCE SCHEMES	48
4.1 Single-Layered Case	48
4.1.1 Problem Description	48
4.1.2 Notations	50
4.1.3 Finite Difference Scheme	52
4.1.4 Algorithm	56
4.2 Double-Layered Case	57
4.2.1 Problem Description	57
4.2.2 Notations	59
4.2.3 Finite Difference Scheme	61
4.2.4 Algorithm	67
CHAPTER 5 NUMERICAL EXAMPLES	69
5.1 One-Dimensional Double-Layered Case	69
5.1.1 Example Description	69
5.1.2 Results and Analysis	70
5.2 Two-Dimensional Single-Layered Case	75
5.2.1 Example Description	75
5.2.2 Results and Analysis	77
5.3 Two-Dimensional Double-Layered Case	90
5.3.1 Example Description	90
5.3.2 Results and Analysis	92
CHAPTER 6 CONCLUSION AND FUTURE WORK	110
APPENDIX A SOURCE CODE FOR 1D DOUBLE-LAYERED CASE	112
APPENDIX B SOURCE CODE FOR 2D SINGLE-LAYERED CASE	117
APPENDIX C SOURCE CODE FOR 2D DOUBLE-LAYERED CASE	125

REFERENCES.....	138
------------------------	------------

LIST OF TABLES

Table 2.1	Phonon-electron coupling factor G , for some noble and transition metals [Qiu 1992].....	15
Table 5.1	Thermal properties of gold and chromium [Chen 2003, Tzou 1996].....	70
Table 5.2	Thermophysical properties of gold [Tzou 2002, Chen 2002, Kaye 1973].....	76
Table 5.3	Thermophysical properties of gold and chromium [Touloukian 1970 a, b, Chen 2003, Tzou 1996].....	91

LIST OF FIGURES

Figure 2.1	Energy transport through phonon collision [Tzou 1996].....	7
Figure 2.2	Phonon interactions in a film of the same order of magnitude as the mean free path, illustrating the challenge of the microscale effect in space to the concept of temperature gradient [Tzou 1996].....	10
Figure 3.1	A 1D double-layered micro thin film.....	27
Figure 3.2	A staggered grid for 1D double-layered thin film.....	36
Figure 4.1	A 2D single-layered micro thin film.....	49
Figure 4.2	A staggered grid for a 2D single-layered thin film	52
Figure 4.3	A 2D double-layered thin film	57
Figure 4.4	A staggered grid for a 2D double-layered thin film.....	61
Figure 5.1	Configuration of a 1D double-layered thin film.....	69
Figure 5.2	Normalized electron temperatures at the front surface of a 100 nm gold and chromium thin film with $\tau_e = 0.00136ps$ and three difference values of τ_l for chromium.....	71
Figure 5.3	Normalized electron temperatures at the front surface of a 100 nm gold and chromium thin film with $\tau_e = 0.0068ps$ and three difference values of τ_l for chromium.....	72
Figure 5.4	Normalized electron temperatures at the front surface of a 100 nm gold and chromium thin film with $\tau_e = 0.0136ps$ and three difference values of τ_l for chromium.....	72
Figure 5.5	Normalized electron temperatures at the front surface of a 100 nm gold and chromium thin film with $\tau_e = 0.00136ps$ and $\tau_l = 0.0136ps$ for chromium, and three different meshes.....	73

Figure 5.6	Calculated electron temperature profiles for a 100 nm gold and chromium thin film with $\tau_e = 0.0068ps$ and $\tau_l = 0.136ps$ for chromium.....	74
Figure 5.7	Calculated lattice temperature profiles for a 100 nm gold and chromium thin film with $\tau_e = 0.0068ps$ and $\tau_l = 0.136ps$ for chromium.....	74
Figure 5.8	Configuration of a 2D single-layered thin film.....	75
Figure 5.9	Change in electron temperature at $x = 0$ and $y = 0$ versus time for various meshes (80×40 , 160×80 and 300×150) comparing with parabolic model [Wang 2006a].....	77
Figure 5.10	Displacement (u) at $x = 0$ and $y = 0$ versus time for various meshes (80×40 , 160×80 and 300×150) with parabolic model [Wang 2006a]	78
Figure 5.11	Comparison of the hyperbolic model, parabolic model [Wang 2006a] and Chen <i>et al.</i> 's method in [Chen 2002a] with regard to the normal stress (σ_x) at $y = 0\mu m$ and $t = 10ps$	79
Figure 5.12	Contour plots of electron temperature distributions at (a) $t = 0.25ps$, (b) $t = 0.5ps$, (c) $t = 1ps$, (d) $t = 10ps$, and (e) $t = 20ps$	80
Figure 5.13	Contour plots of lattice temperature distributions at (a) $t = 0.25ps$, (b) $t = 0.5ps$, (c) $t = 1ps$, (d) $t = 10ps$, and (e) $t = 20ps$	81
Figure 5.14	Contour plots of displacement (u) distributions at (a) $t = 1ps$, (b) $t = 5ps$, (c) $t = 10ps$, (d) $t = 15ps$, and (e) $t = 20ps$	83
Figure 5.15	Contour plots of displacement (v) distributions at (a) $t = 1ps$, (b) $t = 5ps$, (c) $t = 10ps$, (d) $t = 15ps$, and (e) $t = 20ps$	85
Figure 5.16	Contour plots of normal stress (σ_x) distributions at (a) $t = 1ps$, (b) $t = 5ps$, (c) $t = 10ps$, (d) $t = 15ps$, and (e) $t = 20ps$	87
Figure 5.17	Contour plots of normal stress (σ_y) distributions at (a) $t = 1ps$, (b) $t = 5ps$, (c) $t = 10ps$, (d) $t = 15ps$, and (e) $t = 20ps$	88
Figure 5.18	Configuration of a 2D double-layered micro thin film.....	90

Figure 5.19	Change in electron temperature at $x = 0$ and $y = 0$ versus time for various meshes (80×40 , 160×80 and 200×100) with $J = 500 J/m^2$ comparing with parabolic model [Wang 2006b].....	93
Figure 5.20	Displacement (u) at $x = 0$ and $y = 0$ versus time for various meshes (80×40 , 160×80 and 200×100) with $J = 500 J/m^2$ comparing with parabolic model [Wang 2006b].....	93
Figure 5.21	Comparison of electron temperature (T_e) at $y = 0 \mu m$ at (a) $t = 0.25 ps$, (b) $t = 0.5 ps$, (c) $t = 1 ps$, (d) $t = 10 ps$, and (e) $t = 20 ps$ with $J = 500 J/m^2$, $1000 J/m^2$ and $2000 J/m^2$	94
Figure 5.22	Comparison of lattice temperature (T_l) at $y = 0 \mu m$ at (a) $t = 0.25 ps$, (b) $t = 0.5 ps$, (c) $t = 1 ps$, (d) $t = 10 ps$, and (e) $t = 20 ps$ with $J = 500 J/m^2$, $1000 J/m^2$ and $2000 J/m^2$	96
Figure 5.23	Comparison of displacement (u) at $y = 0 \mu m$ at (a) $t = 5 ps$, (b) $t = 10 ps$, (c) $t = 15 ps$, and (d) $t = 20 ps$ with $J = 500 J/m^2$, $1000 J/m^2$ and $2000 J/m^2$	98
Figure 5.24	Comparison of displacement (v) at $y = 0 \mu m$ at (a) $t = 5 ps$, (b) $t = 10 ps$, (c) $t = 15 ps$, and (d) $t = 20 ps$ with $J = 500 J/m^2$, $1000 J/m^2$ and $2000 J/m^2$	99
Figure 5.25	Comparison of normal stress (σ_x) at $y = 0 \mu m$ at (a) $t = 5 ps$, (b) $t = 10 ps$, (c) $t = 15 ps$, and (d) $t = 20 ps$ with $J = 500 J/m^2$, $1000 J/m^2$ and $2000 J/m^2$	100
Figure 5.26	Comparison of normal stress (σ_y) at $y = 0 \mu m$ at (a) $t = 5 ps$, (b) $t = 10 ps$, (c) $t = 15 ps$, and (d) $t = 20 ps$ with $J = 500 J/m^2$, $1000 J/m^2$ and $2000 J/m^2$	101
Figure 5.27	Contour plots of electron temperature (T_e) profiles with $J = 1000 J/m^2$ at (a) $t = 0.25 ps$, (b) $t = 0.5 ps$, (c) $t = 1 ps$ and (d) $t = 10 ps$	103
Figure 5.28	Contour plots of lattice temperature (T_l) profiles with $J = 1000 J/m^2$ at (a) $t = 0.25 ps$, (b) $t = 0.5 ps$, (c) $t = 1 ps$ and (d) $t = 10 ps$	104

Figure 5.29	Contour plots of displacement (u) profiles with $J = 1000 J/m^2$ at (a) $t = 1 ps$, (b) $t = 5 ps$, (c) $t = 10 ps$, and (d) $t = 20 ps$	105
Figure 5.30	Contour plots of displacement (v) profiles with $J = 1000 J/m^2$ at (a) $t = 1 ps$, (b) $t = 5 ps$, (c) $t = 10 ps$, and (d) $t = 20 ps$	107
Figure 5.31	Contour plots of normal stress (σ_x) profiles with $J = 1000 J/m^2$ at (a) $t = 1 ps$, (b) $t = 5 ps$, (c) $t = 10 ps$, and (d) $t = 20 ps$	108
Figure 5.32	Contour plots of normal stress (σ_y) profiles with $J = 1000 J/m^2$ at (a) $t = 1 ps$, (b) $t = 5 ps$, (c) $t = 10 ps$, and (d) $t = 20 ps$	109

NOMENCLATURE

A_e	electron-blast coefficient, $J/(m^3 K^2)$
C_e	electron heat capacity, $J/(m^3 K)$
C_l	lattice heat capacity, $J/(m^3 K)$
E	phonon/electron energy, J
G	electron-lattice coupling factor, $W/(m^3 K)$
J	laser fluence, J/m^2
K	bulk modulus, Pa
k_e	thermal conductivity, $W/(mK)$
L_x	length of micro thin film in x direction, μm
L_y	length of micro thin film in y direction, μm
N_x	number of grid points in x direction
N_y	number of grid points in y direction
S	volumetric heat source, W/m^2
\bar{q}_e	electron heat flux, W/m^2
\bar{q}_l	lattice heat flux, W/m^2
q_e^x	electron heat flux in x direction, W/m^2
q_e^y	electron heat flux in y direction, W/m^2

q_l^x	lattice heat flux in x direction, W/m^2
q_l^y	lattice heat flux in y direction, W/m^2
R	surface reflectivity
T	absolute temperature, K
T_e	electron temperature, K
T_l	lattice temperature, K
S	heat source, W/m^2
t_p	laser pulse duration, s
u	displacement in the x direction, m
v	displacement in the y direction, m
v_1	velocity component in the x direction, m/s
v_2	velocity component in the y direction, m/s
x, y	rectangular coordinates
\vec{n}	unit outward normal vector on the boundary

Greek Symbols

Δt	time increment, s
Δx	rectangular grid size, m
Δy	rectangular grid size, m
ζ	optical penetration depth, m
α_T	thermal expansion coefficient
Δ_{-t}	finite difference operator

δ_x	finite difference operator
δ_y	finite difference operator
Δ_x	finite difference operator
Δ_{-x}	finite difference operator
Δ_y	finite difference operator
Δ_{-y}	finite difference operator
τ_e	electron relaxation time, <i>ps</i>
τ_l	lattice relaxation time, <i>ps</i>
ε_x	normal strain in the <i>x</i> direction
ε_y	normal strain in the <i>y</i> direction
ε_{xy}	shear strain
Λ	electron-blast coefficient, $J/(m^3 K^2)$
λ	Lame's constant, <i>Pa</i>
μ	Lame's constant, <i>Pa</i>
ρ	density, kg/m^3
δ	penetration depth <i>nm</i>
σ	Stefan-Boltzmann's constant
σ_x	normal stress in the <i>x</i> direction
σ_y	normal stress in the <i>y</i> direction
σ_{xy}	shear stress in the <i>xy</i> direction

Subscripts and Superscripts

0	initial value at $t = 0$
e	electron
i	grid index in the x direction
j	grid index in the y direction
l	lattice
n	time level

ACKNOWLEDGEMENTS

This dissertation owes great appreciation to many people for their support and encouragement. I am here to express my sincere gratitude to my advisor, Dr. Weizhong Dai, for his patient guidance, generous help, and abundant encouragement. It is my great luck and honor to be his student. Without his directions and suggestions, this dissertation could not be completed. I would like to thank Dr. Richard Greechie for his termless trust and warmhearted help. In his class, he showed me the views of mathematics so that I can realize how beautiful it is. The special appreciation to Dr. Raja Nassar is for his patience to teach me about statistics and his kindness to give me endless support. Sincere acknowledgement is also extended to Dr. Hisham Hegab and Dr. Andrei Paun for teaching and directing me.

I owe a lot to my parents for their unconditional love and selfless sacrifice. They trust, respect, and support me and try their best to offer me comfortable conditions for living and studying. I would also like to thank my boyfriend, Jian Wu, who accompanies me through sorrow and happiness. Finally, I want to express my appreciation to all my friends. This dissertation is dedicated to all above mentioned.

CHAPTER 1

INTRODUCTION

1.1 General Overview

Heat transport through micro thin films plays a very important role in microtechnology applications [Joseph 1989] [Joshi 1993]. Many microelectronic devices have metal thin films as their key components. In order to enhance the switching speed of the device, we have to reduce the device size to microscale. Meanwhile, size reduction increases the rate of heat generation, which causes a high thermal load on the microelectronic devices. Microscale heat transfer is also important for the thermal processing of materials [Qiu 1992, 1993], including laser micromachining, laser patterning, laser synthesis, and laser surface hardening.

Recently, it has been very popular to use ultrashort-pulsed lasers in thermal processing, which are ultrafast lasers with pulse durations of the order of subpicoseconds to femtoseconds. They have been widely applied in structural monitoring of thin metal films [Opsal 1991], laser micromachining [Knapp 1990], and patterning [Elliot 1989], structural tailoring of microfilms [Grigoropoulos 1994], and laser synthesis and processing in thin-film deposition [Narayan 1991]. The non-contact nature of femtosecond lasers has made them an ideal candidate for precise thermal processing of

functional nanophase materials, and this kind of lasers can limit the undesirable spread of the thermal process zone in the the heated sample [Tzou 2002].

For an ultrashort-pulsed laser, the heating involves high-rate heat flow from electrons to lattices in the picosecond domains. Depending on the temperature, electrons have a heat capacity two to three order of magnitude smaller than that of lattices. When heated by photons (lasers), the laser energy is primarily absorbed by the free electrons that are confined within film depth during the excitation. Electrons first shoot up to several hundreds or thousands of degrees within a few picoseconds without disturbing the metal lattices. A major portion of the thermal energy diffuses to the electrons in the deeper region of the target. Because the pulse duration is so short, the laser is turned off before thermal equilibrium between the electrons and lattices is reached. In this time interval, the heat flux is essentially limited to the region within the electron thermal diffusion length. This stage is termed non-equilibrium heating due to the large difference of temperatures in electrons and lattices [Chen 2001]. The lattice temperature then increases as a result of lattice-electron coupling, resulting in a new thermal property termed lattice-electron coupling factor.

In order to apply high-energy ultrashort-pulsed lasers in real life, we need three main factors [Tzou 2002]: (1) well characterized pulse width, intensity and experimental techniques; (2) reliable microscale heat transfer models, and (3) prevention of thermal damage which is also the most important task in real applications. Here, ultrafast damage induced by sub-picosecond pulses is intrinsically different from that induced by long-pulse or continuous lasers. For the latter, laser damage is caused by the elevated temperatures resulting from the continuous pumping of photon energy into the processed

sample. The “damage threshold” termed in heating by long-pulse lasers, therefore, is often referred to as the laser intensity that drives the heated spot to the melting temperature. Thermal damage induced by ultrashort-pulsed lasers in the picosecond domain, on the other hand, occurs after the heating pulse is over [Wang 2007]. Under a sufficiently high intensity of heating, in fact, experimental results have shown that the ultrafast damage involves shattering of a thin material layer (from the heated surface) without a clear signature of thermal damage by excessive temperatures [Tzou 2002, Wang 2007]. Rather than the melting damage developed at high temperature, obviously, there exists a new driving force that brings about such ultrafast damage; probably in only a few picoseconds after heating is applied [Tzou 2002]. Therefore, preventing thermal damage is our motivation to study the thermal deformation induced by ultrashort-pulsed lasers.

1.2 Research Objectives

The objective of this dissertation is to develop a new numerical method for studying thermal deformation in two-dimensional single-layered and double-layered micro thin films exposed to ultrashort-pulsed lasers in which the numerical method is obtained based on the dynamic equations of motion and hyperbolic two-step heat transport equations. To achieve this objective, a series of steps will be taken as follows:

Step 1: Introduce velocity components into the model and re-write the dynamic equations of motion.

Step 2: Construct a staggered grid.

Step 3: Develop a fourth-order compact finite difference scheme for evaluating stress derivatives and share stress derivatives in the dynamic equations of motion. As such, the third-order derivatives of stresses and shear stresses are disappeared and hence non-physical oscillations in the solutions are eliminated.

Step 4: Develop a finite difference scheme for obtaining temperatures in a 1D double-layered micro thin film heated by ultrashort-pulsed lasers, where the interfaces are perfectly contacted. This scheme is based on the hyperbolic two-step model.

Step 5: Analyze the convergence of the finite difference scheme for 1D situation.

Step 6: Develop a finite difference scheme for obtaining temperatures, stress, strain, and displacement distributions in a 2D single-layered micro thin film based on the hyperbolic two-step model.

Step 7: Develop a finite difference scheme for obtaining temperatures, stress, strain and displacement distributions in a 2D double-layered micro thin film with perfectly contacted interface based on the hyperbolic two-step model.

Step 8: Test the method by numerical examples.

1.3 Organization of the Dissertation

In Chapter 1, a general review of the main idea of our work is given, and the objective of this dissertation is proposed. Chapter 2 provides some background for this research. Heat transfer at micro scale, the dual-phase-lagging behavior, and the parabolic

two-step model for 1D and 2D double-layered micro thin films, as well as a review of previous works, will be reviewed in this chapter.

Chapter 3 gives the mathematical models for 1D double-layered micro thin film. We will consider a 1D micro thin film irradiated by ultrashort pulsed lasers, set up the governing equations, and obtain its energy estimate. Meanwhile, we will develop the finite difference scheme and then show that it satisfies a discrete analogus of the energy estimate.

In Chapter 4, we will set up the governing equations for 2D single-layered and double-layered thin films, respectively. In Chapter 5, a finite difference scheme will be developed for both single-layered and double-layered micro thin film for 2D cases.

In Chapter 6, we will design the numerical algorithms for obtaining the temperature, displacement, stress and strain distributions and give the numerical results based on the developed numerical methods in a micro thin film exposed to an ultrashort pulsed laser. Three cases will be focused on, which will be a 1D double-layered micro thin film with perfectly contacted interface, 2D single-layered micro thin film, and 2D double-layered micro thin film with perfectly contacted interface. Various mesh sizes will be chosen to test the convergence of the method. Also, the electron temperature, the lattice temperature, the displacements, and the stresses will be calculated and discussed. Lastly, in Chapter 7, we give the conclusions of our work and suggest future research work.

CHAPTER 2

BACKGROUND AND PREVIOUS WORK

2.1 Microscale Heat Transfer Model

At the micro scale, the process of heat transfer is determined by phonon-electron interaction in metallic films and by phonon scattering in dielectric films, conductors and semiconductors. The classical theories established at the macro scale, such as heat conduction subjected to Fourier's law, are not expected to be informative enough at the microscale because they describe macroscopic behavior aggregated over many grains. They break down further as the temporal domain becomes extremely small, say, on the order of picoseconds or femtoseconds. A typical case occurs in the ultrafast laser heating in the thermal processing of materials. In this instance, the quasi-equilibrium assumption established in Fourier's law does not hold along with other macroscopic behaviors [Kaba 2004, 2005].

In this part of the dissertation, we give a brief review of the microscopic two-step model (phonon-electron interaction model), which emphasizes the special behavior depicted by the model that might reveal possible lagging behavior. Many articles exist about this two-step model, according to which, we can gain an overall understanding of

the development of the model. The following sections are based on Tzou's book [Tzou 1996].

2.1.1 Microscale Heat Conduction

Regardless of the type of the conducting medium, heat transport requires sufficient collisions among energy carriers. In metals, electrons and phonons are the main energy carriers. In dielectric crystals, insulators, and semiconductors on the other hand, phonons are the primary energy carriers. The phonon gas can be considered as a group of "mass particles" that characterize the energy state of a metal lattice. For a metal lattice vibrating at a frequency ν at a certain temperature T , the energy state of the metal lattice, and hence the energy state of the phonon is

$$E = h\nu, \quad (2.1)$$

with h being the Planck constant. The lattice frequency is of the order of tens of terahertz (10^{13} l/s) at room temperature. We can imagine that the lattice frequency increases with the temperature of the metal lattice. Energy transport from one lattice to the other one can thus be thought of as the consequence of a series of phonon collisions in time history, as illustrated in Figure 2.1.

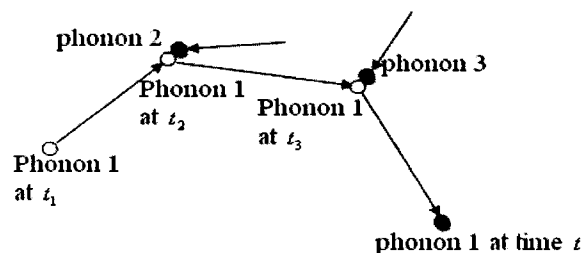


Figure 2.1 Energy transport through phonon collision [Tzou 1996].

Bearing energy $h\nu$ at time t_1 , phonon 1 collides with phonon 2 at t_2 and with phonon 3 at time t_3 . In the process of each successive collision, energy is transferred from phonon 1 to phonons 2 and 3, which causes a successive change of vibrating frequency of phonon 1. To illustrate the phenomenon, the mean free path (d , in space) is defined as the algebraic mean of the distances traveled by phonon 1 between the two successive collisions with phonons 2 and 3:

$$d = \frac{d_1 + d_2 + d_3}{3}. \quad (2.2)$$

The mean free time τ can be defined similarly as the algebraic mean of the times traveled by phonon 1 between the two successive collisions with phonons 2 and 3:

$$\tau = \frac{(\tau_2 - \tau_1) + (\tau_3 - \tau_2) + (t - \tau_3)}{3} = \frac{(t - \tau_1)}{3}. \quad (2.3)$$

We use two collisions for phonon 1 in this example. To have a meaningful statistical ensemble space of course, a “sufficient” number of collisions must be collected to determine the mean free path and the mean free time.

In the macroscopic models, we assume the physical domain for heat transport is so large that it allows hundreds of thousands of phonon collisions before an observation or description is made for the process of heat transport. Since phonon collision requires a finite amount of time to occur, hundreds of thousands of those collisions would require a sufficiently long time for the process of heat transfer to occur. Therefore, it is clear that the macroscopic models not only require a sufficiently large physical domain for conducting heat (much larger than the mean free path), but also a sufficiently long time

for heat conduction to take place (much longer than the mean free time). It should be pointed out that the sufficiently long time for the stabilization of energy transport by phonons should not be confused with the time required for the steady state to be reached. The sufficiently long time required in phonon collisions is to provide a statistically meaningful concept in regards to the mean free path and the mean free time. The heat transport phenomenon can still be time dependent after phonon transport becomes stabilized. In a phenomenological sense, the mean free time as illustrated in Figure 2.2 is parallel to the characteristic time describing the relaxation behavior in the fast-transient process. For metals, the mean free time, or relaxation time is of the order of picoseconds. In dielectrics crystals and insulators, the relaxation time is longer, roughly of the order of nanoseconds to picoseconds. As a rough estimate, any response time being shorter than one nanosecond should be closely investigated. The fast-transient effect, such as wave behavior in heat conduction, may activate and introduce unexpected effects in heat transport. Such a threshold value of nanoseconds, however, depends on the combined effects of geometric configuration (of the specimen) and thermal loading imposed upon the system. It may vary by one order of magnitude if the system involves an abrupt change of geometric curvatures (specifically around a crack or notch tips), or is subject to discontinuous thermal loading (irradiation of a short pulse laser, for instance).

The mean free path for electrons is the order of tens of nanometers ($10^{-8} m$) at room temperature, which is a strong function of temperature. It may increase to the order of millimeters in the liquid helium temperature range, roughly $4 K$. The mean free path in phonon collision or phonon scattering (from the boundaries of the grains) is much longer. Take a type IIa diamond film as an example; its mean free path is of the order of tenths of

a micron ($10^{-7} m$) at room temperature. We can roughly estimate that a physical device with a characteristic dimension in submicrons deserves special attention. The microstructural interaction effect, such as phonon-electron or phonon scattering, may enhance heat transfer in short times dramatically. Enhancement of the heat transfer enlarges the thermal processing zone and promotes the temperature level, which may cause early burnout of micro devices without proper prevention.

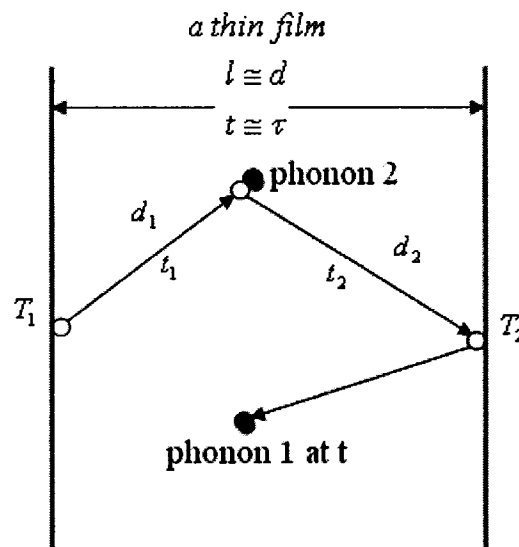


Figure 2.2 Phonon interactions in a film of the same order of magnitude as the mean free path, illustrating the challenge of the microscale effect in space to the concept of temperature gradient [Tzou 1996].

Given that the physical dimensions, under consideration at the micro scale, are of the same order of magnitude as the mean free path, the response time is of the same order of magnitude as the mean free time, and the quantities derived from the concept of aggregation at the macro scale need to be reexamined for their meaning in a microscopic environment. The temperature gradient, which has been simply derived in macro scale

heat transfer, may lose its physical meaning for a thin film of thickness, the same order of magnitude as the mean free path. As illustrated in Figure 2.2, it is proper that we can still divide the temperature difference, $T_2 - T_1$, by the film thickness l ($\cong d$, the mean free path of phonon interaction or scattering) to obtain a “gradient like” quantity, but the temperature gradient obtained in this fashion loses its usual physical meaning for the reason that there is no sufficient energy carriers between the two surfaces of the film and, as a result, the temperature field is discontinuous across the film thickness. The concept of temperature gradient fails, and the usual way to define the heat flux vector according to Fourier’s law turns out to be doubtful. Thus, deciding the concept of both the temperature gradient and the heat flux vector is the first-line challenge that the microscale effect in space has raised against traditional theories in macroscale heat transfer.

A similar situation happens to the response time for the temperature. The typical response time in the thin film is of the same order of magnitude as the mean free time, as a result of phonons traveling in the threshold of the mean free path. If the response time of primary concern (for temperature or heat flux vector) is of the same order of magnitude as the mean free time (relaxation time), the individual effects of phonon interaction and phonon scattering must be considered in the short time transient of heat transport. This is the second challenge raised by the microscale effect in time against conventional theories in macroscale heat transfer. From Figure 2.2, it is clear that the microscale effect in space interferes with the microscale effects in time. They cannot be separated and must be contained simultaneously in the framework seeking to develop a theory of heat transfer at the microscale, which is obvious by considering the finite speed of phonon transport in short time. Phonons propagate at the speed of sound, on average,

which is of the order of 10^4 to 10^5 m/s at room temperature, depending on the type of solid medium. A response time of the order of picoseconds (10^{-12} s) thus implies a traveling distance (the penetration depth of heat by phonon transport) of the order of submicrons (10^{-8} to 10^{-7} m). Such a penetration depth is on the microscopic level, requiring a simultaneous consideration of the microscale effect in space.

2.1.2 Two-Step Model

In Figure 2.1 and Figure 2.2, by replacing phonons with phonons or electrons, it becomes the description for the phonon-electron interaction for heat transfer in metals. For those electron gases with much smaller heat capacity than that of the metal lattice, the heating system involves excitation of the electron gas and heating of the metal lattice through phonon-electron interaction in short times. In microscale, the phonon-electron interaction model was proposed to describe this two-step process for energy transport. The first version of the two step model (phonon-electron interaction model) was proposed by Kaganov *et al.* [Kaganov 1957] and Anisimov *et al.* [Anisimov 1974], but they did not give any rigorous proof. This model was only considered as a phenomenological model until Qiu and Tien [Qiu 1993] set the model on a quantum mechanical and statistical basis. They derived the generalized hyperbolic constitutive equations for heat transfer through the electron gas from the Boltzmann transport equation in the absence of an electrical current during short-time heating. The hyperbolic two-step model can perfectly reduce to the parabolic two-step model proposed by Kaganov *et al.* [Kaganov 1957] and Anisimov *et al.* [Anisimov 1974] by setting the relaxation time of the electron gas calculated at the Fermi surface to be zero.

The two-step model depicts heating of the electron gas and the metal lattice by a two-step process for metals. The equations can be written as:

$$\text{Step 1: } C_e \frac{\partial T_e}{\partial t} = \nabla \cdot (K \nabla T_e) - G(T_e - T_l), \quad (2.4)$$

$$\text{Step 2: } C_l \frac{\partial T_l}{\partial t} = G(T_e - T_l), \quad (2.5)$$

where C denotes the volumetric heat capacity, K the thermal conductivity of electron gas, and subscripts e and l represent the electron and metal lattice, respectively. Equation (2.4) is the mathematical representation for the first step heating of the electron gas, and Equation (2.5) is for the second step heating of the metal lattice. Here, we do not consider the effect of heat conduction through the metal lattice. According to Equation (2.4), the extremely supplied phonons, such as those from an intensified laser, first increase the temperature of the electron gas. At this step, diffusion is assumed to provide a parabolic nature for heat transport through the electron gas. The second step is shown mathematically by Equation (2.5), which is the hot electron gas heating the metal lattice by phonon-electron interaction. The energy exchange between phonons and electrons is illustrated by the phonon-electron coupling factor G [Kaganov 1957]:

$$G = \frac{\pi^2}{6} \frac{m_e n_e v_s^2}{\tau_e T_e} \text{ for } T_e \gg T_l, \quad (2.6)$$

where m_e is the electron mass, n_e the number density of electrons per unit volume, and v_s the speed of sound,

$$v_s = \frac{\sigma}{2\pi\hbar} (6\pi^2 n_a)^{\frac{1}{3}} T_D, \quad (2.7)$$

with the quantity h being Planck's constant, k being the Boltzmann constant, n_a being the atomic number density per unit volume, and T_D representing the Debye temperature. The electron temperature (T_e) is much higher than the lattice temperature (T_l) in the early time response. The condition $T_e \gg T_l$ in Equation (2.6) for the applicability of G is thus valid in the fast-transient process of electron-phonon dynamics. Within the limits of Wiedemann-Frenz's law, which states that for metals at moderate temperatures ($T_l > 0.48T_D$), the ratio of the thermal conductivity to the electrical conductivity is proportional to the temperature, and the constant of proportionality is independent of particular metal, the electron thermal conductivity can be expressed as [Kaganov 1957]

$$k_e = \frac{\pi^2 n_e k^2 \tau_e T_e}{3m_e}, \quad (2.8)$$

therefore

$$m_e = \frac{\pi^2 n_e k^2 \tau_e T_e}{3k_e}. \quad (2.9)$$

Substituting Equation (2.9) into Equation (2.6) for the electron mass yields

$$G = \frac{\pi^4 (n_e v k_s)^2}{18\sigma}. \quad (2.10)$$

This coupling factor is dependent upon the thermal conductivity (K) and the number density (n_e) of the electron gas. The coupling factor does not show a strong dependence on temperature and is not affected by relaxation time [Tzou 1996].

In order to estimate the value of G , the number density (n_e) of the electron gas is a key quantity. Qiu and Tien assumed one free electron per atom for noble metals and employed the s -band approximation for the valence electrons in transition metals [Qiu

1992]. Thus, the value for the number density of the electron gas is chosen as a fraction of the valence electrons. The phonon-electron coupling factor is calculated, and experimentally measured values are listed in Table 2.1 for comparison.

Mathematically, Equation (2.4) and Equation (2.5) are two equations with two unknowns, which are the electron-gas temperature (T_e) and the metal-lattice temperature (T_l). We can solve them in a coupled manner, or we can combine them to a single energy equation depicting heat transport through phonon-electron interaction in microscale. On the other hand, the combined energy equation can also be generated from the phase lag concept in the temporal response. This coincidence supports the dual-phase-lag model that we will discuss in the next section.

Table 2.1 Phonon-electron coupling factor G , for some noble and transition metals [Qiu 1992]

Metal	Calculated, $\times 10^{16} W/m^3K$	Measured, $\times 10^{16} W/m^3K$
Cu	14	4.8 ± 0.7 [Brorson 1990] 10 [Elsayed-Ali 1987]
Ag	3.1	2.8 [Groeneveld 1990]
Au	2.6	2.8 ± 0.5 [Brorson 1990]
Cr	45 ($n_s/n_a = 0.5$)	42 ± 5 [Brorson 1990]
W	27 ($n_s/n_a = 1.0$)	26 ± 3 [Brorson 1990]
V	648 ($n_s/n_a = 2.0$)	523 ± 37 [Brorson 1990]
Nb	138 ($n_s/n_a = 2.0$)	387 ± 36 [Brorson 1990]
Pb	62	12.4 ± 1.4 [Brorson 1990]
Ti	202 ($n_s/n_a = 1.0$)	185 ± 16 [Brorson 1990]

2.1.3 Dual-Phase-Lagging Model

Generally speaking, the lagging response depicts the heat flux vector and the temperature gradient taking place at various times in the heat transfer process. Two situations exist. If the temperature gradient goes before the heat flux, then the temperature gradient is the reason with the heat flux as its result, whereas if the temperature gradient follows the heat flux, the heat flux is the cause, and the temperature gradient becomes the effect.

No such precedence concept is present in the established theory of diffusion because in the traditional theory, it is assumed that the temperature gradient and the heat flux vector happen at the same instant of time. Fourier's law of heat conduction,

$$\vec{q}(\vec{r}, t) = -k\Delta T(\vec{r}, t), \quad (2.11)$$

where \vec{r} is the position vector of the material volume and t the physical time. No time difference between the heat flux vector and the temperature gradient exists; therefore, it causes an infinite speed of heat transmission.

Tzou established the base of the theory for the lagging response in heat transfer conduction [Tzou 1996]. In Tzou's work, a new type of energy equation was established, which includes the traditional theories of diffusion with macroscopic space and time, thermal waves with macroscopic space but microscopic time, and phonon-electron interaction model with microscopic space and time in the same system. Since this model utilizes the two-phase lags to describe the transient process, it is named the dual-phase-lag model. Based on the dual-phase-lag model, it is easy to depict the essential conversion from diffusion to the phonon-electron interaction. Similar to Fourier's law, Tzou wrote the constitutive equation as [Tzou 1989a, b, 1990a, b, and 1992]

$$\bar{q}(\vec{r}, t + \tau) = -k\Delta T(\vec{r}, t), \quad (2.12)$$

with τ as the time delay, named the relaxation time in the wave theory of heat conduction. Applying the first-order expression of τ in Equation (2.12) regarding to t , Equation (2.12) changes to

$$\bar{q}(\vec{r}, t) + \tau \frac{\partial \bar{q}}{\partial t}(\vec{r}, t) = -k\Delta T(\vec{r}, t). \quad (2.13)$$

This is the *CV* wave model derived by Cattaneo [Cattaneo 1958] and Vernotte [Vernotte 1958, 1961], successfully getting rid of the contradiction of infinite speed of heat propagation in Fourier's law. The relationship between the relaxation time and the thermal wave speed is [Chester 1963]

$$\tau = \frac{\alpha}{C^2}, \quad (2.14)$$

where α is the thermal diffusivity and C denotes the thermal wave speed. We can clearly see that as C goes to infinity, τ goes to zero, then the *CV* wave model, Equations (2.12) and (2.13), reduces to the Fourier's law, Equation (2.11). This wave model is one of the main research areas in heat transfer conduction. There are also some detailed reviews by Joseph and Preziosi [Joseph 1989, 1990], Tzou [Tzou 1992] and Ozisik and Tzou [Ozisik 1994].

2.2 Previous Work

Based on the theoretical foundation in the previous section, we first review some detailed parabolic models related with our research in this section. Then we roughly take a glance at those previous research works.

2.2.1 One-Dimensional Parabolic Two-Step Model

The energy equations describing the continuous energy flow from hot electrons to lattices during non-equilibrium heating can be written as [Anisimov 1974, Qiu 1992, 1993, and 1994]:

$$C_e(T_e) \frac{\partial T_e}{\partial t} = \nabla \cdot [k_e(T_e, T_l) \nabla T_e] - G(T_e - T_l) + S, \quad (2.15)$$

$$C_l \frac{\partial T_l}{\partial t} = G(T_e - T_l), \quad (2.16)$$

where $C_e(T_e) = A_e T_e$, $k_e(T_e, T_l) = k_0 \left(\frac{T_e}{T_l} \right)$. In the classical theory of diffusion, $T_e = T_l$ thermal equilibrium between the electrons and lattices is reached. Thus, Equations (2.15) and (2.16) can be reduced to the classical heat conduction equation.

In 2004, Dai developed a nonlinear finite difference scheme for solving the parabolic two-step model with temperature dependent thermal properties in a one-dimensional double-layered thin film heated by ultrashort-pulsed lasers [Dai 2004]. The method was applied to investigating the heat transfer in a gold layer on a chromium layer with perfectly contacted interface, where the double-layered thin film with thickness L of the order $0.1 \mu m$ is subjected to a subpicosecond-pulse irradiation. Based on Equations (2.15) and (2.16), the governing equations for the double-layered thin film are [Dai 2004]

$$C_e^{(m)} \frac{\partial T_e^{(m)}}{\partial t} = \frac{\partial}{\partial x} \left(k_e^{(m)} \frac{\partial T_e^{(m)}}{\partial x} \right) - G^{(m)} (T_e^{(m)} - T_l^{(m)}) + S^{(m)}, \quad (2.17)$$

$$C_l^{(m)} \frac{\partial T_l^{(m)}}{\partial t} = G^{(m)} (T_e^{(m)} - T_l^{(m)}), \quad (2.18)$$

where $C_e^{(m)} = A_e T_e^{(m)}$, $k_e^{(m)} = k_0 \frac{T_e^{(m)}}{T_l^{(m)}}$, $0 \leq x \leq \frac{L}{2}$ when $m = 1$, and $\frac{L}{2} \leq x \leq L$ when $m = 2$.

The heat source for both layers is chosen to be

$$S^{(m)}(x,t) = 0.94J \left[\frac{1-R}{t_p \delta} \right] e^{-\frac{x}{\delta}} I(t), \quad (2.19)$$

where $I(t)$ is the light intensity of the laser beam. The interfacial equations are assumed to be

$$k_e^{(1)} \frac{\partial T_e^{(1)}}{\partial x} = k_e^{(2)} \frac{\partial T_e^{(2)}}{\partial x}, \quad T_e^{(1)} = T_e^{(2)}, \quad x = \frac{L}{2}. \quad (2.20)$$

The initial and boundary conditions are assumed to be

$$T_e^{(m)}(x,0) = T_l^{(m)}(x,0) = T_0 (= 300K), \quad (2.21)$$

$$\frac{\partial T_e^{(1)}(0,t)}{\partial x} = \frac{\partial T_l^{(1)}(0,t)}{\partial x} = 0, \quad \frac{\partial T_e^{(2)}(0,t)}{\partial x} = \frac{\partial T_l^{(2)}(0,t)}{\partial x} = 0. \quad (2.22)$$

Such boundary conditions arise from the fact that there are no heat losses from the film surfaces in the short time response [Tzou 1996].

2.2.2 Two-Dimensional Parabolic Two-Step Model

In 2006, Dai and his colleagues [Wang 2006a] developed a finite difference method for studying thermal deformation in a single-layered thin film exposed to ultrashort-pulsed lasers based on the parabolic two-step heat transport equations. The governing equations for studying thermal deformation in the thin film can be expressed as:

(1) Dynamic equations of motion [Tzou 2002, Chen 2002a, Brorson 1987]

$$\rho \frac{\partial^2 u}{\partial t^2} = \frac{\partial \sigma_x}{\partial x} + \frac{\partial \sigma_{xy}}{\partial y} + 2\lambda T_e \frac{\partial T_e}{\partial x}, \quad (2.23)$$

$$\rho \frac{\partial^2 v}{\partial t^2} = \frac{\partial \sigma_{xy}}{\partial x} + \frac{\partial \sigma_y}{\partial y} + 2\lambda T_e \frac{\partial T_e}{\partial y}, \quad (2.24)$$

where

$$\sigma_x = \lambda(\varepsilon_x + \varepsilon_y) + 2\mu\varepsilon_x - (3\lambda + 2\mu)\alpha_T(T_l - T_0), \quad (2.25)$$

$$\sigma_y = \lambda(\varepsilon_x + \varepsilon_y) + 2\mu\varepsilon_y - (3\lambda + 2\mu)\alpha_T(T_l - T_0), \quad (2.26)$$

$$\sigma_{xy} = \mu\varepsilon_{xy}, \quad (2.27)$$

$$\varepsilon_x = \frac{\partial u}{\partial x}, \varepsilon_y = \frac{\partial u}{\partial y}, \varepsilon_{xy} = \frac{\partial u}{\partial y} + \frac{\partial v}{\partial x}, \quad (2.28)$$

$$\lambda = K - \frac{2}{3}\mu. \quad (2.29)$$

(2) Energy equations [Tzou 2002, Chen 2002a, Qiu 1992]

$$\begin{aligned} C_e(T_e) \frac{\partial T_e}{\partial t} &= \frac{\partial}{\partial x} \left[k_e(T_e, T_l) \frac{\partial T_e}{\partial x} \right] + \frac{\partial}{\partial y} \left[k_e(T_e, T_l) \frac{\partial T_e}{\partial y} \right] \\ &\quad - G(T_e - T_l) + Q, \end{aligned} \quad (2.30)$$

$$C_l \frac{\partial T_l}{\partial t} = G(T_e - T_l) - (3\lambda + 2\mu)\alpha_T \frac{\partial}{\partial t} (\varepsilon_x + \varepsilon_y), \quad (2.31)$$

where the heat source is given by

$$Q = 0.94J \frac{1-R}{t_p x_s} \exp \left[-\frac{x}{x_s} - \left(\frac{y}{y_s} \right)^2 - 2.77 \left(\frac{t-2t_p}{t_p} \right)^2 \right]. \quad (2.32)$$

Here, $C_e(T_e) = A_e T_e$, $k_e(T_e, T_l) = k_0 \left(\frac{T_e}{T_l} \right)$. Equations (2.30) and (2.31) are referred to as

parabolic two-step heat transport equations. The boundary conditions are assumed to be

$$\sigma_x = 0, \sigma_{xy} = 0, \text{ at } x = 0, L_x, \quad (2.33)$$

$$\sigma_y = 0, \sigma_{xy} = 0, \text{ at } y = 0, L_y, \quad (2.34)$$

$$\frac{\partial T_e}{\partial \bar{n}} = 0, \frac{\partial T_l}{\partial \bar{n}} = 0. \quad (2.35)$$

The initial conditions are assumed to be

$$T_e = T_l = T_0, u = v = 0, u_t = v_t = 0, \text{ at } t = 0. \quad (2.36)$$

They further presented a finite difference method for studying thermal deformation in a double-layered thin film with perfectly contacted interface exposed to ultrashort-pulsed lasers [Wang 2006b]. The governing equations are written as follows:

(1) Dynamic equations of motion [Brorson 1987, Chen 2002a, Tzou 2002]

$$\rho^{(m)} \frac{\partial^2 u^{(m)}}{\partial t^2} = \frac{\partial \sigma_x^{(m)}}{\partial x} + \frac{\partial \sigma_{xy}^{(m)}}{\partial y} + 2\Lambda^{(m)} T_e^{(m)} \frac{\partial T_e^{(m)}}{\partial x}, \quad (2.37)$$

$$\rho^{(m)} \frac{\partial^2 v^{(m)}}{\partial t^2} = \frac{\partial \sigma_{xy}^{(m)}}{\partial x} + \frac{\partial \sigma_y^{(m)}}{\partial y} + 2\Lambda^{(m)} T_e^{(m)} \frac{\partial T_e^{(m)}}{\partial y}, \quad (2.38)$$

where

$$\sigma_x^{(m)} = \lambda^{(m)} (\varepsilon_x^{(m)} + \varepsilon_y^{(m)}) + 2\mu^{(m)} \varepsilon_x^{(m)} - (3\lambda^{(m)} + 2\mu^{(m)}) \alpha_T^{(m)} (T_l^{(m)} - T_0), \quad (2.39)$$

$$\sigma_y^{(m)} = \lambda^{(m)} (\varepsilon_x^{(m)} + \varepsilon_y^{(m)}) + 2\mu^{(m)} \varepsilon_y^{(m)} - (3\lambda^{(m)} + 2\mu^{(m)}) \alpha_T^{(m)} (T_l^{(m)} - T_0), \quad (2.40)$$

$$\varepsilon_x^{(m)} = \frac{\partial u^{(m)}}{\partial x}, \quad \varepsilon_y^{(m)} = \frac{\partial v^{(m)}}{\partial y}, \quad \varepsilon_{xy}^{(m)} = \frac{\partial u^{(m)}}{\partial y} + \frac{\partial v^{(m)}}{\partial x}. \quad (2.41)$$

Here, $m = 1, 2$, denotes layer 1 and 2, respectively.

(2) Energy equations [Chen 2002a, Qiu 1992, Tzou 2002]

$$\begin{aligned} (C_e(T_e))^{(m)} \frac{\partial T_e^{(m)}}{\partial t} &= \frac{\partial}{\partial x} \left[(k_e(T_e, T_l))^{(m)} \frac{\partial T_e^{(m)}}{\partial x} \right] + \frac{\partial}{\partial y} \left[(k_e(T_e, T_l))^{(m)} \frac{\partial T_e^{(m)}}{\partial y} \right] \\ &\quad - G^{(m)} (T_e^{(m)} - T_l^{(m)}) + Q, \end{aligned} \quad (2.42)$$

$$C_l^{(m)} \frac{\partial T_l^{(m)}}{\partial t} = G^{(m)} (T_e^{(m)} - T_l^{(m)}) - (3\lambda^{(m)} + 2\mu^{(m)}) \alpha_T^{(m)} \frac{\partial}{\partial t} (\varepsilon_x^{(m)} + \varepsilon_y^{(m)}), \quad (2.43)$$

where the heat source is given by

$$Q = 0.94J \frac{1-R}{t_p x_s} \exp \left[-\frac{x}{x_s} - \left(\frac{y}{y_s} \right)^2 - 2.77 \left(\frac{t-2t_p}{t_p} \right)^2 \right]. \quad (2.44)$$

The boundary conditions are

$$\sigma_x^{(1)} = 0, \sigma_{xy}^{(1)} = 0, \text{ at } x = 0, \text{ and } \sigma_x^{(2)} = 0, \sigma_{xy}^{(2)} = 0, \text{ at } x = L_x, \quad (2.45)$$

$$\sigma_y^{(1)} = 0, \sigma_{xy}^{(1)} = 0, \text{ at } y = 0, \text{ and } \sigma_y^{(2)} = 0, \sigma_{xy}^{(2)} = 0, \text{ at } y = L_x, \quad (2.46)$$

$$\frac{\partial T_e^{(m)}}{\partial \vec{n}} = 0, \frac{\partial T_l^{(m)}}{\partial \vec{n}} = 0. \quad (2.47)$$

The initial conditions are assumed to be

$$T_e^{(m)} = T_l^{(m)} = T_0, \mathbf{u}^{(m)} = \mathbf{v}^{(m)} = 0, u_t^{(m)} = v_t^{(m)} = 0, \text{ at } t = 0. \quad (2.48)$$

The interfacial conditions are assumed to be, at $x = L_x/2$,

$$\mathbf{u}^{(1)} = \mathbf{u}^{(2)}, \mathbf{v}^{(1)} = \mathbf{v}^{(2)}, \quad (2.49)$$

$$\sigma_x^{(1)} = \sigma_x^{(2)}, \sigma_{xy}^{(1)} = \sigma_{xy}^{(2)}, \quad (2.50)$$

$$T_e^{(1)} = T_e^{(2)}, k_e^{(1)} \frac{\partial T_e^{(1)}}{\partial x} = k_e^{(2)} \frac{\partial T_e^{(2)}}{\partial x}. \quad (2.51)$$

Numerical results show that the method allows avoiding non-physical oscillations in the solution.

2.2.3 Other Work

As shown in the previous section, the parabolic two-step micro heat transport equations have been widely applied in analysis of microscale heat transfer. However, when the laser pulse duration is much shorter than the electron-lattice thermal relaxation

time that is the characteristic time for the activation of ballistic behavior in the electron gas, the parabolic two-step model may lose accuracy [Qiu 1993] [Tzou 1995b]. As Qiu and Tien point out [Qiu 1994], the relaxation time increases dramatically, as the temperature decreases, from 0.04 ps at room temperature to about 10 ps at 10 K. They developed the hyperbolic two-step heat transport equations based on the macroscopic averages of the electric and heat currents carried by electrons in the momentum space [Qiu 1993]. The generalized hyperbolic two-step model can be written as follows [Chen 2001] [Qiu 1994] [Chen 2003]:

$$C_e \frac{\partial T_e}{\partial t} = -\nabla \cdot \vec{q}_e - G(T_e - T_l) + S, \quad (2.52)$$

$$\tau_e \frac{\partial \vec{q}_e}{\partial t} + \vec{q}_e = -k_e \nabla T_e, \quad (2.53)$$

$$C_l \frac{\partial T_l}{\partial t} = -\nabla \cdot \vec{q}_l + G(T_e - T_l), \quad (2.54)$$

$$\tau_l \frac{\partial \vec{q}_l}{\partial t} + \vec{q}_l = -k_l \nabla T_l. \quad (2.55)$$

Here, $\tau_e = \frac{1}{A_e T_e^2 + B_l T_l}$ is the electron relaxation time, and $\tau_l = \frac{3k_l}{C_l v_s^2}$ is the lattice

relaxation time. It can be seen that if τ_e , τ_l and k_l are zero, the hyperbolic two-step model will reduce to the parabolic two-step model.

Many articles try to provide the numerical methods for solving Equations (2.52) to (2.55) [Tzou 1995a-d, 2001] [Ozisik 1994] [Chiffell 1994] [Wang 2000, 2001] [Antaki 1998] [Tang 1999] [Lin 1997] [Dai 1999, 2000, 2001a, b].

Chen *et al.* [Chen 2001, 2003] employed finite-difference and finite-element methods to solve the hyperbolic two-step model for investigation of thermal response in a

single-layered metal thin film caused by pulse laser heating. Al-Nimr and his colleagues [Al-Nimr 1999, 2000, 2003] [Al-Odat 2002] [Naji 2003] studied the thermal behavior of thin metal films in the hyperbolic two-step model with constant thermal properties.

From a recent report, using the temperature-dependent conductivity instead of constant conductivity can gain better agreement between temperature predictions and corresponding measurements for short-pulse laser heating [Antaki 2002]. Tzou and Chiu studied the temperature-dependent thermal lagging [Tzou 2001], developing an explicit finite difference algorithm to perform the nonlinear analysis.

Wang and his colleagues [Wang 2000, 2001] gave methods of measuring the phase-lags of the heat flux and the temperature gradient and obtained analytical solutions for 1D, 2D and 3D heat conduction domains under essentially arbitrary initial and boundary conditions. They provided solution system for both mixed and Cauchy problems of dual-phase-lagging (DPL) heat conduction equations. The DPL heat conduction equation is well-posed in a finite 1D region under Dirichlet, Neumann or Robin boundary conditions [Wang 2000]. Under linear boundary conditions, two solution systems exist. For a finite region of dimension n ($n \geq 2$) under Dirichlet, Neumann or Robin boundary conditions, the DPL heat conduction equation has a unique solution, which is stable regarding to the initial conditions [Wang 2001].

In order to solve the transient heat conduction problems in finite rigid slabs irradiated by short-pulse lasers, Tang and Araki [Tang 1999] developed a generalized macroscopic model with the solution derived from Green's function method and finite integral transform technique.

Many works about heat transfer models with ultrashort-pulsed lasers are published; however, only a few mathematical models have been derived to study the deformation caused by ultrashort-pulsed lasers [Tzou 2002, Chen 2002a, b, Chen 2003]. Tzou [Tzou 2002] developed a one-dimensional model in a double-layered thin film and solved it using the differential-difference approach. Chen and his co-workers considered a two-dimensional axisymmetric cylindrical thin film and applied an explicit finite difference method. They added an artificial viscosity term to eliminate numerical oscillations.

As mentioned above, the parabolic two-step model may lose accuracy when the laser pulse duration is much shorter than the electron-lattice thermal relaxation time. Therefore, it is needed to employ a hyperbolic two-step model for studying thermal deformation in thin films exposed to ultrashort-pulse lasers, which is also the motivation of our research.

CHAPTER 3

ONE-DIMENSIONAL MATHEMATICAL MODEL AND FINITE DIFFERENCE SCHEME

3.1 Governing Equations

3.1.1 Problem Description

Hyperbolic two-step micro heat transport equations have attracted attention in thermal analysis of thin metal films exposed to ultrashort-pulsed lasers. Exploration of temperature-dependent thermal properties is absolutely necessary to advance our fundamental understanding of microscale heat transport. In this chapter, we consider the case where the heat transport is a one-dimensional micro thin film with perfectly contacted two layers. By obtaining an energy estimate, we develop a finite difference scheme, which has a discrete analogue of the energy estimate, to solve the hyperbolic two-step model with temperature-dependent thermal properties in the thin film exposed to ultrashort-pulsed lasers.

It should be pointed out that double (or multi)-layered thin films are widely used in engineering applications since a single metal layer cannot satisfy all mechanical,

thermal and electronic requirements. For example, chromium can be used to act as a heat sink which significantly reduces the temperature rise in the top gold layer.

3.1.2 Governing Equations

Consider a double-layered metal thin film exposed to ultrashort-pulsed lasers, as shown in Figure 3.1.

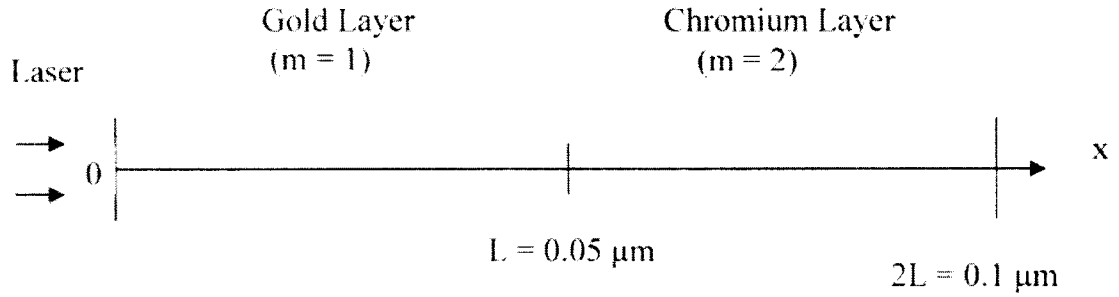


Figure 3.1 A 1D double-layered micro thin film.

Based on Equations (2.52)-(2.55), the hyperbolic two-step heat transport equations in the one-dimensional double-layered micro thin film can be expressed as follows:

$$C_e^{(m)} \frac{\partial T_e^{(m)}}{\partial t} = -\frac{\partial q_e^{(m)}}{\partial x} - G(T_e^{(m)} - T_l^{(m)}) + S^{(m)}, \quad (3.1)$$

$$\tau_e^{(m)} \frac{\partial q_e^{(m)}}{\partial t} + q_e^{(m)} = -k_e^{(m)} \frac{\partial T_e^{(m)}}{\partial x}, \quad (3.2)$$

$$C_l^{(m)} \frac{\partial T_l^{(m)}}{\partial t} = -\frac{\partial q_l^{(m)}}{\partial x} + G(T_e^{(m)} - T_l^{(m)}), \quad (3.3)$$

$$\tau_l^{(m)} \frac{\partial q_l^{(m)}}{\partial t} + q_l^{(m)} = -k_l^{(m)} \frac{\partial T_l^{(m)}}{\partial x}, \quad (3.4)$$

where $C_e^{(m)} = A_e^{(m)} T_e^{(m)}$, $k_e^{(m)} = k_0 \frac{T_e^{(m)}}{T_l^{(m)}}$, $0 \leq x \leq L$ when $m = 1$, and $L \leq x \leq 2L$ when

$m = 2$. For simplicity, we assume that $\tau_e^{(m)}$, $\tau_l^{(m)}$, $k_l^{(m)}$ and $G^{(m)}$ are positive constants.

We assume that the interface is perfectly thermal contact, and hence, the interfacial conditions are, at $x = L$,

$$q_e^{(1)} = q_e^{(2)}, T_e^{(1)} = T_e^{(2)}, \quad (3.5a)$$

$$q_l^{(1)} = q_l^{(2)}, T_l^{(1)} = T_l^{(2)}. \quad (3.5b)$$

The initial and boundary conditions are

$$T_e^{(m)}(x,0) = T_l^{(m)}(x,0) = T_0, q_e^{(m)}(x,0) = q_l^{(m)}(x,0) = 0, \quad (3.6)$$

$$q_e^{(1)}(0,t) = q_e^{(2)}(2L,t) = 0, \quad (3.7a)$$

$$q_l^{(1)}(0,t) = q_l^{(2)}(2L,t) = 0. \quad (3.7b)$$

3.1.3 Energy Estimate

In this section, we seek an energy estimate for the above problem. Assume that $k_e^{(m)}$ and the solutions of Equations (3.1)-(3.7) are smooth, and $T_e^{(m)} \geq T_0$ and $T_l^{(m)} \geq T_0$.

For this purpose, we first introduce the L^p - norm:

$$\|u^{(m)}\|_{L^p} = \left(\int_{I^{(m)}} |u^{(m)}|^p dx \right)^{\frac{1}{p}}, 1 < p < +\infty, \quad (3.8)$$

where $I^{(m)}$ is the interval $[0, L]$ when $m = 1$ and $[L, 2L]$ when $m = 2$, respectively.

Multiplying Equation (3.1) by $T_e^{(m)}$ and Equation (3.3) by $T_l^{(m)}$, integrating them over $I^{(m)}$, and then summing the results over m , we obtain

$$\begin{aligned}
& \sum_{m=1}^2 \int_{\Gamma^{(m)}} \left[A_e^{(m)} (T_e^{(m)})^2 \frac{\partial T_e^{(m)}}{\partial t} + C_l^{(m)} T_l^{(m)} \frac{\partial T_l^{(m)}}{\partial t} \right] dx \\
&= \sum_{m=1}^2 \int_{\Gamma^{(m)}} - \left(\frac{\partial q_e^{(m)}}{\partial x} T_e^{(m)} + \frac{\partial q_l^{(m)}}{\partial x} T_l^{(m)} \right) dx - \sum_{m=1}^2 \int_{\Gamma^{(m)}} G^{(m)} (T_e^{(m)} - T_l^{(m)})^2 dx \\
&+ \sum_{m=1}^2 \int_{\Gamma^{(m)}} S^{(m)} T_e^{(m)} dx. \tag{3.9}
\end{aligned}$$

Using the integration by parts and then applying the interfacial conditions, Equations (3.5a) and (3.5b), the boundary conditions, and Equations (3.7a) and (3.7b), we can obtain

$$\begin{aligned}
& - \sum_{m=1}^2 \int_{\Gamma^{(m)}} \frac{\partial q_e^{(m)}}{\partial x} T_e^{(m)} dx = -T_e^{(1)} q_e^{(1)} \Big|_0^L - T_e^{(2)} q_e^{(2)} \Big|_L^{2L} + \sum_{m=1}^2 \int_{\Gamma^{(m)}} q_e^{(m)} \frac{\partial T_e^{(m)}}{\partial x} dx \\
&= T_e^{(1)}(0,t) q_e^{(1)}(0,t) - T_e^{(1)}(L,t) q_e^{(1)}(L,t) \\
&+ T_e^{(2)}(L,t) q_e^{(2)}(L,t) - T_e^{(2)}(2L,t) q_e^{(2)}(2L,t) \\
&+ \sum_{m=1}^2 \int_{\Gamma^{(m)}} q_e^{(m)} \frac{\partial T_e^{(m)}}{\partial x} dx \\
&= \sum_{m=1}^2 \int_{\Gamma^{(m)}} q_e^{(m)} \frac{\partial T_e^{(m)}}{\partial x} dx \tag{3.10}
\end{aligned}$$

and

$$\begin{aligned}
& - \sum_{m=1}^2 \int_{\Gamma^{(m)}} \frac{\partial q_l^{(m)}}{\partial x} T_l^{(m)} dx = T_l^{(1)}(0,t) q_l^{(1)}(0,t) - T_l^{(1)}(L,t) q_l^{(1)}(L,t) \\
&+ T_l^{(2)}(L,t) q_l^{(2)}(L,t) - T_l^{(2)}(2L,t) q_l^{(2)}(2L,t) \\
&+ \sum_{m=1}^2 \int_{\Gamma^{(m)}} q_l^{(m)} \frac{\partial T_l^{(m)}}{\partial x} dx
\end{aligned}$$

$$= \sum_{m=1}^2 \int_{J^{(m)}} q_l^{(m)} \frac{\partial T_l^{(m)}}{\partial x} dx. \quad (3.11)$$

Further, we have

$$\begin{aligned} \sum_{m=1}^2 \int_{J^{(m)}} A_e^{(m)} (T_e^{(m)})^2 \frac{\partial T_e^{(m)}}{\partial t} dx &= \sum_{m=1}^2 \frac{1}{3} \int_{J^{(m)}} A_e^{(m)} \frac{\partial (T_e^{(m)})^3}{\partial t} dx \\ &= \sum_{m=1}^2 \frac{d}{dt} \int_{J^{(m)}} \frac{1}{3} A_e^{(m)} (T_e^{(m)})^3 dx \\ &= \sum_{m=1}^2 \frac{d}{dt} \left(\frac{1}{3} A_e^{(m)} \|T_e^{(m)}\|_{L^3}^3 \right) \end{aligned} \quad (3.12)$$

and

$$\begin{aligned} \sum_{m=1}^2 \int_{J^{(m)}} C_l^{(m)} T_l^{(m)} \frac{\partial T_l^{(m)}}{\partial t} dx &= \sum_{m=1}^2 \frac{1}{2} \int_{J^{(m)}} C_l^{(m)} \frac{\partial (T_l^{(m)})^2}{\partial t} dx \\ &= \sum_{m=1}^2 \frac{d}{dt} \int_{J^{(m)}} \frac{1}{2} C_l^{(m)} (T_l^{(m)})^2 dx \\ &= \sum_{m=1}^2 \frac{d}{dt} \left(\frac{1}{2} C_l^{(m)} \|T_l^{(m)}\|_{L^2}^2 \right). \end{aligned} \quad (3.13)$$

By Young's inequality with ε (i.e., $ab \leq \varepsilon a^p + (\varepsilon p)^{-\frac{q}{p}} q^{-1} b^q$, $\frac{1}{p} + \frac{1}{q} = 1$, [Evans 1998]),

one may obtain, by choosing $\varepsilon = \frac{1}{3} A_e^{(m)}$, $p = 3$, and $q = \frac{3}{2}$,

$$\begin{aligned} \int_{J^{(m)}} S^{(m)} T_e^{(m)} dx &\leq \frac{1}{3} A_e^{(m)} \int_{J^{(m)}} (T_e^{(m)})^3 dx + \left(\frac{1}{3} A_e^{(m)} 3 \right)^{-\frac{1}{2}} \frac{2}{3} \int_{J^{(m)}} (S^{(m)})^{\frac{3}{2}} dx \\ &= \frac{1}{3} A_e^{(m)} \|T_e^{(m)}\|_{L^3}^3 + \frac{2}{3\sqrt{A_e^{(m)}}} \|S^{(m)}\|_{L^2}^{\frac{3}{2}}. \end{aligned} \quad (3.14)$$

Substituting Equations (3.10)-(3.14) into Equation (3.9) gives

$$\begin{aligned}
& \sum_{m=1}^2 \frac{d}{dt} \left(\frac{1}{3} A_e^{(m)} \|T_e^{(m)}\|_{L^3}^3 \right) + \sum_{m=1}^2 \frac{d}{dt} \left(\frac{1}{2} C_l^{(m)} \|T_l^{(m)}\|_{L^2}^2 \right) \\
& - \sum_{m=1}^2 \int_{J^{(m)}} q_e^{(m)} \frac{\partial T_e^{(m)}}{\partial x} dx - \sum_{m=1}^2 \int_{J^{(m)}} q_l^{(m)} \frac{\partial T_l^{(m)}}{\partial x} dx \\
& + \sum_{m=1}^2 \int_{J^{(m)}} G^{(m)} (T_e^{(m)} - T_l^{(m)})^2 dx \\
& \leq \sum_{m=1}^2 \frac{1}{3} A_e^{(m)} \|T_e^{(m)}\|_{L^3}^3 + \sum_{m=1}^2 \frac{2}{3\sqrt{A_e^{(m)}}} \|S^{(m)}\|_{L^2}^{\frac{3}{2}}. \tag{3.15}
\end{aligned}$$

Integrating Equation (3.15) with respect to t over the time interval $[0, t]$, we can obtain

$$\begin{aligned}
& \sum_{m=1}^2 \left(\frac{1}{3} A_e^{(m)} \|T_e^{(m)}(t)\|_{L^3}^3 \right) + \sum_{m=1}^2 \left(\frac{1}{2} C_l^{(m)} \|T_l^{(m)}(t)\|_{L^2}^2 \right) \\
& - \sum_{m=1}^2 \left(\frac{1}{3} A_e^{(m)} \|T_e^{(m)}(0)\|_{L^3}^3 \right) - \sum_{m=1}^2 \left(\frac{1}{2} C_l^{(m)} \|T_l^{(m)}(0)\|_{L^2}^2 \right) \\
& - \sum_{m=1}^2 \int_{J^{(m)}} \int_0^t q_e^{(m)} \frac{\partial T_e^{(m)}}{\partial x} ds dx - \sum_{m=1}^2 \int_{J^{(m)}} \int_0^t q_l^{(m)} \frac{\partial T_l^{(m)}}{\partial x} ds dx \\
& + \sum_{m=1}^2 \int_{J^{(m)}} \int_0^t G^{(m)} (T_e^{(m)} - T_l^{(m)})^2 ds dx \\
& \leq \sum_{m=1}^2 \int_0^t \frac{1}{3} A_e^{(m)} \|T_e^{(m)}(s)\|_{L^3}^3 ds + \sum_{m=1}^2 \int_0^t \frac{2}{3\sqrt{A_e^{(m)}}} \|S^{(m)}(s)\|_{L^2}^{\frac{3}{2}} ds. \tag{3.16}
\end{aligned}$$

We now claim that the term $-\sum_{m=1}^2 \int_{J^{(m)}} \int_0^t q_e^{(m)} \frac{\partial T_e^{(m)}}{\partial x} ds dx$ is nonnegative in Equation (3.16).

In fact, multiplying Equation (3.2) with $\frac{q_e^{(m)}}{\tau_e^{(m)}}$, we obtain

$$\frac{1}{2} \frac{\partial (q_e^{(m)})^2}{\partial t} + \frac{1}{\tau_e^{(m)}} (q_e^{(m)})^2 = -\frac{1}{\tau_e^{(m)}} k_e^{(m)} \frac{\partial T_e^{(m)}}{\partial x} q_e^{(m)}. \tag{3.17}$$

Solving Equation (3.17) for $(q_e^{(m)})^2$ gives, for any $t \geq 0$,

$$\begin{aligned} 0 &\leq (q_e^{(m)}(x, t))^2 = (q_e^{(m)}(x, t))^2 - (q_e^{(m)}(x, 0))^2 \\ &= -\frac{2}{\tau_e^{(m)}} \exp\left(-\frac{2t}{\tau_e^{(m)}}\right) \int_0^t \exp\left(\frac{2s}{\tau_e^{(m)}}\right) k_e^{(m)} \frac{\partial T_e^{(m)}}{\partial x} q_e^{(m)} ds. \end{aligned} \quad (3.18)$$

If there exists a $t_0 > 0$ such that $\int_0^{t_0} \frac{\partial T_e^{(m)}}{\partial x} q_e^{(m)} ds > 0$, then we have, by the Mean-Value

Theorem for integral (since $k_e^{(m)}$ is smooth),

$$\begin{aligned} \int_0^{t_0} \exp\left(\frac{2s}{\tau_e^{(m)}}\right) k_e^{(m)} \frac{\partial T_e^{(m)}}{\partial x} q_e^{(m)} ds &= \exp\left(\frac{2\xi}{\tau_e^{(m)}}\right) k_e^{(m)}(\xi) \int_0^{t_0} \frac{\partial T_e^{(m)}}{\partial x} q_e^{(m)} ds \\ &> 0, \end{aligned} \quad (3.19)$$

where $0 \leq \xi \leq t_0$. This implies

$$\begin{aligned} (q_e^{(m)}(x, t_0))^2 &= -\frac{2}{\tau_e^{(m)}} \exp\left(-\frac{2t_0}{\tau_e^{(m)}}\right) \int_0^{t_0} \exp\left(\frac{2s}{\tau_e^{(m)}}\right) k_e^{(m)} \frac{\partial T_e^{(m)}}{\partial x} q_e^{(m)} ds \\ &< 0, \end{aligned} \quad (3.20)$$

which is a contradiction with Equation (3.18). Therefore, we can conclude that

$\int_0^t q_e^{(m)} \frac{\partial T_e^{(m)}}{\partial x} ds \leq 0$ and hence

$$-\sum_{m=1}^2 \int_{I^{(m)}} \int_0^t q_e^{(m)} \frac{\partial T_e^{(m)}}{\partial x} ds dx \geq 0. \quad (3.21)$$

We now simplify the term $-\int_{I^{(m)}} \int_0^t q_l^{(m)} \frac{\partial T_l^{(m)}}{\partial x} ds dx$ in Equation (3.16). By Equation (3.4),

we obtain

$$-\int_{I^{(m)}} \int_0^t q_l^{(m)} \frac{\partial T_l^{(m)}}{\partial x} ds dx = \frac{\tau_l^{(m)}}{k_l^{(m)}} \int_{I^{(m)}} \int_0^t q_l^{(m)} \frac{\partial q_l^{(m)}}{\partial t} ds dx + \frac{1}{k_l^{(m)}} \int_{I^{(m)}} \int_0^t (q_l^{(m)})^2 ds dx$$

$$\begin{aligned}
&= \frac{\tau_l^{(m)}}{2k_l^{(m)}} \int_{I^{(m)}_0}^t \int \frac{\partial (q_l^{(m)})^2}{\partial t} ds dx + \frac{1}{k_l^{(m)}} \int_{I^{(m)}_0}^t \int (q_l^{(m)})^2 ds dx \\
&\geq \frac{\tau_l^{(m)}}{2k_l^{(m)}} \left(\|q_l^{(m)}(t)\|_{L^2}^2 - \|q_l^{(m)}(0)\|_{L^2}^2 \right). \tag{3.22}
\end{aligned}$$

As such, Equation (3.16) can be simplified as follows

$$\begin{aligned}
&\sum_{m=1}^2 \frac{1}{3} A_e^{(m)} \|T_e^{(m)}(t)\|_{L^3}^3 + \sum_{m=1}^2 \frac{1}{2} C_l^{(m)} \|T_l^{(m)}(t)\|_{L^2}^2 + \sum_{m=1}^2 \frac{\tau_l^{(m)}}{2k_l^{(m)}} \|q_l^{(m)}(t)\|_{L^2}^2 \\
&- \left(\sum_{m=1}^2 \frac{1}{3} A_e^{(m)} \|T_e^{(m)}(0)\|_{L^3}^3 + \sum_{m=1}^2 \frac{1}{2} C_l^{(m)} \|T_l^{(m)}(0)\|_{L^2}^2 + \sum_{m=1}^2 \frac{\tau_l^{(m)}}{2k_l^{(m)}} \|q_l^{(m)}(0)\|_{L^2}^2 \right) \\
&\leq \sum_{m=1}^2 \int_0^t \frac{1}{3} A_e^{(m)} \|T_e^{(m)}(s)\|_{L^3}^3 ds + \sum_{m=1}^2 \int_0^t \frac{2}{3\sqrt{A_e^{(m)}}} \|S^{(m)}(s)\|_{L^2}^{\frac{3}{2}} ds. \tag{3.23}
\end{aligned}$$

Introducing

$$F(t) = \sum_{m=1}^2 \left[\frac{1}{3} A_e^{(m)} \|T_e^{(m)}(t)\|_{L^3}^3 + \frac{1}{2} C_l^{(m)} \|T_l^{(m)}(t)\|_{L^2}^2 + \frac{\tau_l^{(m)}}{2k_l^{(m)}} \|q_l^{(m)}(t)\|_{L^2}^2 \right] \tag{3.24}$$

and

$$Q(t) = \sum_{m=1}^2 \frac{2}{3\sqrt{A_e^{(m)}}} \|S^{(m)}(t)\|_{L^2}^{\frac{3}{2}}, \tag{3.25}$$

Equation (3.23) can be further simplified to

$$F(t) - F(0) \leq \int_0^t F(s) ds + \int_0^t Q(s) ds. \tag{3.26}$$

By Gronwall's lemma (*i.e.*, if $\phi(t) \geq 0$ and $\psi(t) \geq 0$ are continuous functions such that

$$\phi(t) \leq K + L \int_{t_0}^t \psi(s) \phi(s) ds \text{ holds on } t_0 \leq t \leq t_1, \text{ where } K \text{ and } L \text{ are positive constants,}$$

then $\phi(t) \leq K \exp(L \int_{t_0}^t \psi(s) ds)$ on $t_0 \leq t \leq t_1$, [Atkinson 2005]), we can get for $0 \leq t \leq t_0$,

$$\begin{aligned}
F(t) &\leq \int_0^t 1 \cdot F(s) ds + F(0) + \int_0^t Q(s) ds \\
&\leq \int_0^t 1 \cdot F(s) ds + F(0) + \int_0^t Q(s) ds \\
&\leq e^t \{F(0) + \int_0^t Q(s) ds\}, \tag{3.27}
\end{aligned}$$

and thus we can get the following theorem.

THEOREM 1. Assume that $k_e^{(m)}$, the solutions of Equations (3.1)-(3.7) are smooth, and $T_e^{(m)} \geq T_0$ and $T_l^{(m)} \geq T_0$. Then the solution of Equations (3.1)-(3.7) satisfies an energy estimate as follows

$$\begin{aligned}
&\sum_{m=1}^2 \left[\frac{1}{3} A_e^{(m)} \|T_e^{(m)}(t)\|_{L^3}^3 + \frac{1}{2} C_l^{(m)} \|T_l^{(m)}(t)\|_{L^2}^2 + \frac{\tau_l^{(m)}}{2k_l^{(m)}} \|q_l^{(m)}(t)\|_{L^2}^2 \right] \\
&\leq e^{t_0} \sum_{m=1}^2 \left\{ \frac{1}{3} A_e^{(m)} \|T_e^{(m)}(0)\|_{L^3}^3 + \frac{1}{2} C_l^{(m)} \|T_l^{(m)}(0)\|_{L^2}^2 + \frac{\tau_l^{(m)}}{2k_l^{(m)}} \|q_l^{(m)}(0)\|_{L^2}^2 \right. \\
&\quad \left. + \int_0^t \frac{2}{3\sqrt{A_e^{(m)}}} \|S^{(m)}(s)\|_{L^2}^{\frac{3}{2}} ds \right\} \\
&\leq e^{t_0} \sum_{m=1}^3 \left\{ \frac{1}{3} A_e^{(m)} \|T_e^{(m)}(0)\|_{L^3}^3 + \frac{1}{2} C_l^{(m)} \|T_l^{(m)}(0)\|_{L^2}^2 + \frac{\tau_l^{(m)}}{2k_l^{(m)}} \|q_l^{(m)}(0)\|_{L^2}^2 \right\} \\
&\quad + \int_0^{t_0} \frac{2}{3\sqrt{A_e^{(m)}}} \|S^{(m)}(s)\|_{L^2}^{\frac{3}{2}} ds + \frac{\tau_e^{(m)}}{2} \int_0^{t_0} (\|q_e^{(m)}(s)\|_{L^2}^2 + \left\| \frac{q_e^{(m)}(t)}{k_e^{(m)}} \right\|_{L^2}^2) ds, \tag{3.28}
\end{aligned}$$

for $0 \leq t \leq t_0$.

3.2 Finite Difference Scheme

3.2.1 Notations

We denote $(T_e^{(m)})_j^n, (T_l^{(m)})_j^n, (q_e^{(m)})_j^n$, and $(q_l^{(m)})_j^n$ as the numerical approximation of $(T_e^{(m)})(j\Delta x, n\Delta t), (T_l^{(m)})(j\Delta x, n\Delta t), (q_e^{(m)})(j\Delta x, n\Delta t)$ and $(q_l^{(m)})(j\Delta x, n\Delta t)$, respectively, where Δx and Δt are the x directional spatial and temporal mesh sizes, respectively, and $1 \leq j \leq N$ so that $(N+1)\Delta x = L$. We further introduce the inner products and l^p - norms for mesh functions u_j and v_j as follows

$$(u, v) = \Delta x \sum_{j=1}^N u_j v_j, \quad (3.29)$$

$$(u, v)_1 = \Delta x \sum_{j=2}^N u_j v_j, \quad (3.30)$$

$$\|u\|_{l^p} = \left(\Delta x \sum_{j=1}^N |u_j|^p \right)^{\frac{1}{p}}, \quad (3.31)$$

and

$$\|u\|_{1l^p} = \left(\Delta x \sum_{j=2}^N |u_j|^p \right)^{\frac{1}{p}}. \quad (3.32)$$

The first-order forward and backward finite difference operators are defined as follows

$$\nabla_x u_j = \frac{u_{j+1} - u_j}{\Delta x}, \quad (3.33)$$

$$\nabla_{\bar{x}} u_j = \frac{u_j - u_{j-1}}{\Delta x}. \quad (3.34)$$

3.2.2 Finite Difference Scheme

We now develop a finite difference scheme, satisfying a discrete analogue of Equation (3.28). To this end, we design a staggered grid, as shown in Figure 3.2.

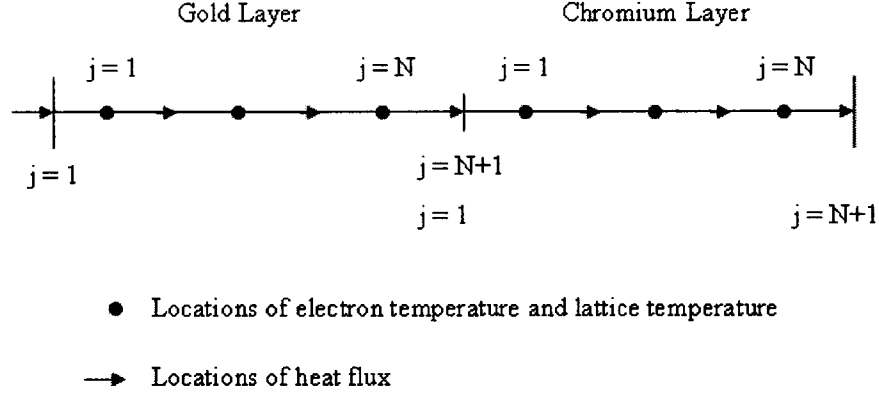


Figure 3.2 A staggered grid for 1D double-layered thin film.

Based on the continuous energy estimate Equation (3.28), we develop a finite difference scheme for solving Equations (3.1)-(3.7) as

$$\begin{aligned}
 A_e^{(m)} \frac{|(T_e^{(m)})_j^{n+1}|^3 - |(T_e^{(m)})_j^n|^3}{3\Delta t} &= -\nabla_x \frac{(q_e^{(m)})_j^{n+1} + (q_e^{(m)})_j^n}{2} \\
 &- G^{(m)} \left[\frac{(T_e^{(m)})_j^{n+1} + (T_e^{(m)})_j^n}{2} - \frac{(T_l^{(m)})_j^{n+1} + (T_l^{(m)})_j^n}{2} \right] \\
 &+ (S^{(m)})_j^{n+\frac{1}{2}}, \quad j = 1, \dots, N,
 \end{aligned} \tag{3.35}$$

$$\begin{aligned}
 \tau_e^{(m)} \frac{(q_e^{(m)})_j^{n+1} - (q_e^{(m)})_j^n}{\Delta t} + \frac{1}{2} [(q_e^{(m)})_j^{n+1} + (q_e^{(m)})_j^n] &= -(k_e^{(m)})_{j-\frac{1}{2}}^{n+\frac{1}{2}} \cdot \nabla_{\bar{x}} \frac{(T_e^{(m)})_j^{n+1} + (T_e^{(m)})_j^n}{2}, \\
 &j = 2, \dots, N,
 \end{aligned} \tag{3.36}$$

$$C_l^{(m)} \frac{(T_l^{(m)})_j^{n+1} - (T_l^{(m)})_j^n}{\Delta t} = G^{(m)} \left[\frac{(T_e^{(m)})_j^{n+1} + (T_e^{(m)})_j^n}{2} - \frac{(T_l^{(m)})_j^{n+1} + (T_l^{(m)})_j^n}{2} \right]$$

$$-\nabla_x \frac{(q_l^{(m)})_j^{n+1} + (q_l^{(m)})_j^n}{2}, \quad j = 1, \dots, N, \quad (3.37)$$

$$\tau_l^{(m)} \frac{(q_l^{(m)})_j^{n+1} - (q_l^{(m)})_j^n}{\Delta t} + \frac{1}{2} [(q_l^{(m)})_j^{n+1} + (q_l^{(m)})_j^n] = -k_l^{(m)} \cdot \nabla_{\bar{x}} \frac{(T_l^{(m)})_j^{n+1} + (T_l^{(m)})_j^n}{2},$$

$$j = 2, \dots, N, \quad (3.38)$$

where $m = 1, 2$, and

$$(k_e^{(m)})_{j-\frac{1}{2}}^{n+\frac{1}{2}} = \frac{1}{2} k_0 \left| \frac{(T_e^{(m)})_j^{n+1} + (T_e^{(m)})_j^n}{(T_l^{(m)})_j^{n+1} + (T_l^{(m)})_j^n} \right| + \frac{1}{2} k_0 \left| \frac{(T_e^{(m)})_{j-1}^{n+1} + (T_e^{(m)})_{j-1}^n}{(T_l^{(m)})_{j-1}^{n+1} + (T_l^{(m)})_{j-1}^n} \right|. \quad (3.39)$$

The interfacial equations are discretized as follows:

$$(q_e^{(1)})_{N+1}^n = (q_e^{(2)})_1^n, \quad (3.40a)$$

$$(q_l^{(1)})_{N+1}^n = (q_l^{(2)})_1^n, \quad (3.40b)$$

$$(T_e^{(1)})_N^n = (T_e^{(2)})_1^n, \quad (3.40c)$$

$$(T_l^{(1)})_N^n = (T_l^{(2)})_1^n, \quad (3.40d)$$

for any time level n , while the initial and boundary conditions are

$$(T_e^{(m)})_j^0 = (T_l^{(m)})_j^0 = T_0, (q_e^{(m)})_j^0 = (q_l^{(m)})_j^0 = 0, \quad (3.41a)$$

$$(q_e^{(1)})_1^n = (q_l^{(1)})_1^n = 0, \quad (3.41b)$$

$$(q_e^{(2)})_{N+1}^n = (q_l^{(2)})_{N+1}^n = 0, \quad (3.41c)$$

for any time level n .

3.2.3 Energy Estimate

The truncation error for Equations (3.35)-(3.41) is $O(\Delta x^2 + \Delta t^2)$. In order to get an energy estimate which is an analogue to Equation (3.28), we multiply Equation (3.35)

by $\Delta x \frac{(T_e^{(m)})_j^{n+1} + (T_e^{(m)})_j^n}{2}$ and Equation (3.37) by $\Delta x \frac{(T_l^{(m)})_j^{n+1} + (T_l^{(m)})_j^n}{2}$; make a summation of j over $1 \leq j \leq N$ and m over 1 and 2, then add the results together. The result is

$$\begin{aligned}
& \frac{1}{\Delta t} \sum_{m=1}^2 \frac{1}{3} A_e^{(m)} \left[\|(T_e^{(m)})^{n+1}\|_{l^3}^3 - \|(T_e^{(m)})^n\|_{l^3}^3 \right] \\
& + \frac{1}{\Delta t} \sum_{m=1}^2 \frac{1}{2} C_l^{(m)} \left[\|(T_l^{(m)})^{n+1}\|_{l^2}^2 - \|(T_l^{(m)})^n\|_{l^2}^2 \right] \\
& + \Delta x \sum_{m=1}^2 G^{(m)} \sum_{j=1}^N \left[\frac{(T_e^{(m)})_j^{n+1} + (T_e^{(m)})_j^n}{2} - \frac{(T_l^{(m)})_j^{n+1} + (T_l^{(m)})_j^n}{2} \right]^2 \\
& = -\Delta x \sum_{m=1}^2 \sum_{j=1}^N \nabla_x \frac{(q_e^{(m)})_j^{n+1} + (q_e^{(m)})_j^n}{2} \cdot \frac{(T_e^{(m)})_j^{n+1} + (T_e^{(m)})_j^n}{2} \\
& - \Delta x \sum_{m=1}^2 \sum_{j=1}^N \nabla_x \frac{(q_l^{(m)})_j^{n+1} + (q_l^{(m)})_j^n}{2} \cdot \frac{(T_l^{(m)})_j^{n+1} + (T_l^{(m)})_j^n}{2} \\
& + \sum_{m=1}^2 \left((S^{(m)})^{n+\frac{1}{2}}, \frac{(T_e^{(m)})^{n+1} + (T_e^{(m)})^n}{2} \right). \tag{3.42}
\end{aligned}$$

Applying the summation by parts and then using Equation (3.36), Equations (3.40a)-(3.40d) and Equations (3.41a)-(3.41c), we can simplify the first term on the right-hand-side (RHS) of Equation (3.42) as follows

$$\begin{aligned}
\text{First Term} & = -\Delta x \sum_{m=1}^2 \sum_{j=1}^N \frac{(q_e^{(m)})_{j+1}^{n+1} + (q_e^{(m)})_{j+1}^n}{2\Delta x} \cdot \frac{(T_e^{(m)})_{j+1}^{n+1} + (T_e^{(m)})_{j+1}^n}{2} \\
& + \Delta x \sum_{m=1}^2 \sum_{j=1}^N \frac{(q_e^{(m)})_j^{n+1} + (q_e^{(m)})_j^n}{2\Delta x} \cdot \frac{(T_e^{(m)})_j^{n+1} + (T_e^{(m)})_j^n}{2} \\
& = -\Delta x \sum_{m=1}^2 \sum_{j=2}^{N+1} \frac{(q_e^{(m)})_j^{n+1} + (q_e^{(m)})_j^n}{2\Delta x} \cdot \frac{(T_e^{(m)})_{j-1}^{n+1} + (T_e^{(m)})_{j-1}^n}{2}
\end{aligned}$$

$$\begin{aligned}
& + \Delta x \sum_{m=1}^2 \sum_{j=2}^{N+1} \frac{(q_e^{(m)})_j^{n+1} + (q_e^{(m)})_j^n}{2\Delta x} \cdot \frac{(T_e^{(m)})_j^{n+1} + (T_e^{(m)})_j^n}{2} \\
& = \Delta x \sum_{m=1}^2 \sum_{j=2}^{N+1} \frac{(q_e^{(m)})_j^{n+1} + (q_e^{(m)})_j^n}{2\Delta x} \cdot \nabla_{\bar{x}} \frac{(T_e^{(m)})_j^{n+1} + (T_e^{(m)})_j^n}{2} \\
& \quad + \sum_{m=1}^2 \frac{(q_e^{(m)})_1^{n+1} + (q_e^{(m)})_1^n}{2} \cdot \frac{(T_e^{(m)})_1^{n+1} + (T_e^{(m)})_1^n}{2} \\
& \quad - \sum_{m=1}^2 \frac{(q_e^{(m)})_{N+1}^{n+1} + (q_e^{(m)})_{N+1}^n}{2} \cdot \frac{(T_e^{(m)})_N^{n+1} + (T_e^{(m)})_N^n}{2} \\
& = \Delta x \sum_{m=1}^2 \sum_{j=2}^N \frac{(q_e^{(m)})_j^{n+1} + (q_e^{(m)})_j^n}{2\Delta x} \cdot \nabla_{\bar{x}} \frac{(T_e^{(m)})_j^{n+1} + (T_e^{(m)})_j^n}{2} \\
& = -\Delta x \sum_{m=1}^2 \sum_{j=2}^N \frac{(q_e^{(m)})_j^{n+1} + (q_e^{(m)})_j^n}{2\Delta x} \cdot \frac{\tau_e^{(m)} \frac{(q_e^{(m)})_j^{n+1} - (q_e^{(m)})_j^n}{\Delta t} + \frac{1}{2} ((q_e^{(m)})_j^{n+1} + (q_e^{(m)})_j^n)}{(k_e^{(m)})_{j-\frac{1}{2}}^{n+\frac{1}{2}}} \\
& = -\Delta x \sum_{m=1}^2 \sum_{j=2}^N \frac{\tau_e^{(m)} [((q_e^{(m)})_j^{n+1})^2 + ((q_e^{(m)})_j^n)^2]}{2\Delta t \cdot (k_e^{(m)})_{j-\frac{1}{2}}^{n+\frac{1}{2}}} \\
& \quad - \Delta x \sum_{m=1}^2 \sum_{j=2}^N \frac{[(q_e^{(m)})_j^{n+1} + (q_e^{(m)})_j^n]^2}{4 \cdot (k_e^{(m)})_{j-\frac{1}{2}}^{n+\frac{1}{2}}}. \tag{3.43}
\end{aligned}$$

Similarly, we can simplify the second term on the RHS of Equation (3.42) as

$$\begin{aligned}
\text{Second Term} & = -\Delta x \sum_{m=1}^2 \sum_{j=2}^N \frac{\tau_l^{(m)} [((q_e^{(m)})_j^{n+1})^2 - ((q_e^{(m)})_j^n)^2]}{2\Delta t \cdot k_l^{(m)}} \\
& \quad - \Delta x \sum_{m=1}^2 \sum_{j=2}^N \frac{[(q_e^{(m)})_j^{n+1} - (q_e^{(m)})_j^n]^2}{4 \cdot k_l^{(m)}}. \tag{3.44}
\end{aligned}$$

Besides, by Young's inequality with ε , we have

$$\begin{aligned}
& \sum_{m=1}^2 \left((S^{(m)})^{n+\frac{1}{2}}, \frac{(T_e^{(m)})^{n+1} + (T_e^{(m)})^n}{2} \right) \\
& \leq \frac{1}{2} \sum_{m=1}^2 \left[\left\| \left((S^{(m)})^{n+\frac{1}{2}}, (T_e^{(m)})^{n+1} \right) \right\| + \left\| \left((S^{(m)})^{n+\frac{1}{2}}, (T_e^{(m)})^n \right) \right\| \right] \\
& \leq \frac{1}{2} \sum_{m=1}^2 \left[\frac{1}{3} A_e^{(m)} \|(T_e^{(m)})^{n+1}\|_{l^3}^3 + \frac{2}{3\sqrt{A_e^{(m)}}} \left\| (S^{(m)})^{n+\frac{1}{2}} \right\|_{l^{\frac{3}{2}}}^3 \right] \\
& \quad + \frac{1}{2} \sum_{m=1}^2 \left[\frac{1}{3} A_e^{(m)} \|(T_e^{(m)})^n\|_{l^3}^3 + \frac{2}{3\sqrt{A_e^{(m)}}} \left\| (S^{(m)})^{n+\frac{1}{2}} \right\|_{l^{\frac{3}{2}}}^3 \right] \\
& \leq \frac{1}{2} \sum_{m=1}^2 \left[\frac{1}{3} A_e^{(m)} \|(T_e^{(m)})^{n+1}\|_{l^3}^3 + \frac{1}{3} A_e^{(m)} \|(T_e^{(m)})^n\|_{l^3}^3 \right] \\
& \quad + \sum_{m=1}^2 \frac{2}{3\sqrt{A_e^{(m)}}} \left\| (S^{(m)})^{n+\frac{1}{2}} \right\|_{l^{\frac{3}{2}}}^3. \tag{3.45}
\end{aligned}$$

Substituting Equations (3.43)-(3.45) into Equation (3.42) gives

$$\begin{aligned}
& \frac{1}{\Delta t} \sum_{m=1}^2 \frac{1}{3} A_e^{(m)} \left[\|(T_e^{(m)})^{n+1}\|_{l^3}^3 - \|(T_e^{(m)})^n\|_{l^3}^3 \right] \\
& + \frac{1}{\Delta t} \sum_{m=1}^2 \frac{1}{2} C_l^{(m)} \left[\|(T_l^{(m)})^{n+1}\|_{l^2}^2 - \|(T_l^{(m)})^n\|_{l^2}^2 \right] \\
& + \Delta x \sum_{m=1}^2 G^{(m)} \sum_{j=1}^N \left[\frac{(T_e^{(m)})_j^{n+1} + (T_e^{(m)})_j^n}{2} - \frac{(T_l^{(m)})_j^{n+1} + (T_l^{(m)})_j^n}{2} \right]^2 \\
& + \Delta x \sum_{m=1}^2 \sum_{j=2}^N \frac{\tau_e^{(m)} [((q_e^{(m)})_j^{n+1})^2 + ((q_e^{(m)})_j^n)^2]}{2\Delta t \cdot (k_e^{(m)})_{j-\frac{1}{2}}^{n+\frac{1}{2}}} + \Delta x \sum_{m=1}^2 \sum_{j=2}^N \frac{[(q_e^{(m)})_j^{n+1} + (q_e^{(m)})_j^n]^2}{4 \cdot (k_e^{(m)})_{j-\frac{1}{2}}^{n+\frac{1}{2}}}
\end{aligned}$$

$$\begin{aligned}
& + \Delta x \sum_{m=1}^2 \sum_{j=2}^N \frac{\tau_l^{(m)} [((q_e^{(m)})_j^{n+1})^2 - ((q_e^{(m)})_j^n)^2]}{2\Delta t \cdot k_l^{(m)}} + \Delta x \sum_{m=1}^2 \sum_{j=2}^N \frac{[(q_e^{(m)})_j^{n+1} - (q_e^{(m)})_j^n]^2}{4 \cdot k_l^{(m)}} \\
& \leq \frac{1}{2} \sum_{m=1}^2 \left[\frac{1}{3} A_e^{(m)} \|(T_e^{(m)})^{n+1}\|_{l^3}^3 + \frac{1}{3} A_e^{(m)} \|(T_e^{(m)})^n\|_{l^3}^3 \right] \\
& \quad + \sum_{m=1}^2 \frac{2}{3\sqrt{A_e^{(m)}}} \left\| (S^{(m)})^{n+\frac{1}{2}} \right\|_{l^{\frac{3}{2}}}^{\frac{3}{2}}. \tag{3.46}
\end{aligned}$$

Since the third, fifth, and seventh terms on the left-hand-side (LHS) of Equation (3.46) are all nonnegative, we just eliminate them from Equation (3.46) and simplify it as follows

$$\begin{aligned}
& \sum_{m=1}^2 \frac{1}{3} A_e^{(m)} \left[\|(T_e^{(m)})^{n+1}\|_{l^3}^3 - \|(T_e^{(m)})^n\|_{l^3}^3 \right] + \sum_{m=1}^2 \frac{1}{2} C_l^{(m)} \left[\|(T_l^{(m)})^{n+1}\|_{l^2}^2 - \|(T_l^{(m)})^n\|_{l^2}^2 \right] \\
& + \Delta x \sum_{m=1}^2 \sum_{j=2}^N \tau_e^{(m)} \left[\frac{((q_e^{(m)})_j^{n+1})^2 - ((q_e^{(m)})_j^n)^2}{2 \cdot (k_e^{(m)})_{j-\frac{1}{2}}^{n+\frac{1}{2}}} \right] + \Delta x \sum_{m=1}^2 \sum_{j=2}^N \tau_l^{(m)} \left[\frac{((q_l^{(m)})_j^{n+1})^2 - ((q_l^{(m)})_j^n)^2}{2 \cdot k_l^{(m)}} \right] \\
& \leq \frac{\Delta t}{2} \sum_{m=1}^2 \left[\frac{1}{3} A_e^{(m)} \|(T_e^{(m)})^{n+1}\|_{l^3}^3 + \frac{1}{3} A_e^{(m)} \|(T_e^{(m)})^n\|_{l^3}^3 \right] + \Delta t \sum_{m=1}^2 \frac{2}{3\sqrt{A_e^{(m)}}} \left\| (S^{(m)})^{n+\frac{1}{2}} \right\|_{l^{\frac{3}{2}}}^{\frac{3}{2}}. \tag{3.47}
\end{aligned}$$

Since the term $\Delta x \sum_{m=1}^2 \sum_{j=2}^N \tau_e^{(m)} \frac{((q_e^{(m)})_j^{n+1})^2}{2(k_e^{(m)})_{j-\frac{1}{2}}^{n+\frac{1}{2}}}$ is positive, it can be dropped from the LHS of

Equation (3.47). The term $-\Delta x \sum_{m=1}^2 \sum_{j=2}^N \tau_e^{(m)} \frac{((q_e^{(m)})_j^n)^2}{2(k_e^{(m)})_{j-\frac{1}{2}}^{n+\frac{1}{2}}}$ may be moved to the RHS and then

bounded by using the Cauchy-Schwarz inequality to obtain

$$\Delta x \sum_{m=1}^2 \sum_{j=2}^N \tau_e^{(m)} \frac{((q_e^{(m)})_j)^2}{2(k_e^{(m)})^{n+\frac{1}{2}} j^{-\frac{1}{2}}} \leq \sum_{m=1}^2 \frac{\tau_e^{(m)}}{2} \left[\|(q_e^{(m)})^n\|_{l^2}^2 + \left\| \frac{(q_e^{(m)})^n}{(k_e^{(m)})^{n+\frac{1}{2}}} \right\|_{l^2}^2 \right]. \quad (3.48)$$

Now we denote

$$\begin{aligned} \tilde{F}(n) &= \sum_{m=1}^2 \frac{1}{3} A_e^{(m)} \|(T_e^{(m)})^n\|_{l^3}^3 + \sum_{m=1}^2 \frac{1}{2} C_l^{(m)} \|(T_l^{(m)})^n\|_{l^2}^2 \\ &\quad + \sum_{m=1}^2 \frac{\tau_l^{(m)}}{k_l^{(m)}} \|(q_l^{(m)})^n\|_{l^2}^2 \end{aligned} \quad (3.49)$$

and

$$\tilde{Q}(n) = \sum_{m=1}^2 \frac{2}{3\sqrt{A_e^{(m)}}} \left\| (S^{(m)})^{n+\frac{1}{2}} \right\|_{l^2}^{\frac{3}{2}} + \sum_{m=1}^2 \frac{\tau_e^{(m)}}{2} \|(q_e^{(m)})^{n-1}\|_{l^2}^2 + \sum_{m=1}^2 \frac{\tau_e^{(m)}}{2} \left\| \frac{(q_e^{(m)})^{n-1}}{(k_e^{(m)})^{n-\frac{1}{2}}} \right\|_{l^2}^2, \quad (3.50)$$

then Equation (3.47) can be further simplified as

$$\left(1 - \frac{\Delta t}{2}\right) \tilde{F}(n+1) \leq \left(1 + \frac{\Delta t}{2}\right) \tilde{F}(n) + \Delta t \tilde{Q}(n+1). \quad (3.51)$$

Here, from Equation (3.51), we have

$$\begin{aligned} \tilde{F}(n) &\leq \frac{1 + \frac{\Delta t}{2}}{1 - \frac{\Delta t}{2}} \tilde{F}(n-1) + \frac{\Delta t}{1 - \frac{\Delta t}{2}} \tilde{Q}(n) \\ &\leq \frac{1 + \frac{\Delta t}{2}}{1 - \frac{\Delta t}{2}} \left[\frac{1 + \frac{\Delta t}{2}}{1 - \frac{\Delta t}{2}} \tilde{F}(n-2) + \frac{\Delta t}{1 - \frac{\Delta t}{2}} \tilde{Q}(n-1) \right] + \frac{\Delta t}{1 - \frac{\Delta t}{2}} \tilde{Q}(n) \\ &\leq \dots \\ &\leq \left(\frac{1 + \frac{\Delta t}{2}}{1 - \frac{\Delta t}{2}} \right)^n \tilde{F}(0) \end{aligned}$$

$$\begin{aligned}
& + \frac{\Delta t}{1 - \frac{\Delta t}{2}} \left[1 + \left(\frac{1 + \frac{\Delta t}{2}}{1 - \frac{\Delta t}{2}} \right) + \left(\frac{1 + \frac{\Delta t}{2}}{1 - \frac{\Delta t}{2}} \right)^2 + \dots + \left(\frac{1 + \frac{\Delta t}{2}}{1 - \frac{\Delta t}{2}} \right)^{n-1} \right] \max_{0 \leq k \leq n} \tilde{Q}(k) \\
& = \left(\frac{1 + \frac{\Delta t}{2}}{1 - \frac{\Delta t}{2}} \right)^n \tilde{F}(0) + \frac{\Delta t}{1 - \frac{\Delta t}{2}} \left[\frac{1 - \left(\frac{1 + \frac{\Delta t}{2}}{1 - \frac{\Delta t}{2}} \right)^n}{1 - \left(\frac{1 + \frac{\Delta t}{2}}{1 - \frac{\Delta t}{2}} \right)} \right] \max_{0 \leq k \leq n} \tilde{Q}(k) \\
& = \left(\frac{1 + \frac{\Delta t}{2}}{1 - \frac{\Delta t}{2}} \right)^n \tilde{F}(0) - \left[1 - \left(\frac{1 + \frac{\Delta t}{2}}{1 - \frac{\Delta t}{2}} \right)^n \right] \max_{0 \leq k \leq n} \tilde{Q}(k) \\
& \leq \left(\frac{1 + \frac{\Delta t}{2}}{1 - \frac{\Delta t}{2}} \right)^n \left[\tilde{F}(0) + \frac{2}{c+1} \max_{0 \leq k \leq n} \tilde{Q}(k) \right]. \tag{3.52}
\end{aligned}$$

By applying the inequalities $(1 + \varepsilon)^n \leq e^{n\varepsilon}$ for $\varepsilon > 0$, and $(1 - \varepsilon)^{-1} \leq e^{2\varepsilon}$ when $0 < \varepsilon \leq \frac{1}{2}$,

we obtain for sufficiently small Δt ,

$$\begin{aligned}
\tilde{F}(n) & \leq e^{\frac{n c \Delta t}{2}} \cdot e^{n \Delta t} \left[\tilde{F}(0) + \max_{0 \leq k \leq n} \tilde{Q}(k) \right] \\
& \leq e^{\frac{3n \Delta t}{2}} \left[\tilde{F}(0) + \max_{0 \leq k \leq n} \tilde{Q}(k) \right]. \tag{3.53}
\end{aligned}$$

Therefore, we get the following theorem.

THEOREM 2. When Δt is sufficiently small, the solutions of the scheme Equations (3.1)-(3.7) satisfies

$$\begin{aligned}
& \sum_{m=1}^2 \frac{1}{3} A_e^{(m)} \|(T_e^{(m)})^n\|_{l^3}^3 + \sum_{m=1}^2 \frac{1}{2} C_l^{(m)} \|(T_l^{(m)})^n\|_{l^2}^2 + \sum_{m=1}^2 \frac{\tau_l^{(m)}}{k_l^{(m)}} \|(q_l^{(m)})^n\|_{l^2}^2 \\
& \leq e^{\frac{3}{2}t_0} \cdot \left\{ \sum_{m=1}^2 \frac{1}{3} A_e^{(m)} \|(T_e^{(m)})^0\|_{l^3}^3 + \sum_{m=1}^2 \frac{1}{2} C_l^{(m)} \|(T_l^{(m)})^0\|_{l^2}^2 + \sum_{m=1}^2 \frac{\tau_l^{(m)}}{k_l^{(m)}} \|(q_l^{(m)})^0\|_{l^2}^2 \right. \\
& \quad \left. + \max_{0 \leq k \leq n} \sum_{m=1}^2 \left[\frac{2}{3\sqrt{A_e^{(m)}}} \left\| (S^{(m)})^{k-\frac{1}{2}} \right\|_{l^3}^{\frac{3}{2}} + \frac{\tau_e^{(m)}}{2} \|(q_e^{(m)})^{k-1}\|_{l^2}^2 + \frac{\tau_e^{(m)}}{2} \left\| \frac{(q_e^{(m)})^{k-1}}{(k_e^{(m)})^{k-\frac{1}{2}}} \right\|_{l^2}^2 \right] \right\}, \quad (3.54)
\end{aligned}$$

for any n with $0 \leq n\Delta t \leq t_0$. Here, we assume $(k_e^{(m)})_j^{-\frac{1}{2}}$ to be $k_0^{(m)}$.

Equation (3.54) can be considered as a discrete analogue of Equation (3.28).

3.2.4 Algorithm

Since the finite difference scheme (see Equations (3.35)-(3.41)) is nonlinear, it must be solved by an iterative method. Here, we develop an iterative method as follows:

$$\begin{aligned}
& A_e^{(m)} \frac{[(T_e^{(m)})_j^{n+1(i)}]^2 + (T_e^{(m)})_j^{n+1(i)} \cdot (T_e^{(m)})_j^n + [(T_e^{(m)})_j^n]^2}{\frac{3}{2}[(T_e^{(m)})_j^{n+1(i)} + (T_e^{(m)})_j^n]} \cdot \frac{(T_e^{(m)})_j^{n+1(i+1)} - (T_e^{(m)})_j^n}{\Delta t} \\
& = -\nabla_x \frac{(q_e^{(m)})_j^{n+1(i+1)} + (q_e^{(m)})_j^n}{2} \\
& \quad - G^{(m)} \left[\frac{(T_e^{(m)})_j^{n+1(i+1)} + (T_e^{(m)})_j^n}{2} - \frac{(T_l^{(m)})_j^{n+1(i)} + (T_l^{(m)})_j^n}{2} \right] + (S^{(m)})_j^{n+\frac{1}{2}}, \quad (3.55)
\end{aligned}$$

$$\begin{aligned}
& \tau_e^{(m)} \frac{(q_e^{(m)})_j^{n+1(i+1)} - (q_e^{(m)})_j^n}{\Delta t} + \frac{1}{2} [(q_e^{(m)})_j^{n+1(i+1)} + (q_e^{(m)})_j^n] \\
& = -(k_e^{(m)})_j^{n+\frac{1}{2}(i)} \cdot \nabla_x \frac{(T_e^{(m)})_j^{n+1(i+1)} + (T_e^{(m)})_j^n}{2}, \quad (3.56)
\end{aligned}$$

$$C_l^{(m)} \frac{(T_l^{(m)})_j^{n+1(i+1)} - (T_l^{(m)})_j^n}{\Delta t} = G^{(m)} \left[\frac{(T_e^{(m)})_j^{n+1(i+1)} + (T_e^{(m)})_j^n}{2} - \frac{(T_l^{(m)})_j^{n+1(i+1)} + (T_l^{(m)})_j^n}{2} \right] - \nabla_x \frac{(q_l^{(m)})_j^{n+1(i+1)} + (q_l^{(m)})_j^n}{2}, \quad (3.57)$$

$$\begin{aligned} \tau_l^{(m)} \frac{(q_l^{(m)})_j^{n+1(i+1)} - (q_l^{(m)})_j^n}{\Delta t} + \frac{1}{2} [(q_l^{(m)})_j^{n+1(i+1)} + (q_l^{(m)})_j^n] \\ = -k_l^{(m)} \cdot \nabla_{\bar{x}} \frac{(T_l^{(m)})_j^{n+1(i+1)} + (T_l^{(m)})_j^n}{2}, \end{aligned} \quad (3.58)$$

where $m = 1, 2$ and

$$(k_e^{(m)})_{j-\frac{1}{2}}^{n+\frac{1}{2}(i)} = \frac{1}{2} k_0 \left| \frac{(T_e^{(m)})_j^{n+1(i)} + (T_e^{(m)})_j^n}{(T_l^{(m)})_j^{n+1(i)} + (T_l^{(m)})_j^n} \right| + \frac{1}{2} k_0 \left| \frac{(T_e^{(m)})_{j-1}^{n+1(i)} + (T_e^{(m)})_{j-1}^n}{(T_l^{(m)})_{j-1}^{n+1(i)} + (T_l^{(m)})_{j-1}^n} \right|. \quad (3.59)$$

Here, j is $1 \leq j \leq N$ in (3.56) and (3.58) and $2 \leq j \leq N$ in (3.55) and (3.57).

The interfacial equations are discretized as follows:

$$\frac{(q_e^{(1)})_{N+1}^n + (q_e^{(1)})_{N+1}^{n+1(i+1)}}{2} = \frac{(q_e^{(2)})_1^n + (q_e^{(2)})_1^{n+1(i+1)}}{2}, \quad (3.60a)$$

$$\frac{(q_l^{(1)})_{N+1}^n + (q_l^{(1)})_{N+1}^{n+1(i+1)}}{2} = \frac{(q_l^{(2)})_1^n + (q_l^{(2)})_1^{n+1(i+1)}}{2}, \quad (3.60b)$$

$$\frac{(T_e^{(1)})_N^n + (T_e^{(1)})_N^{n+1(i+1)}}{2} = \frac{(T_e^{(2)})_1^n + (T_e^{(2)})_1^{n+1(i+1)}}{2}, \quad (3.60c)$$

$$\frac{(T_l^{(1)})_N^n + (T_l^{(1)})_N^{n+1(i+1)}}{2} = \frac{(T_l^{(2)})_1^n + (T_l^{(2)})_1^{n+1(i+1)}}{2}, \quad (3.60d)$$

for any time level n , $i = 0, 1, 2, \dots$, and $(T_e^{(m)})_j^{n+1(0)} = (T_e^{(m)})_j^n$, and $(T_l^{(m)})_j^{n+1(0)} = (T_l^{(m)})_j^n$.

The initial and boundary conditions are

$$(T_e^{(m)})_j^0 = (T_l^{(m)})_j^0 = T_0 (= 300K), \quad (3.61a)$$

$$(q_e^{(m)})_j^0 = (q_l^{(m)})_j^0 = 0, \quad (3.61b)$$

$$(q_e^{(1)})_1^n = (q_e^{(2)})_{N+1}^n = 0, \quad (3.61c)$$

$$(q_l^{(1)})_1^n = (q_l^{(2)})_{N+1}^n = 0, \quad (3.61d)$$

for any time level n .

Hence, the algorithm for computing $T_e^{(m)}, q_e^{(m)}, T_l^{(m)}, q_l^{(m)}, m = 1, 2$, can be written as follows:

Step 1: Solve for $(q_e^{(m)})_j^{n+1(i+1)}$ from Equation (3.56), and substitute it into Equation (3.55) to obtain an equation with only one unknown variable $(T_e^{(m)})_j^{n+1(i+1)}$.

Step 2: Set a tridiagonal linear system for $(T_e^{(m)})_j^{n+1(i+1)}$ from the obtained equation in Step 1 with the interfacial condition Equation (3.60a), (3.60c), and boundary condition Equation (3.61c), and then solve for $(T_e^{(m)})_j^{n+1(i+1)}$. Once $(T_e^{(m)})_j^{n+1(i+1)}$ is calculated, $(q_e^{(m)})_j^{n+1(i+1)}$ is then obtained from Equation (3.56).

Step 3: Check if $\max_{1 \leq j \leq N} |(T_e^{(m)})_j^{n+1(i+1)} - (T_e^{(m)})_j^n| < \varepsilon$. If yes, $(T_e^{(m)})_j^{n+1(i+1)}$ is then saved as $(T_e^{(m)})_j^{n+1}$ and $(q_e^{(m)})_j^{n+1(i+1)}$ as $(q_e^{(m)})_j^{n+1}$. The calculation goes to Step 4. If no, $(T_e^{(m)})_j^{n+1(i+1)}$ is then saved as $(T_e^{(m)})_j^{n+1(i)}$ and $(q_e^{(m)})_j^{n+1(i+1)}$ as $(q_e^{(m)})_j^{n+1(i)}$. The calculation then goes back to Step 2.

Step 4: Solve for $(q_l^{(m)})_j^{n+1(i+1)}$ from Equation (3.58), and substitute it into Equation (3.57) to obtain an equation which has only one unknown variable $(T_l^{(m)})_j^{n+1(i+1)}$.

Step 5: Develop a tridiagonal linear system for $(T_l^{(m)})_j^{n+1(i+1)}$ from the obtained equation in Step 4 with the interfacial condition Equations (3.60b), (3.60d), and the boundary condition Equation (3.61d), and then solve for $(T_l^{(m)})_j^{n+1(i+1)}$. Once $(T_l^{(m)})_j^{n+1(i+1)}$ is calculated, $(q_l^{(m)})_j^{n+1(i+1)}$ is then obtained from Equation (3.58).

Step 6: Check if $\max_{1 \leq j \leq N} |(T_l^{(m)})_j^{n+1(i+1)} - (T_l^{(m)})_j^n| < \varepsilon$. If yes, $(T_l^{(m)})_j^{n+1(i+1)}$ is then saved as $(T_l^{(m)})_j^{n+1}$ and $(q_l^{(m)})_j^{n+1(i+1)}$ as $(q_l^{(m)})_j^{n+1}$. The calculation goes to Step 1, and move on to the next time step. If no, $(T_l^{(m)})_j^{n+1(i+1)}$ is then saved as $(T_l^{(m)})_j^{n+1(i)}$ and $(q_l^{(m)})_j^{n+1(i+1)}$ as $(q_l^{(m)})_j^{n+1(i)}$. The calculation then goes back to Step 5.

Step 7: Repeat the calculation until the required time steps have been reached.

CHAPTER 4

TWO-DIMENSIONAL MATHEMATICAL MODELS

AND

FINITE DIFFERENCE SCHEMES

4.1 Single-Layered Case

4.1.1 Problem Description

In this chapter, we consider a two-dimensional micro thin film exposed to ultrashort-pulsed lasers. We will employ the hyperbolic two-step model and the finite difference scheme developed in the previous chapter coupled with dynamic equations of motion to study thermal deformation in a two-dimensional single-layered thin film.

The two-dimensional single-layered thin film in rectangular coordinates, which is exposed to ultrashort-pulsed lasers, is shown as in Figure 4.1.

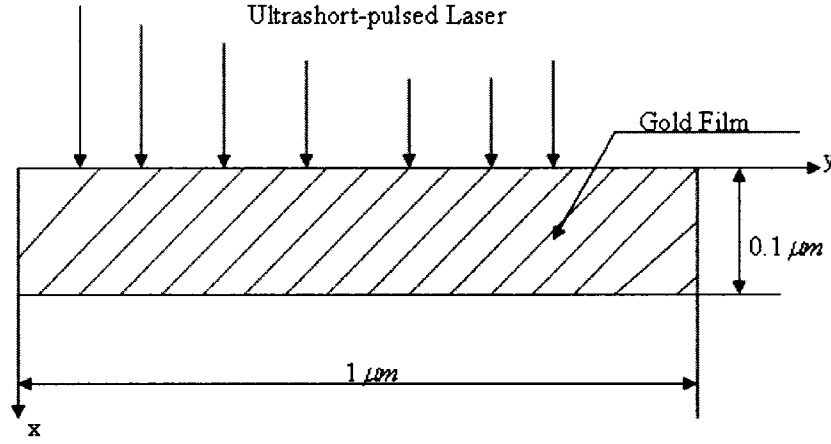


Figure 4.1 A 2D single-layered micro thin film.

The governing equations for studying thermal deformation in this two-dimensional single-layered micro thin film are expressed as follows:

(1) Dynamic equations of motion [Tzou 2002, Chen 2002, Brorson 1987, Wang 2006a]

$$\rho \frac{\partial^2 u}{\partial t^2} = \frac{\partial \sigma_x}{\partial x} + \frac{\partial \sigma_{xy}}{\partial y} + 2\Lambda T_e \frac{\partial T_e}{\partial x}, \quad (4.1)$$

$$\rho \frac{\partial^2 v}{\partial t^2} = \frac{\partial \sigma_{xy}}{\partial x} + \frac{\partial \sigma_y}{\partial y} + 2\Lambda T_e \frac{\partial T_e}{\partial y}, \quad (4.2)$$

where

$$\sigma_x = \lambda(\varepsilon_x + \varepsilon_y) + 2\mu\varepsilon_x - (3\lambda + 2\mu)\alpha_T(T_l - T_0), \quad (4.3)$$

$$\sigma_y = \lambda(\varepsilon_x + \varepsilon_y) + 2\mu\varepsilon_y - (3\lambda + 2\mu)\alpha_T(T_l - T_0), \quad (4.4)$$

$$\sigma_{xy} = \mu\varepsilon_{xy}, \quad (4.5)$$

$$\varepsilon_x = \frac{\partial u}{\partial x}, \varepsilon_y = \frac{\partial v}{\partial y}, \varepsilon_{xy} = \frac{\partial u}{\partial y} + \frac{\partial v}{\partial x}, \quad (4.6)$$

$$\lambda = K - \frac{2}{3}\mu. \quad (4.7)$$

(2) Energy equations [Chen 2001, Qiu 1994, Chen 2003]:

$$C_e \frac{\partial T_e}{\partial t} = -\frac{\partial q_e^x}{\partial x} - \frac{\partial q_e^y}{\partial y} - G(T_e - T_l) + S, \quad (4.8)$$

$$\tau_e \frac{\partial q_e^x}{\partial t} + q_e^x = -k_e \frac{\partial T_e}{\partial x}, \quad (4.9)$$

$$\tau_e \frac{\partial q_e^y}{\partial t} + q_e^y = -k_e \frac{\partial T_e}{\partial y}, \quad (4.10)$$

$$C_l \frac{\partial T_l}{\partial t} = -\frac{\partial q_l^x}{\partial x} - \frac{\partial q_l^y}{\partial y} + G(T_e - T_l) - (3\lambda + 2\mu)\alpha_T T_0 \frac{\partial}{\partial t}(\varepsilon_x + \varepsilon_y), \quad (4.11)$$

$$\tau_l \frac{\partial q_l^x}{\partial t} + q_l^x = -k_l \frac{\partial T_l}{\partial x}, \quad (4.12)$$

$$\tau_l \frac{\partial q_l^y}{\partial t} + q_l^y = -k_l \frac{\partial T_l}{\partial y}. \quad (4.13)$$

Equations (4.8)-(4.13) are called as hyperbolic two-step heat transport equations.

The boundary conditions are assumed to be

$$\sigma_x = 0, \sigma_{xy} = 0, \text{ at } x = 0, L_x, \quad (4.14a)$$

$$\sigma_y = 0, \sigma_{xy} = 0, \text{ at } y = 0, L_y, \quad (4.14b)$$

$$\frac{\partial T_e}{\partial \bar{n}} = 0, \quad (4.15a)$$

$$\frac{\partial T_l}{\partial \bar{n}} = 0. \quad (4.15b)$$

The initial conditions are assumed to be

$$T_e = T_l = T_0, u = v = 0, u_t = v_t = 0, \text{ at } t = 0. \quad (4.16)$$

4.1.2 Notations

To avoid the nonphysical oscillations in the numerical solutions, we employ the idea in [Wang 2006a, Wang 2007] and introduce two velocity components v_1 and v_2 in

the dynamic equations of motion, and hence, the Equations (4.1)-(4.6) are rewritten as follows:

$$v_1 = \frac{\partial u}{\partial t}, v_2 = \frac{\partial v}{\partial t}, \quad (4.17)$$

$$\rho \frac{\partial v_1}{\partial t} = \frac{\partial \sigma_x}{\partial x} + \frac{\partial \sigma_{xy}}{\partial y} + \Lambda \frac{\partial T_e^2}{\partial x}, \quad (4.18)$$

$$\rho \frac{\partial v_2}{\partial t} = \frac{\partial \sigma_{xy}}{\partial x} + \frac{\partial \sigma_y}{\partial y} + \Lambda \frac{\partial T_e^2}{\partial y}, \quad (4.19)$$

$$\frac{\partial \varepsilon_x}{\partial t} = \frac{\partial v_1}{\partial x}, \frac{\partial \varepsilon_y}{\partial t} = \frac{\partial v_2}{\partial x}, \frac{\partial \varepsilon_{xy}}{\partial t} = \frac{\partial v_2}{\partial x} + \frac{\partial v_1}{\partial y}, \quad (4.20)$$

$$\sigma_x = \lambda(\varepsilon_x + \varepsilon_y) + 2\mu\varepsilon_x - (3\lambda + 2\mu)\alpha_T(T_l - T_0), \quad (4.21)$$

$$\sigma_y = \lambda(\varepsilon_x + \varepsilon_y) + 2\mu\varepsilon_y - (3\lambda + 2\mu)\alpha_T(T_l - T_0), \quad (4.22)$$

$$\sigma_{xy} = \mu\varepsilon_{xy}. \quad (4.23)$$

We denote $(v_1)_{i+\frac{1}{2},j}^n$ and $(v_2)_{i,j+\frac{1}{2}}^n$ as numerical approximations of $v_1((i+\frac{1}{2})\Delta x, j\Delta y, n\Delta t)$

and $v_2(i\Delta x, (j+\frac{1}{2})\Delta y, n\Delta t)$, respectively, where $\Delta t, \Delta x$ and Δy are time increment and

spatial step sizes, respectively. Similar notations are used here for other variables. We

also introduce some finite difference operators, $\Delta_{-t}, \delta_x, \delta_y, \nabla_x, \nabla_{\bar{x}}, \nabla_y$ and $\nabla_{\bar{y}}$ as

follows:

$$\Delta_{-t} u_{i,j}^n = u_{i,j}^n - u_{i,j}^{n-1},$$

$$\delta_x u_{i,j}^n = u_{i+\frac{1}{2},j}^n - u_{i-\frac{1}{2},j}^n, \delta_y u_{i,j}^n = u_{i,j+\frac{1}{2}}^n - u_{i,j-\frac{1}{2}}^n,$$

$$\nabla_x u_{i,j}^n = \frac{u_{i+1,j}^n - u_{i,j}^n}{\Delta x}, \nabla_{\bar{x}} u_{i,j}^n = \frac{u_{i,j}^n - u_{i-1,j}^n}{\Delta x},$$

$$\nabla_y u_{i,j}^n = \frac{u_{i,j+1}^n - u_{i,j}^n}{\Delta y}, \quad \nabla_x u_{i,j}^n = \frac{u_{i,j}^n - u_{i,j-1}^n}{\Delta x}.$$

4.1.3 Finite Difference Scheme

We first set up a staggered grid as shown in Figure 4.2.

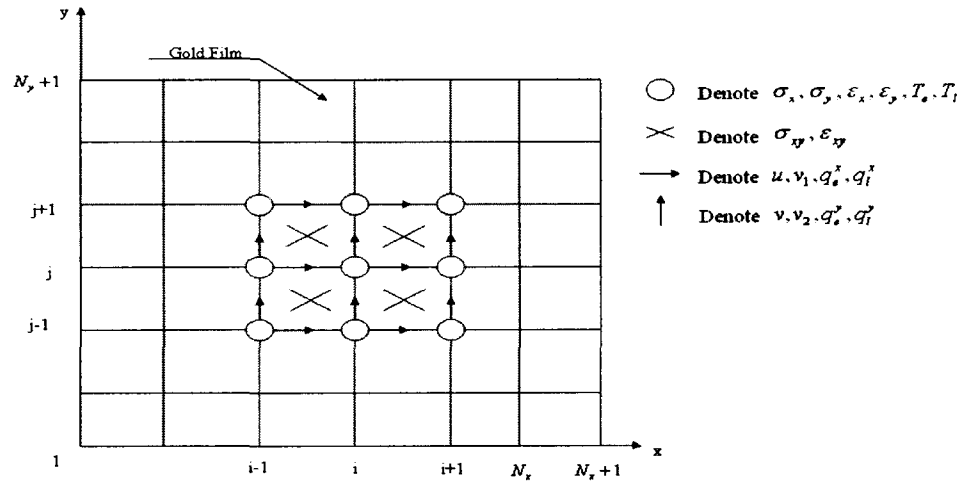


Figure 4.2 A staggered grid for 2D single-layered thin film.

In Figure 4.2, v_1 , q_e^x and q_i^x are placed at $(x_{i+1/2}, y_j)$, v_2 , q_e^y and q_i^y at $(x_i, y_{j+1/2})$, ϵ_{xy} and σ_{xy} are placed at $(x_{i+1/2}, y_{j+1/2})$ and $\epsilon_x, \epsilon_y, \sigma_x, \sigma_y, T_e$ and T_i are at (x_i, y_j) with $1 \leq i \leq N_x + 1$ and $1 \leq j \leq N_y + 1$.

The staggered-grid method is used in computational fluid dynamics to prevent the solution from oscillations [Patanka 1980]. For example, if v_1 and ϵ_x in Equation (4.20) are placed at the same location, employing a central finite difference scheme may produce a velocity component v_1 , a wave solution, implying oscillation.

We develop a finite difference method for solving Equations (4.18)-(4.20). For this purpose, we discretize these equations using a backward finite difference scheme as follows:

$$\begin{aligned} \rho \frac{1}{\Delta t} \Delta_{-t}(v_1)_{i+\frac{1}{2},j}^{n+1} &= \frac{1}{\Delta x} \delta_x (\sigma_x)_{i+\frac{1}{2},j}^{n+1} + \frac{1}{\Delta y} \delta_y (\sigma_{xy})_{i+\frac{1}{2},j}^{n+1} \\ &+ \Lambda \frac{1}{\Delta x} \delta_x (T_e^2)_{i+\frac{1}{2},j}^{n+1}, \end{aligned} \quad (4.24)$$

$$\begin{aligned} \rho \frac{1}{\Delta t} \Delta_{-t}(v_2)_{i,j+\frac{1}{2}}^{n+1} &= \frac{1}{\Delta x} \delta_x (\sigma_{xy})_{i,j+\frac{1}{2}}^{n+1} + \frac{1}{\Delta y} \delta_y (\sigma_y)_{i,j+\frac{1}{2}}^{n+1} (i, j+1/2)^{n+1} \\ &+ \Lambda \frac{1}{\Delta y} \delta_y (T_e^2)_{i,j+\frac{1}{2}}^{n+1}, \end{aligned} \quad (4.25)$$

$$\frac{1}{\Delta t} \Delta_{-t}(\varepsilon_x)_{i,j}^{n+1} = \frac{1}{\Delta x} \delta_x (v_1)_{i,j}^{n+1}, \quad (4.26)$$

$$\frac{1}{\Delta t} \Delta_{-t}(\varepsilon_y)_{i,j}^{n+1} = \frac{1}{\Delta x} \delta_y (v_2)_{i,j}^{n+1}, \quad (4.27)$$

$$\frac{1}{\Delta t} \Delta_{-t}(\varepsilon_{xy})_{i+\frac{1}{2},j+\frac{1}{2}}^{n+1} = \frac{1}{\Delta x} \delta_x (v_2)_{i+\frac{1}{2},j+\frac{1}{2}}^{n+1} + \frac{1}{\Delta y} \delta_y (v_1)_{i+\frac{1}{2},j+\frac{1}{2}}^{n+1}, \quad (4.28)$$

and Equations (4.21)-(4.23) are discretized as:

$$(\sigma_x)_{i,j}^{n+1} = \lambda[(\varepsilon_x)_{i,j}^{n+1} + (\varepsilon_y)_{i,j}^{n+1}] + 2\mu(\varepsilon_x)_{i,j}^{n+1} - (3\lambda + 2\mu)\alpha_T[(T_l)_{i,j}^n - T_0], \quad (4.29)$$

$$(\sigma_y)_{i,j}^{n+1} = \lambda[(\varepsilon_x)_{i,j}^{n+1} + (\varepsilon_y)_{i,j}^{n+1}] + 2\mu(\varepsilon_y)_{i,j}^{n+1} - (3\lambda + 2\mu)\alpha_T[(T_l)_{i,j}^n - T_0], \quad (4.30)$$

$$(\sigma_{xy})_{i+\frac{1}{2},j+\frac{1}{2}}^{n+1} = \mu(\varepsilon_{xy})_{i+\frac{1}{2},j+\frac{1}{2}}^{n+1}. \quad (4.31)$$

Then we discretize the Equations (4.8)-(4.13) as follows:

$$A_e \frac{|(T_e)_{i,j}^{n+1}|^3 - |(T_e)_{i,j}^n|^3}{\frac{3}{2} \Delta t [(T_e)_{i,j}^{n+1} + (T_e)_{i,j}^n]} = -\nabla_{\bar{x}} \left[\frac{(q_e^x)_{i,j}^{n+1} + (q_e^x)_{i,j}^n}{2} \right] - \nabla_{\bar{y}} \left[\frac{(q_e^y)_{i,j}^{n+1} + (q_e^y)_{i,j}^n}{2} \right]$$

$$-G \left[\frac{(T_e)_{i,j}^{n+1} + (T_e)_{i,j}^n}{2} - \frac{(T_l)_{i,j}^{n+1} + (T_l)_{i,j}^n}{2} \right] + S_{i,j}^{n+\frac{1}{2}}, \quad (4.32)$$

$$\tau_e \frac{(q_e^x)_{i,j}^{n+1} - (q_e^x)_{i,j}^n}{\Delta t} + \frac{(q_e^x)_{i,j}^{n+1} + (q_e^x)_{i,j}^n}{2} = -(k_e)_{i-\frac{1}{2},j}^{n+\frac{1}{2}} \cdot \nabla_x \left[\frac{(T_e)_{i,j}^{n+1} + (T_e)_{i,j}^n}{2} \right], \quad (4.33)$$

$$\tau_e \frac{(q_e^y)_{i,j}^{n+1} - (q_e^y)_{i,j}^n}{\Delta t} + \frac{(q_e^y)_{i,j}^{n+1} + (q_e^y)_{i,j}^n}{2} = -(k_e)_{i,j-\frac{1}{2}}^{n+\frac{1}{2}} \cdot \nabla_y \left[\frac{(T_e)_{i,j}^{n+1} + (T_e)_{i,j}^n}{2} \right], \quad (4.34)$$

$$\begin{aligned} C_l \frac{(T_l)_{i,j}^{n+1} - (T_l)_{i,j}^n}{\Delta t} &= -\nabla_{\bar{x}} \left[\frac{(q_l^x)_{i,j}^{n+1} + (q_l^x)_{i,j}^n}{2} \right] - \nabla_{\bar{y}} \left[\frac{(q_l^y)_{i,j}^{n+1} + (q_l^y)_{i,j}^n}{2} \right] \\ &\quad - G \left[\frac{(T_e)_{i,j}^{n+1} + (T_e)_{i,j}^n}{2} - \frac{(T_l)_{i,j}^{n+1} + (T_l)_{i,j}^n}{2} \right] \\ &\quad - (3\lambda + 2\mu) \alpha_T T_0 \cdot \frac{\Delta_{-t}(\varepsilon_x)_{i,j}^{n+1} + \Delta_{-t}(\varepsilon_y)_{i,j}^{n+1}}{\Delta t}, \end{aligned} \quad (4.35)$$

$$\tau_l \frac{(q_l^x)_{i,j}^{n+1} - (q_l^x)_{i,j}^n}{\Delta t} + \frac{(q_l^x)_{i,j}^{n+1} + (q_l^x)_{i,j}^n}{2} = -k_l \cdot \nabla_x \left[\frac{(T_l)_{i,j}^{n+1} + (T_l)_{i,j}^n}{2} \right], \quad (4.36)$$

$$\tau_l \frac{(q_l^y)_{i,j}^{n+1} - (q_l^y)_{i,j}^n}{\Delta t} + \frac{(q_l^y)_{i,j}^{n+1} + (q_l^y)_{i,j}^n}{2} = -k_l \cdot \nabla_y \left[\frac{(T_l)_{i,j}^{n+1} + (T_l)_{i,j}^n}{2} \right], \quad (4.37)$$

Here, $i = 2, \dots, N_x$ and $j = 2, \dots, N_y$ in Equations (4.32)-(4.37).

We can obtain the displacements, u and v , by the Euler backward scheme of Equation (4.17) as:

$$\frac{1}{\Delta t} \Delta_{-t} u_{i+\frac{1}{2},j}^{n+1} = (v_1)_{i+\frac{1}{2},j}^{n+1}, \quad (4.38)$$

$$\frac{1}{\Delta t} \Delta_{-t} v_{i+\frac{1}{2},j}^{n+1} = (v_2)_{i+\frac{1}{2},j}^{n+1}. \quad (4.39)$$

The boundary conditions, Equations (4.14a), (4.14b), (4.15a), and (4.15b), are discretized as follows:

$$(\sigma_x)_{1,j}^n = 0, (\sigma_x)_{N_x+1,j}^n = 0, 1 \leq j \leq N_y + 1, \quad (4.40a)$$

$$(\sigma_{xy})_{1+\frac{1}{2},j+\frac{1}{2}}^n = 0, (\sigma_{xy})_{N_x+\frac{1}{2},j+\frac{1}{2}}^n = 0, 1 \leq j \leq N_y, \quad (4.40b)$$

$$(\sigma_y)_{i,1}^n = 0, (\sigma_y)_{i,N_y+1}^n = 0, 1 \leq i \leq N_x + 1, \quad (4.41a)$$

$$(\sigma_{xy})_{i+\frac{1}{2},1+\frac{1}{2}}^n = 0, (\sigma_{xy})_{i+\frac{1}{2},N_y+\frac{1}{2}}^n = 0, 1 \leq i \leq N_x, \quad (4.41b)$$

$$(T_e)_{i,j}^n = (T_e)_{2,j}^n, (T_e)_{N_x+1,j}^n = (T_e)_{N_x,j}^n, 1 \leq j \leq N_y + 1, \quad (4.42a)$$

$$(T_e)_{i,1}^n = (T_e)_{i,2}^n, (T_e)_{i,N_y+1}^n = (T_e)_{i,N_y}^n, 1 \leq i \leq N_x + 1, \quad (4.42b)$$

$$(T_l)_{1,j}^n = (T_l)_{2,j}^n, (T_l)_{N_x+1,j}^n = (T_l)_{N_x,j}^n, 1 \leq j \leq N_y + 1, \quad (4.42c)$$

$$(T_l)_{i,1}^n = (T_l)_{i,2}^n, (T_l)_{i,N_y+1}^n = (T_l)_{i,N_y}^n, 1 \leq i \leq N_x + 1, \quad (4.42d)$$

for any time level n . The initial conditions, Equation (4.16), are discretized as

$$u_{i+\frac{1}{2},j}^0 = 0, v_{i,j+\frac{1}{2}}^0 = 0, 1 \leq i \leq N_x, 1 \leq j \leq N_y, \quad (4.43a)$$

$$(v_1)_{i+\frac{1}{2},j}^0 = 0, (v_2)_{i,j+\frac{1}{2}}^0 = 0, 1 \leq i \leq N_x, 1 \leq j \leq N_y, \quad (4.43b)$$

$$(T_e)_{i,j}^0 = (T_l)_{i,j}^0 = T_0, 1 \leq i \leq N_x + 1, 1 \leq j \leq N_y + 1, \quad (4.43c)$$

$$(\varepsilon_x)_{i,j}^0 = (\varepsilon_y)_{i,j}^0 = 0, 1 \leq i \leq N_x + 1, 1 \leq j \leq N_y + 1, \quad (4.43d)$$

$$(\sigma_x)_{i,j}^0 = (\sigma_y)_{i,j}^0 = 0, 1 \leq i \leq N_x + 1, 1 \leq j \leq N_y + 1, \quad (4.43e)$$

$$(\sigma_{xy})_{i+\frac{1}{2},j+\frac{1}{2}}^0 = (\varepsilon_{xy})_{i+\frac{1}{2},j+\frac{1}{2}}^0 = 0, 1 \leq i \leq N_x, 1 \leq j \leq N_y. \quad (4.43f)$$

4.1.4 Algorithm

For the finite difference scheme developed in the previous section, we can see that the truncation error of Equations (4.24) and (4.25) is $O(\Delta t + \Delta x^2 + \Delta y^2)$, and the truncation error of Equations (4.32)-(4.37) is $O(\Delta t^2 + \Delta x^2 + \Delta y^2)$. We should notice that Equations (4.24) and (4.25) are nonlinear since they contain nonlinear terms $\delta_x (T_e^2)_{i+\frac{1}{2},j}^{n+1}$ and $\delta_y (T_e^2)_{i,j+\frac{1}{2}}^{n+1}$. Similarly, Equations (4.32)-(4.37) are also nonlinear. Therefore, we have to solve the above scheme iteratively. The following algorithm is an iterative method for solving the finite difference scheme at time level $n+1$ developed in the previous section.

Step 1: Guess $(\varepsilon_x)^{n+1}$, $(\varepsilon_y)^{n+1}$ and $(\varepsilon_{xy})^{n+1}$ using their values at previous time step.

Solve $(q_e^x)^{n+1}$, $(q_e^y)^{n+1}$, $(q_i^x)^{n+1}$ and $(q_i^y)^{n+1}$ from Equations (4.33), (4.34), (4.36) and (4.37), respectively, and substitute them into Equations (4.32) and (4.35). Then solve for $(T_e)^{n+1}$ and $(T_i)^{n+1}$ iteratively based on the guessed $(\varepsilon_x)^{n+1}$, $(\varepsilon_y)^{n+1}$ and $(\varepsilon_{xy})^{n+1}$.

Step 2: Solve Equations (4.29)-(4.31) for $(\sigma_x)^{n+1}$, $(\sigma_y)^{n+1}$ and $(\sigma_{xy})^{n+1}$.

Step 3: Solve Equations (4.24) and (4.25) for $(v_1)^{n+1}$ and $(v_2)^{n+1}$.

Step 4: Update $(\varepsilon_x)^{n+1}$, $(\varepsilon_y)^{n+1}$ and $(\varepsilon_{xy})^{n+1}$ by using Equations (4.26)-(4.28).

Given the required accuracy, repeat the above steps until a convergent solution is obtained based on the following criteria

$$\max |(\varepsilon_x)^{n+1(new)} - (\varepsilon_x)^{n+1(old)}| \leq \varepsilon,$$

$$\max |(\varepsilon_y)^{n+1(new)} - (\varepsilon_y)^{n+1(old)}| \leq \varepsilon,$$

$$\max |(\varepsilon_{xy})^{n+1(new)} - (\varepsilon_{xy})^{n+1(old)}| \leq \varepsilon.$$

Step 5: Solve Equations (4.38) and (4.39) for u^{n+1} and v^{n+1} .

4.2 Double-Layered Case

4.2.1 Problem Description

In this section, we consider a two-dimensional double-layered micro thin film exposed to ultrashort pulsed lasers, which has a perfectly thermal contact interface, as shown in Figure 4.3.

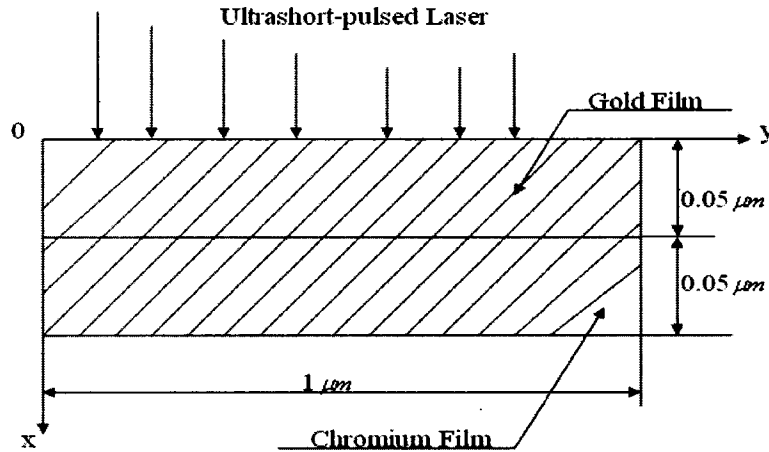


Figure 4.3 A 2D double-layered thin film.

The governing equations for studying thermal deformation in the two-dimensional double-layered micro thin film can be expressed as:

(1) Dynamic equations of motion [Tzou 2002, Chen 2002a, Brorson 1987, Wang 2006b]

$$\rho^{(m)} \frac{\partial^2 u^{(m)}}{\partial t^2} = \frac{\partial \sigma_x^{(m)}}{\partial x} + \frac{\partial \sigma_{xy}^{(m)}}{\partial y} + 2\Lambda^{(m)} T_e^{(m)} \frac{\partial T_e^{(m)}}{\partial x}, \quad (4.44)$$

$$\rho^{(m)} \frac{\partial^2 v^{(m)}}{\partial t^2} = \frac{\partial \sigma_{xy}^{(m)}}{\partial x} + \frac{\partial \sigma_y^{(m)}}{\partial y} + 2\Lambda^{(m)} T_e^{(m)} \frac{\partial T_e^{(m)}}{\partial y}, \quad (4.45)$$

where

$$\sigma_x^{(m)} = \lambda^{(m)}(\varepsilon_x^{(m)} + \varepsilon_y^{(m)}) + 2\mu^{(m)}\varepsilon_x^{(m)} - (3\lambda^{(m)} + 2\mu^{(m)})\alpha_T^{(m)}(T_l^{(m)} - T_0), \quad (4.46)$$

$$\sigma_y^{(m)} = \lambda^{(m)}(\varepsilon_x^{(m)} + \varepsilon_y^{(m)}) + 2\mu^{(m)}\varepsilon_y^{(m)} - (3\lambda^{(m)} + 2\mu^{(m)})\alpha_T^{(m)}(T_l^{(m)} - T_0), \quad (4.47)$$

$$\sigma_{xy}^{(m)} = \mu^{(m)}\varepsilon_{xy}^{(m)}, \quad (4.48)$$

$$\varepsilon_x^{(m)} = \frac{\partial u^{(m)}}{\partial x}, \varepsilon_y^{(m)} = \frac{\partial v^{(m)}}{\partial y}, \varepsilon_{xy}^{(m)} = \frac{\partial u^{(m)}}{\partial y} + \frac{\partial v^{(m)}}{\partial x}. \quad (4.49)$$

Here, $m = 1, 2$, standing for layer 1 and 2, respectively.

(2) Energy equations [Chen 2001, Qiu 1994, Chen 2003]:

$$C_e^{(m)} \frac{\partial T_e^{(m)}}{\partial t} = -\frac{\partial q_e^{x(m)}}{\partial x} - \frac{\partial q_e^{y(m)}}{\partial y} - G^{(m)}(T_e^{(m)} - T_l^{(m)}) + S^{(m)}, \quad (4.50)$$

$$\tau_e^{(m)} \frac{\partial q_e^{x(m)}}{\partial t} + q_e^{x(m)} = -k_e^{(m)} \frac{\partial T_e^{(m)}}{\partial x}, \quad (4.51)$$

$$\tau_e^{(m)} \frac{\partial q_e^{y(m)}}{\partial t} + q_e^{y(m)} = -k_e^{(m)} \frac{\partial T_e^{(m)}}{\partial y}, \quad (4.52)$$

$$C_l^{(m)} \frac{\partial T_l^{(m)}}{\partial t} = -\frac{\partial q_l^{x(m)}}{\partial x} - \frac{\partial q_l^{y(m)}}{\partial y} + G^{(m)}(T_e^{(m)} - T_l^{(m)}) - (3\lambda^{(m)} + 2\mu^{(m)})\alpha_T^{(m)}T_0 \frac{\partial}{\partial t}(\varepsilon_x^{(m)} + \varepsilon_y^{(m)}), \quad (4.53)$$

$$\tau_l^{(m)} \frac{\partial q_l^{x(m)}}{\partial t} + q_l^{x(m)} = -k_l^{(m)} \frac{\partial T_l^{(m)}}{\partial x}, \quad (4.54)$$

$$\tau_l^{(m)} \frac{\partial q_l^{y(m)}}{\partial t} + q_l^{y(m)} = -k_l^{(m)} \frac{\partial T_l^{(m)}}{\partial y}. \quad (4.55)$$

Here, $C_e^{(m)} = A_e^{(m)} \cdot T_e^{(m)}$, $k_e^{(m)} = k_0^{(m)} \frac{T_e^{(m)}}{T_l^{(m)}}$. Equations (4.50)-(4.55) are often referred to as

hyperbolic two-step heat transport equations.

The boundary conditions are assumed to be

$$\sigma_x^{(1)} = 0, \sigma_{xy}^{(1)} = 0, \text{ at } x = 0, \text{ and } \sigma_x^{(2)} = 0, \sigma_{xy}^{(2)} = 0, \text{ at } x = L_x, \quad (4.56a)$$

$$\sigma_y^{(1)} = 0, \sigma_{xy}^{(1)} = 0, \text{ at } y = 0, \text{ and } \sigma_y^{(2)} = 0, \sigma_{xy}^{(2)} = 0, \text{ at } y = L_y, \quad (4.56b)$$

$$\frac{\partial T_e^{(m)}}{\partial \vec{n}} = 0, \quad (4.57a)$$

$$\frac{\partial T_l^{(m)}}{\partial \vec{n}} = 0. \quad (4.57b)$$

The initial conditions are assumed to be

$$T_e^{(m)} = T_l^{(m)} = T_0, u^{(m)} = v^{(m)} = 0, u_t^{(m)} = v_t^{(m)} = 0, \text{ at } t = 0, \quad (4.58)$$

where $m = 1, 2$.

The interfacial equations are assumed to be, at $x = L_x/2$,

$$u^{(1)} = u^{(2)}, v^{(1)} = v^{(2)}, \quad (4.59a)$$

$$\sigma_x^{(1)} = \sigma_x^{(2)}, \sigma_{xy}^{(1)} = \sigma_{xy}^{(2)}, \quad (4.59b)$$

$$T_e^{(1)} = T_e^{(2)}, q_e^{x(1)} = q_e^{x(2)}, T_l^{(1)} = T_l^{(2)}, q_l^{x(1)} = q_l^{x(2)}. \quad (4.59c)$$

4.2.2 Notations

For the double-layered case, we follow the idea in [Wang 2006b, Wang 2007] and introduce two velocity components $v_1^{(m)}$ and $v_2^{(m)}$ into the model to prevent the solution from oscillations. The dynamic equations of motion, Equations (4.44)-(4.49), are rewritten as follows:

$$v_1^{(m)} = \frac{\partial u^{(m)}}{\partial t}, v_2^{(m)} = \frac{\partial v^{(m)}}{\partial t}, \quad (4.60)$$

$$\frac{\partial \varepsilon_x^{(m)}}{\partial t} = \frac{\partial v_1^{(m)}}{\partial x}, \quad \frac{\partial \varepsilon_y^{(m)}}{\partial t} = \frac{\partial v_2^{(m)}}{\partial y}, \quad \frac{\partial \varepsilon_{xy}^{(m)}}{\partial t} = \frac{\partial v_2^{(m)}}{\partial x} + \frac{\partial v_1^{(m)}}{\partial y}, \quad (4.61)$$

$$\rho^{(m)} \frac{\partial v_1^{(m)}}{\partial t} = \frac{\partial \sigma_x^{(m)}}{\partial x} + \frac{\partial \sigma_{xy}^{(m)}}{\partial y} + \Lambda^{(m)} \frac{\partial (T_e^2)^{(m)}}{\partial x}, \quad (4.62)$$

$$\rho^{(m)} \frac{\partial v_2^{(m)}}{\partial t} = \frac{\partial \sigma_{xy}^{(m)}}{\partial x} + \frac{\partial \sigma_y^{(m)}}{\partial y} + \Lambda^{(m)} \frac{\partial (T_e^2)^{(m)}}{\partial y}, \quad (4.63)$$

$$\sigma_x^{(m)} = \lambda^{(m)} (\varepsilon_x^{(m)} + \varepsilon_y^{(m)}) + 2\mu^{(m)} \varepsilon_x^{(m)} - (3\lambda^{(m)} + 2\mu^{(m)}) \alpha_T^{(m)} (T_l^{(m)} - T_0), \quad (4.64)$$

$$\sigma_y^{(m)} = \lambda^{(m)} (\varepsilon_x^{(m)} + \varepsilon_y^{(m)}) + 2\mu^{(m)} \varepsilon_y^{(m)} - (3\lambda^{(m)} + 2\mu^{(m)}) \alpha_T^{(m)} (T_l^{(m)} - T_0), \quad (4.65)$$

$$\sigma_{xy}^{(m)} = \mu^{(m)} \varepsilon_{xy}^{(m)}. \quad (4.66)$$

Here, we use $(v_1^{(m)})_{i+\frac{1}{2},j}^n$ and $(v_2^{(m)})_{i,j+\frac{1}{2}}^n$ to denote the numerical approximations of

$v_1^{(m)}((i+1/2)\Delta x, j\Delta y, n\Delta t)$ and $v_2^{(m)}(i\Delta x, (j+1/2)\Delta y, n\Delta t)$, respectively. Similar notations

are used for other variables. Furthermore, we also provide some finite difference

operators, Δ_{-t} , δ_x , δ_y , ∇_x , $\nabla_{\bar{x}}$, ∇_y and $\nabla_{\bar{y}}$ as follows:

$$\Delta_{-t} u_{i,j}^n = u_{i,j}^n - u_{i,j}^{n-1},$$

$$\delta_x u_{i,j}^n = u_{i+\frac{1}{2},j}^n - u_{i-\frac{1}{2},j}^n, \quad \delta_y u_{i,j}^n = u_{i,j+\frac{1}{2}}^n - u_{i,j-\frac{1}{2}}^n,$$

$$\nabla_x u_{i,j}^n = \frac{u_{i+1,j}^n - u_{i,j}^n}{\Delta x}, \quad \nabla_{\bar{x}} u_{i,j}^n = \frac{u_{i,j}^n - u_{i-1,j}^n}{\Delta x},$$

$$\nabla_y u_{i,j}^n = \frac{u_{i,j+1}^n - u_{i,j}^n}{\Delta y}, \quad \nabla_{\bar{y}} u_{i,j}^n = \frac{u_{i,j}^n - u_{i,j-1}^n}{\Delta y}.$$

4.2.3 Finite Difference Scheme

We first set up a staggered grid as shown in Figure 4.4, where $v_1^{(m)}$, $q_e^{x(m)}$ and $q_l^{x(m)}$ are laid at $(x_{i+1/2}, y_j)$, and $v_2^{(m)}$, $q_e^{y(m)}$ and $q_l^{y(m)}$ are laid at $(x_i, y_{j+1/2})$. $\varepsilon_{xy}^{(m)}$ and $\sigma_{xy}^{(m)}$ are placed at $(x_{i+1/2}, y_{j+1/2})$, and $\varepsilon_x^{(m)}$, $\varepsilon_y^{(m)}$, $\sigma_x^{(m)}$, $\sigma_y^{(m)}$, $T_e^{(m)}$ and $T_l^{(m)}$ are placed as (x_i, y_j) . Here, i and j are indices with $1 \leq i \leq N_x + 1, 1 \leq j \leq N_y + 1$ and $m = 1, 2$.

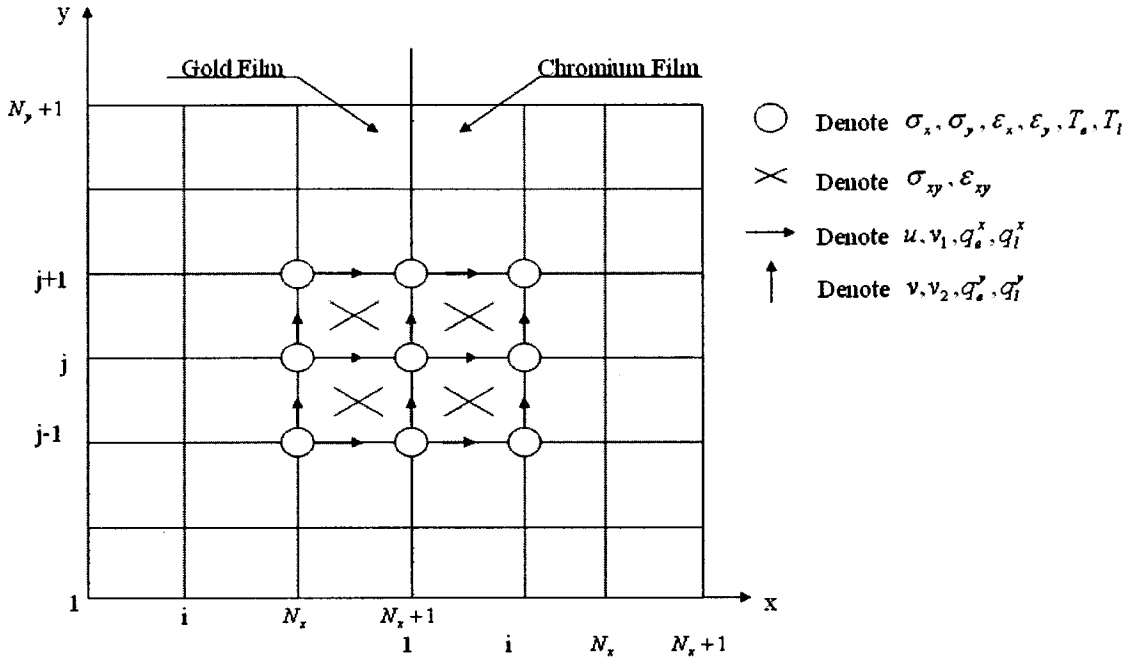


Figure 4.4 A staggered grid for 2D double-layered thin film.

Now, we develop a finite difference method to solve the governing equations discussed in section 4.2.1. For this purpose, we first discretize Equations (4.61)-(4.66) using an implicit finite difference scheme as

$$\frac{1}{\Delta t} \Delta_{-t} (\varepsilon_x^{(m)})_{i,j}^{n+1} = \frac{1}{\Delta x} \delta_x (v_1^{(m)})_{i,j}^{n+1}, \quad (4.67a)$$

$$\frac{1}{\Delta t} \Delta_{-t} (\varepsilon_y^{(m)})_{i,j}^{n+1} = \frac{1}{\Delta y} \delta_y (v_2^{(m)})_{i,j}^{n+1}, \quad (4.67b)$$

$$\frac{1}{\Delta t} \Delta_{-t} (\varepsilon_{xy}^{(m)})_{i+\frac{1}{2}, j+\frac{1}{2}}^{n+1} = \frac{1}{\Delta x} \delta_x (v_2^{(m)})_{i+\frac{1}{2}, j+\frac{1}{2}}^{n+1} + \frac{1}{\Delta y} \delta_y (v_1^{(m)})_{i+\frac{1}{2}, j+\frac{1}{2}}^{n+1}, \quad (4.67c)$$

$$\begin{aligned} \rho^{(m)} \frac{1}{\Delta t} \Delta_{-t} (v_1^{(m)})_{i+\frac{1}{2}, j}^{n+1} &= \frac{1}{\Delta x} \delta_x (\sigma_x^{(m)})_{i+\frac{1}{2}, j}^{n+1} + \frac{1}{\Delta y} \delta_y (\sigma_{xy}^{(m)})_{i+\frac{1}{2}, j}^{n+1} \\ &\quad + \Lambda^{(m)} \frac{1}{\Delta x} \delta_x ((T_e^2)^{(m)})_{i+\frac{1}{2}, j}^{n+1}, \end{aligned} \quad (4.68)$$

$$\begin{aligned} \rho^{(m)} \frac{1}{\Delta t} \Delta_{-t} (v_2^{(m)})_{i, j+\frac{1}{2}}^{n+1} &= \frac{1}{\Delta x} \delta_x (\sigma_{xy}^{(m)})_{i, j+\frac{1}{2}}^{n+1} + \frac{1}{\Delta y} \delta_y (\sigma_y^{(m)})_{i, j+\frac{1}{2}}^{n+1} \\ &\quad + \Lambda^{(m)} \frac{1}{\Delta y} \delta_y ((T_e^2)^{(m)})_{i, j+\frac{1}{2}}^{n+1}, \end{aligned} \quad (4.69)$$

$$\begin{aligned} (\sigma_x^{(m)})_{i, j}^{n+1} &= \lambda^{(m)} [(\varepsilon_x^{(m)})_{i, j}^{n+1} + (\varepsilon_y^{(m)})_{i, j}^{n+1}] + 2\mu^{(m)} (\varepsilon_x^{(m)})_{i, j}^{n+1} \\ &\quad - (3\lambda^{(m)} + 2\mu^{(m)}) \alpha_T^{(m)} [(T_l^{(m)})_{i, j}^{n+1} - T_0], \end{aligned} \quad (4.70)$$

$$\begin{aligned} (\sigma_y^{(m)})_{i, j}^{n+1} &= \lambda^{(m)} [(\varepsilon_x^{(m)})_{i, j}^{n+1} + (\varepsilon_y^{(m)})_{i, j}^{n+1}] + 2\mu^{(m)} (\varepsilon_y^{(m)})_{i, j}^{n+1} \\ &\quad - (3\lambda^{(m)} + 2\mu^{(m)}) \alpha_T^{(m)} [(T_l^{(m)})_{i, j}^{n+1} - T_0], \end{aligned} \quad (4.71)$$

$$(\sigma_{xy}^{(m)})_{i+\frac{1}{2}, j+\frac{1}{2}}^{n+1} = \mu^{(m)} \cdot (\varepsilon_{xy}^{(m)})_{i+\frac{1}{2}, j+\frac{1}{2}}^{n+1}. \quad (4.72)$$

We then discretize Equations (4.50)-(4.55) as

$$\begin{aligned} A_e^{(m)} \frac{|(T_e^{(m)})_{i, j}^{n+1}|^3 - |(T_e^{(m)})_{i, j}^n|^3}{3\Delta t \frac{(T_e^{(m)})_{i, j}^{n+1} + (T_e^{(m)})_{i, j}^n}{2}} &= -\nabla_{\bar{x}} \frac{(q_e^{x(m)})_{i, j}^{n+1} + (q_e^{x(m)})_{i, j}^n}{2} - \nabla_{\bar{y}} \frac{(q_e^{y(m)})_{i, j}^{n+1} + (q_e^{y(m)})_{i, j}^n}{2} \\ &\quad - G^{(m)} \left[\frac{(T_e^{(m)})_{i, j}^{n+1} + (T_e^{(m)})_{i, j}^n}{2} - \frac{(T_l^{(m)})_{i, j}^{n+1} + (T_l^{(m)})_{i, j}^n}{2} \right] \\ &\quad + (S^{(m)})_{i, j}^{n+\frac{1}{2}}, \end{aligned} \quad (4.73)$$

$$\tau_e^{(m)} \frac{(q_e^{x(m)})_{i, j}^{n+1} - (q_e^{x(m)})_{i, j}^n}{\Delta t} + \frac{1}{2} [(q_e^{x(m)})_{i, j}^{n+1} + (q_e^{x(m)})_{i, j}^n]$$

$$= -(k_e^{(m)})_{i-\frac{1}{2},j}^{n+\frac{1}{2}} \cdot \nabla_x \frac{(T_e^{(m)})_{i,j}^{n+1} + (T_e^{(m)})_{i,j}^n}{2}, \quad (4.74)$$

$$\begin{aligned} & \tau_e^{(m)} \frac{(q_e^{y(m)})_{i,j}^{n+1} - (q_e^{y(m)})_{i,j}^n}{\Delta t} + \frac{1}{2} [(q_e^{y(m)})_{i,j}^{n+1} + (q_e^{y(m)})_{i,j}^n] \\ &= -(k_e^{(m)})_{i,j-\frac{1}{2}}^{n+\frac{1}{2}} \cdot \nabla_y \frac{(T_e^{(m)})_{i,j}^{n+1} + (T_e^{(m)})_{i,j}^n}{2}, \end{aligned} \quad (4.75)$$

$$\begin{aligned} C_l^{(m)} \frac{(T_l^{(m)})_{i,j}^{n+1} - (T_l^{(m)})_{i,j}^n}{\Delta t} &= -\nabla_{\bar{x}} \frac{(q_l^{x(m)})_{i,j}^{n+1} + (q_l^{x(m)})_{i,j}^n}{2} - \nabla_{\bar{y}} \frac{(q_l^{y(m)})_{i,j}^{n+1} + (q_l^{y(m)})_{i,j}^n}{2} \\ &+ G^{(m)} \left[\frac{(T_e^{(m)})_{i,j}^{n+1} + (T_e^{(m)})_{i,j}^n}{2} - \frac{(T_l^{(m)})_{i,j}^{n+1} + (T_l^{(m)})_{i,j}^n}{2} \right] \\ &- \frac{(3\lambda^{(m)} + 2\mu^{(m)})\alpha_T^{(m)}T_0}{\Delta t} [(\varepsilon_x^{(m)})_{i,j}^{n+1} + (\varepsilon_y^{(m)})_{i,j}^{n+1} \\ &- (\varepsilon_x^{(m)})_{i,j}^n - (\varepsilon_y^{(m)})_{i,j}^n], \end{aligned} \quad (4.76)$$

$$\begin{aligned} & \tau_l^{(m)} \frac{(q_l^{x(m)})_{i,j}^{n+1} - (q_l^{x(m)})_{i,j}^n}{\Delta t} + \frac{1}{2} [(q_l^{x(m)})_{i,j}^{n+1} + (q_l^{x(m)})_{i,j}^n] \\ &= -k_l^{(m)} \cdot \nabla_x \frac{(T_l^{(m)})_{i,j}^{n+1} + (T_l^{(m)})_{i,j}^n}{2}, \end{aligned} \quad (4.77)$$

$$\begin{aligned} & \tau_l^{(m)} \frac{(q_l^{y(m)})_{i,j}^{n+1} - (q_l^{y(m)})_{i,j}^n}{\Delta t} + \frac{1}{2} [(q_l^{y(m)})_{i,j}^{n+1} + (q_l^{y(m)})_{i,j}^n] \\ &= -k_l^{(m)} \cdot \nabla_y \frac{(T_l^{(m)})_{i,j}^{n+1} + (T_l^{(m)})_{i,j}^n}{2}, \end{aligned} \quad (4.78)$$

where, in Equations (4.73) and (4.76), $2 \leq i \leq N_x$, $2 \leq j \leq N_y$ and $m = 1, 2$; in Equations (4.74) and (4.77), $1 \leq i \leq N_x$ and $2 \leq j \leq N_y$ when $m = 1$ and $1 \leq i \leq N_x - 1$ and $2 \leq j \leq N_y$ when $m = 2$; and in Equations (4.75) and (4.78), $2 \leq i \leq N_x$ and $1 \leq j \leq N_y$ when $m = 1$ and $1 \leq i \leq N_x - 1$ and $1 \leq j \leq N_y$ when $m = 2$. Here,

$$(k_e^{(m)})_{i-\frac{1}{2},j}^{n+\frac{1}{2}} = \frac{1}{2} k_0^{(m)} \left| \frac{(T_e^{(m)})_{i,j}^{n+1} + (T_e^{(m)})_{i,j}^n}{(T_l^{(m)})_{i,j}^{n+1} + (T_l^{(m)})_{i,j}^n} \right| + \frac{1}{2} k_0^{(m)} \left| \frac{(T_e^{(m)})_{i-1,j}^{n+1} + (T_e^{(m)})_{i-1,j}^n}{(T_l^{(m)})_{i-1,j}^{n+1} + (T_l^{(m)})_{i-1,j}^n} \right|$$

and

$$(k_e^{(m)})_{i,j-\frac{1}{2}}^{n+\frac{1}{2}} = \frac{1}{2} k_0^{(m)} \left| \frac{(T_e^{(m)})_{i,j}^{n+1} + (T_e^{(m)})_{i,j}^n}{(T_l^{(m)})_{i,j}^{n+1} + (T_l^{(m)})_{i,j}^n} \right| + \frac{1}{2} k_0^{(m)} \left| \frac{(T_e^{(m)})_{i,j-1}^{n+1} + (T_e^{(m)})_{i,j-1}^n}{(T_l^{(m)})_{i,j-1}^{n+1} + (T_l^{(m)})_{i,j-1}^n} \right|.$$

It should be pointed out that the above scheme, Equations (4.76)-(4.78) without the term $-\frac{(3\lambda^{(m)} + 2\mu^{(m)})\alpha_T^{(m)}}{\Delta t} [(\varepsilon_x^{(m)})_{i,j}^{n+1} + (\varepsilon_y^{(m)})_{i,j}^{n+1} - (\varepsilon_x^{(m)})_{i,j}^n - (\varepsilon_y^{(m)})_{i,j}^n]$, is obtained

based on an energy estimate and is shown to be unconditionally stable in Chapter 3.

Finally, we can obtain the displacements $u^{(m)}$ and $v^{(m)}$ by the Euler backward scheme for Equation (4.60) as follows:

$$\frac{1}{\Delta t} \Delta_{-t} (u^{(m)})_{i+\frac{1}{2},j}^{n+1} = (v_1^{(m)})_{i+\frac{1}{2},j}^{n+1}, \quad (4.79a)$$

$$\frac{1}{\Delta t} \Delta_{-t} (v^{(m)})_{i,j+\frac{1}{2}}^{n+1} = (v_2^{(m)})_{i,j+\frac{1}{2}}^{n+1}. \quad (4.79b)$$

The boundary conditions, Equations (4.56a), (4.56b), (4.57a) and (4.57b), are discretized as

$$(\sigma_x^{(1)})_{1,j}^{n+1} = 0, (\sigma_x^{(2)})_{N_x+1}^{n+1} = 0, (\sigma_{xy}^{(1)})_{1,j}^{n+1} = 0, (\sigma_{xy}^{(2)})_{N_x+1,j}^{n+1} = 0, \quad (4.80a)$$

$$(\sigma_y^{(1)})_{i,1}^{n+1} = 0, (\sigma_y^{(2)})_{i,N_y+1}^{n+1} = 0, (\sigma_{xy}^{(1)})_{i,1}^{n+1} = 0, (\sigma_{xy}^{(2)})_{i,N_y+1}^{n+1} = 0, \quad (4.80b)$$

$$(T_e^{(1)})_{1,j}^{n+1} = (T_e^{(1)})_{2,j}^{n+1}, (T_e^{(2)})_{N_x+1,j}^{n+1} = (T_e^{(2)})_{N_x,j}^{n+1}, \quad (4.81a)$$

$$(T_e^{(1)})_{i,1}^{n+1} = (T_e^{(1)})_{i,2}^{n+1}, (T_e^{(2)})_{i,N_y+1}^{n+1} = (T_e^{(2)})_{i,N_y}^{n+1}, \quad (4.81b)$$

$$(T_l^{(1)})_{1,j}^{n+1} = (T_l^{(1)})_{2,j}^{n+1}, (T_l^{(2)})_{N_x+1,j}^{n+1} = (T_l^{(2)})_{N_x,j}^{n+1}, \quad (4.82a)$$

$$(T_l^{(1)})_{i,1}^{n+1} = (T_l^{(1)})_{i,2}^{n+1}, (T_l^{(2)})_{i,N_y+1}^{n+1} = (T_l^{(2)})_{i,N_y}^{n+1}, \quad (4.82b)$$

for any time level n . Here, in Equations (4.80a), (4.81a) and (4.82a), $1 \leq j \leq N_y + 1$ and in Equations (4.80b), (4.81b) and (4.82b), $1 \leq i \leq N_x + 1$.

First, based on Equation (4.59a), we can write the interfacial conditions for velocity components $v_1^{(m)}$ and $v_2^{(m)}$ as $v_1^{(1)} = v_1^{(2)}$ and $v_2^{(1)} = v_2^{(2)}$ on the interface. Thus, we assume that

$$(v_1^{(1)})_{N_x+1,j}^{n+1} = (v_1^{(2)})_{1,j}^{n+1}, \quad (4.83a)$$

$$(v_2^{(1)})_{N_x+1,j}^{n+1} = (v_2^{(2)})_{1,j}^{n+1}. \quad (4.83b)$$

Second, we can discretize Equation (4.59b) using Equations (4.64)-(4.66) as follows:

$$\begin{aligned} & (\lambda^{(1)} + 2\mu^{(1)})(\varepsilon_x^{(1)})_{N_x+1,j}^{n+1} + \lambda^{(1)}(\varepsilon_y^{(1)})_{N_x+1,j}^{n+1} - (3\lambda^{(1)} + 2\mu^{(1)})\alpha_T^{(1)}[(T_l^{(1)})_{N_x+1,j}^{n+1} - T_0] \\ & = (\lambda^{(2)} + 2\mu^{(2)})(\varepsilon_x^{(2)})_{1,j}^{n+1} + \lambda^{(2)}(\varepsilon_y^{(2)})_{1,j}^{n+1} - (3\lambda^{(2)} + 2\mu^{(2)})\alpha_T^{(2)}[(T_l^{(2)})_{1,j}^{n+1} - T_0], \end{aligned} \quad (4.84a)$$

$$\mu^{(1)}(\varepsilon_{xy}^{(1)})_{N_x+1,j}^{n+1} = \mu^{(2)}(\varepsilon_{xy}^{(2)})_{1,j}^{n+1}, \quad (4.84b)$$

where $(\varepsilon_x^{(1)})_{N_x+1,j}^{n+1}$, $(\varepsilon_x^{(2)})_{1,j}^{n+1}$, $(\varepsilon_y^{(1)})_{N_x+1,j}^{n+1}$, $(\varepsilon_y^{(2)})_{1,j}^{n+1}$, $(\varepsilon_{xy}^{(1)})_{N_x+1,j}^{n+1}$ and $(\varepsilon_{xy}^{(2)})_{1,j}^{n+1}$ can be obtained by

Equations (4.67a)-(4.67c) as follows:

$$(\varepsilon_x^{(1)})_{N_x+1,j}^{n+1} = \frac{(v_1^{(1)})_{N_x+1,j}^{n+1} - (v_1^{(1)})_{N_x,j}^{n+1}}{\Delta x} \Delta t + (\varepsilon_x^{(1)})_{N_x+1,j}^n, \quad (4.85a)$$

$$(\varepsilon_x^{(2)})_{1,j}^{n+1} = \frac{(v_1^{(2)})_{2,j}^{n+1} - (v_1^{(2)})_{1,j}^{n+1}}{\Delta x} \Delta t + (\varepsilon_x^{(2)})_{1,j}^n, \quad (4.85b)$$

$$(\varepsilon_y^{(1)})_{N_x+1,j}^{n+1} = \frac{(v_2^{(1)})_{N_x+1,j}^{n+1} - (v_2^{(1)})_{N_x+1,j-1}^{n+1}}{\Delta y} \Delta t + (\varepsilon_y^{(1)})_{N_x+1,j}^n, \quad (4.86a)$$

$$(\varepsilon_y^{(2)})_{1,j}^{n+1} = \frac{(v_2^{(2)})_{1,j}^{n+1} - (v_2^{(2)})_{1,j-1}^{n+1}}{\Delta y} \Delta t + (\varepsilon_y^{(2)})_{1,j}^n, \quad (4.86b)$$

$$\begin{aligned}
(\varepsilon_{xy}^{(1)})_{N_x+1,j}^{n+1} &= \frac{\Delta t}{\Delta y} [(v_1^{(1)})_{N_x+1,j+1}^{n+1} - (v_1^{(1)})_{N_x+1,j}^{n+1}] + \frac{\Delta t}{\Delta x} [(v_2^{(1)})_{N_x+1,j}^{n+1} - (v_2^{(1)})_{N_x,j}^{n+1}] \\
&+ (\varepsilon_{xy}^{(1)})_{N_x+1,j}^n,
\end{aligned} \tag{4.87a}$$

$$\begin{aligned}
(\varepsilon_{xy}^{(2)})_{1,j}^{n+1} &= \frac{\Delta t}{\Delta y} [(v_1^{(2)})_{1,j+1}^{n+1} - (v_1^{(2)})_{1,j}^{n+1}] + \frac{\Delta t}{\Delta x} [(v_2^{(2)})_{2,j}^{n+1} - (v_2^{(2)})_{1,j}^{n+1}] \\
&+ (\varepsilon_{xy}^{(2)})_{1,j}^n,
\end{aligned} \tag{4.87b}$$

where $1 \leq j \leq N_y + 1$.

Third, Equation (4.59c) can be discretized as

$$(T_e^{(1)})_{N_x+1,j}^{n+1} = (T_e^{(2)})_{1,j}^{n+1}, \tag{4.88a}$$

$$(T_l^{(1)})_{N_x+1,j}^{n+1} = (T_l^{(2)})_{1,j}^{n+1}, \tag{4.88b}$$

$$(q_e^{x(1)})_{N_x,j}^{n+1} = (q_e^{x(2)})_{1,j}^{n+1}, \tag{4.88c}$$

$$(q_l^{x(1)})_{N_x,j}^{n+1} = (q_l^{x(2)})_{1,j}^{n+1}, \tag{4.88d}$$

for any time level n and $1 \leq j \leq N_y + 1$.

For the initial conditions, Equation (4.58), we can approximate it as

$$(u^{(m)})_{i+\frac{1}{2},j}^0 = 0, (v^{(m)})_{i,j+\frac{1}{2}}^0 = 0, \tag{4.89a}$$

$$(v_1^{(m)})_{i+\frac{1}{2},j}^0 = 0, (v_2^{(m)})_{i,j+\frac{1}{2}}^0 = 0, \tag{4.89b}$$

$$(T_e^{(m)})_{i,j}^0 = (T_l^{(m)})_{i,j}^0 = T_0, \tag{4.89c}$$

where $1 \leq i \leq N_x + 1, 1 \leq j \leq N_y + 1$ and $m = 1, 2$.

4.2.4 Algorithm

In the finite difference scheme shown in the previous section, the truncation error of Equations (4.67)-(4.69) is $O(\Delta t + \Delta x^2 + \Delta y^2)$ and the truncation error of Equations (4.73)-(4.78) is $O(\Delta t^2 + \Delta x^2 + \Delta y^2)$. We should notice that Equations (4.67) and (4.69) are nonlinear since they contain nonlinear terms $\delta_x (T_e^2)_{i+1/2,j}^{n+1}$ and $\delta_y (T_e^2)_{i,j+1/2}^{n+1}$. Similarly, Equations (4.73)-(4.78) are also nonlinear. Therefore, we have to solve the scheme iteratively. The following algorithm is an iterative method for solving the finite difference scheme at time level $n + 1$ developed in the previous section.

Step 1: Guess $(\varepsilon_x^{(m)})^{n+1}$, $(\varepsilon_y^{(m)})^{n+1}$ and $(\varepsilon_{xy}^{(m)})^{n+1}$ using their values at previous time step. Obtain $(q_e^{x(m)})^{n+1}$, $(q_e^{y(m)})^{n+1}$, $(q_l^{x(m)})^{n+1}$ and $(q_l^{y(m)})^{n+1}$ based on Equations (4.74), (4.75), (4.77), (4.78) and the interfacial conditions (4.88), and substitute into Equation (4.73) and (4.76) to obtain $(T_e^{(m)})^{n+1}$ and $(T_l^{(m)})^{n+1}$.

Step 2: Solve Equations (4.70)-(4.72) for $(\sigma_x^{(m)})^{n+1}$, $(\sigma_y^{(m)})^{n+1}$ and $(\sigma_{xy}^{(m)})^{n+1}$.

Step 3: Solve Equations (4.68) and (4.69) for $(v_1^{(m)})^{n+1}$ and $(v_2^{(m)})^{n+1}$.

Step 4: Update $(\varepsilon_x^{(m)})^{n+1}$, $(\varepsilon_y^{(m)})^{n+1}$ and $(\varepsilon_{xy}^{(m)})^{n+1}$ by using Equations (4.67a)-(4.67c). Given the required accuracy, repeat the above steps until a convergent solution is obtained based on the following criteria:

$$\max |(\varepsilon_x^{(m)})^{n+1(new)} - (\varepsilon_x^{(m)})^{n+1(old)}| \leq \varepsilon, \quad (4.90a)$$

$$\max |(\varepsilon_y^{(m)})^{n+1(new)} - (\varepsilon_y^{(m)})^{n+1(old)}| \leq \varepsilon, \quad (4.90b)$$

$$\max |(\varepsilon_{xy}^{(m)})^{n+1(new)} - (\varepsilon_{xy}^{(m)})^{n+1(old)}| \leq \varepsilon. \quad (4.90c)$$

Step 5: Solve Equations (4.79a) and (4.79b) for $(u^{(m)})^{n+1}$ and $(v^{(m)})^{n+1}$.

CHAPTER 5

NUMERICAL EXAMPLES

5.1 One-Dimensional Double-Layered Case

In this chapter, we will consider three cases in order to test our scheme.

5.1.1 Example Description

To demonstrate the applicability of the numerical scheme mentioned in section 3.2, we investigate the temperature rise in a one-dimensional double-layered thin film, namely a gold layer on a chromium layer, where each layer is $0.05 \mu\text{m}$ in thickness as shown in Figure 5.1.

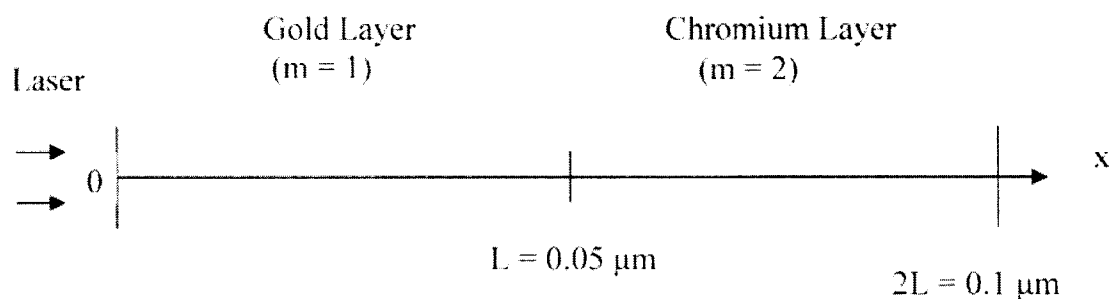


Figure 5.1 Configuration of a 1D double-layered thin film.

The heat source was chosen to be

$$S^{(m)}(x,t) = 0.94J \left[\frac{1-R}{t_p \delta} \right] \exp \left(-\frac{x + L(m-1)}{\delta} - 2.77 \left(\frac{t - 2t_p}{t_p} \right)^2 \right). \quad (5.1)$$

where $m = 1, 2$, $L = 0.05 \mu\text{m}$, $t_p = 0.1 \text{ps}$, $\delta = 15.3 \text{nm}$, $R = 0.93$ and $J = 13.4 \text{J}/\text{m}^2$.

The initial temperature T_0 for T_e and T_l is chosen to be 300K .

The thermal properties for gold and chromium used in this analysis are shown in Table 5.1. Due to the lack of information on τ_e and τ_l for chromium, we use various values of τ_e and τ_l for chromium based on the analysis in [Tzou 1996].

Table 5.1 Thermal properties of gold and chromium [Chen 2003, Tzou 1996]

Parameters	Gold ($m = 1$)	Chromium ($m = 2$)
$k_0 (\text{J}/\text{mmKps})$	3.15×10^{-13}	9.4×10^{-14}
$C_l (\text{J}/\text{mm}^3 \text{K})$	2.5×10^{-3}	3.3×10^{-3}
$G (\text{J}/\text{mm}^3 \text{Kps})$	2.6×10^{-5}	42×10^{-5}
$A_e (\text{J}/\text{mm}^3 \text{K}^2)$	7.0×10^{-8}	1.933×10^{-7}
$\tau_e (\text{ps})$	0.04	
$\tau_l (\text{ps})$	0.8	

5.1.2 Results and Analysis

Figure 5.2 shows the change in temperature ($\Delta T_e / (\Delta T_e)_{\max}$) on the surface of the gold layer with the fluence of $J = 13.4 \text{J}/\text{m}^2$, where τ_e for chromium is chosen to be 0.00136ps and τ_l for chromium to be 0.0136ps , 0.0272ps and 0.0544ps , respectively.

Results are obtained with a mesh of 200 points for each layer and a time increment, Δt , of 0.005 ps . The maximum electron temperature is 759.1 K . We also make a comparison between our result and that of the parabolic two-step model, which is calculated using the Crank-Nicholson method. It is clear that there is no significant difference among the solutions with various values of τ_l for chromium. However, there is a slight difference between the parabolic model and our hyperbolic model, which indicates the effect of τ_e and τ_l .

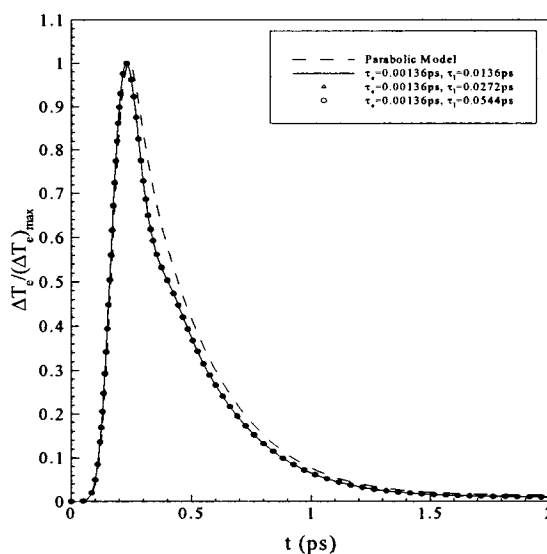


Figure 5.2 Normalized electron temperatures at the front surface of a 100 nm gold and chromium thin film with $\tau_e = 0.00136 \text{ ps}$ and three difference values of τ_l for chromium.

Furthermore, we obtain similar results for the case when τ_e for chromium is changed to be 0.0068 ps and τ_l for chromium to be 0.068 ps , 0.136 ps and 0.272 ps , respectively, as shown in Figure 5.3, and for the other case when τ_e for chromium is

chosen to be 0.0136 ps and τ_l for chromium to be 0.136 ps , 0.272 ps and 0.544 ps , respectively, which is shown in Figure 5.4.

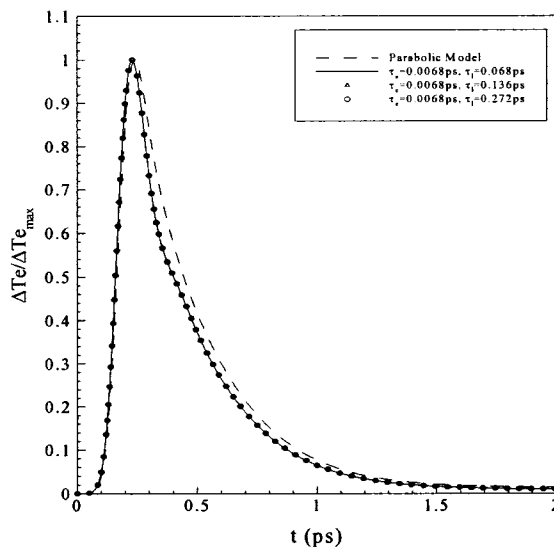


Figure 5.3 Normalized electron temperatures at the front surface of a 100 nm gold and chromium thin film with $\tau_e = 0.0068 \text{ ps}$ and three difference values of τ_l for chromium.

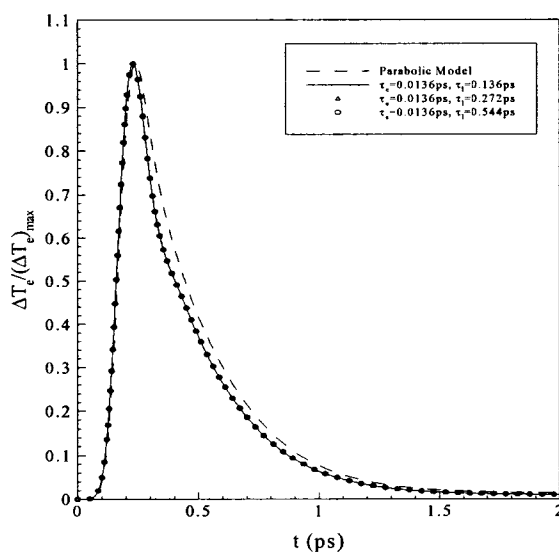


Figure 5.4 Normalized electron temperatures at the front surface of a 100 nm gold and chromium thin film with $\tau_e = 0.0136 \text{ ps}$ and three difference values of τ_l for chromium.

In order to check the effect of grid size, we plot the change in temperature ($\Delta T_e / (\Delta T_e)_{\max}$) on the surface of the gold layer utilizing three different meshes of 100, 200, and 400 for each layer, as shown in Figure 5.5. From it, we can conclude that grid size has no significant effect on the solution. Therefore, our method is grid independent.

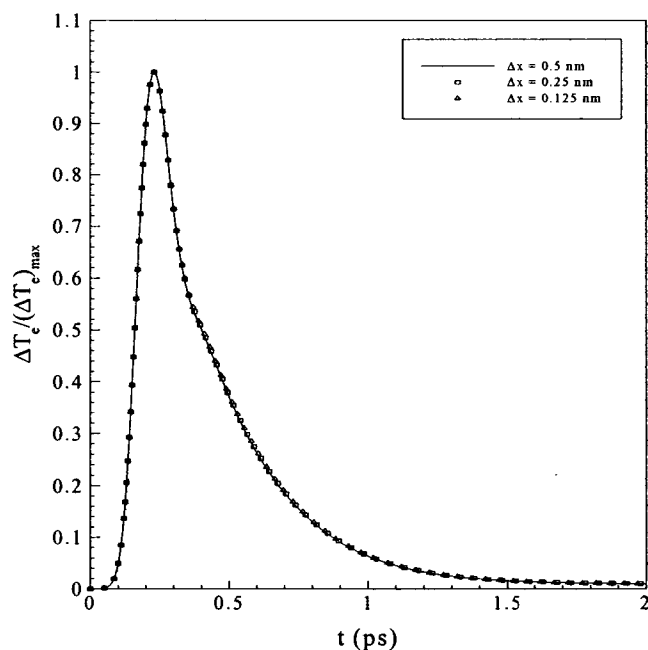


Figure 5.5 Normalized electron temperatures at the front surface of a 100 nm gold and chromium thin film with $\tau_e = 0.00136 ps$ and $\tau_l = 0.0136 ps$ for chromium and three different meshes.

Figures 5.6 and 5.7 provide the electron temperature profiles and lattice temperature profiles along the x-axis for time $t = 0.2, 0.3,$ and $1.2 ps$, respectively. Results are obtained using a time increment of $0.005 ps$ and a mesh of 200 points for each layer.

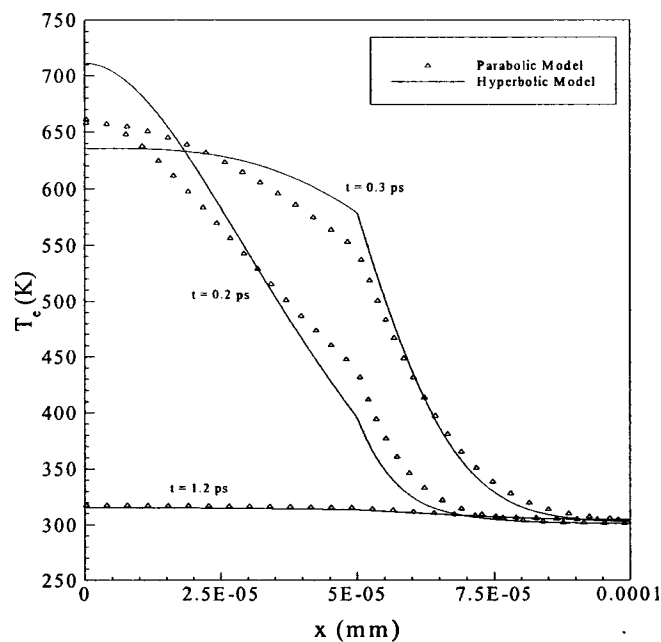


Figure 5.6 Calculated electron temperature profiles for a 100 nm gold and chromium thin film with $\tau_e = 0.0068 ps$ and $\tau_l = 0.136 ps$ for chromium.

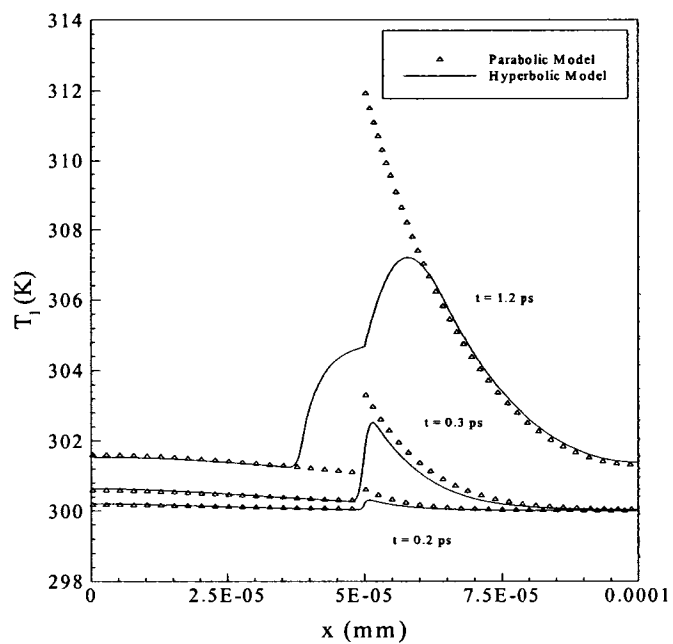


Figure 5.7 Calculated lattice temperature profiles for a 100 nm gold and chromium thin film with $\tau_e = 0.0068 ps$ and $\tau_l = 0.136 ps$ for chromium.

5.2 Two-Dimensional Single-Layered Case

5.2.1 Example Description

In this example, we want to test the applicability of the finite different scheme developed in section 4.1, Equations (4.24)-(4.43). For this purpose, we investigate the temperature rise and deformation in a two-dimensional single-layered micro thin film with the dimensions $0.1\mu m$ (thickness) $\times 1\mu m$ (length), as shown in Figure 5.8. The heat source is given by

$$S(x, y, t) = 0.94J \frac{1-R}{t_p x_s} \exp \left[-\frac{x}{x_s} - \left(\frac{y}{y_s} \right)^2 - 2.77 \left(\frac{t-2t_p}{t_p} \right)^2 \right], \quad (5.2)$$

where $J = 500 J/m^2$, $R = 0.93$, $t_p = 0.1 \times 10^{-12} s$, $x_s = 15.3 \times 10^{-9} m$ and $y_s = 1.0 \times 10^{-6} m$.

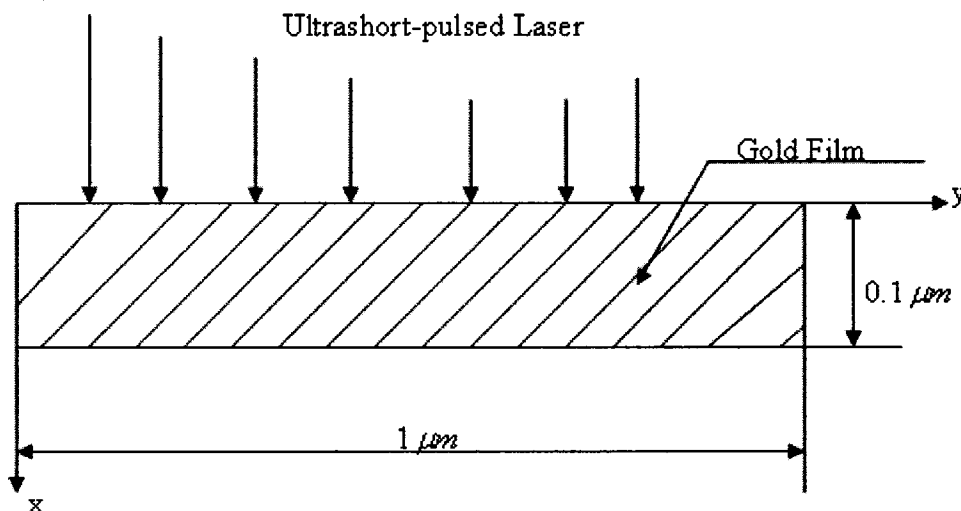


Figure 5.8 Configuration of a 2D single-layered thin film.

In order to test the convergence of the scheme, we choose three different meshes of 80×40 , 160×80 , 300×150 . The time increment is 0.005 ps . The initial temperature T_0 is chosen to be 300 K .

The thermophysical properties for gold are listed in Table 5.2 [Tzou 2002, Chen 2002a, Kaye 1973].

Table 5.2 Thermophysical properties of gold [Tzou 2002, Chen 2002a, Kaye 1973]

Properties	Unit	Value
ρ	kg/m^3	19300
Λ	$J/m^3 K^2$	70
K	Pa	217×10^9
μ	Pa	27×10^9
α_T	K^{-1}	14.2×10^{-6}
A_e	$J/m^3 K^2$	70
C_l	$J/m^3 K$	2.5×10^6
G	$W/m^3 K$	2.6×10^{16}
τ_e	ps	0.04
τ_l	ps	0.8
$k_0(k_l)$	W/mK	315

5.2.2 Results and Analysis

Figure 5.9 shows the change in electron temperature ($\Delta T_e / (\Delta T_e)_{\max}$) at $x = 0$ and $y = 0$ versus time for various meshes (80×40 , 160×80 and 300×150). The maximum temperature rise of T_e , which is $(\Delta T_e)_{\max}$, is about 3943 K, which is close to that obtained by Qiu and Tien [Qiu 1994]. Meanwhile, by comparing our results with that of the parabolic model [Wang 2006a] in Figure 5.9, we can see a slight difference between the parabolic model and our hyperbolic model, which indicates the effect of relaxation time τ_e and τ_l . Figure 5.10 shows the displacement (u) at $x = 0$ and $y = 0$ versus time for various meshes (80×40 , 160×80 and 300×150). Both figures show that the solutions are convergent as the mesh is getting better.

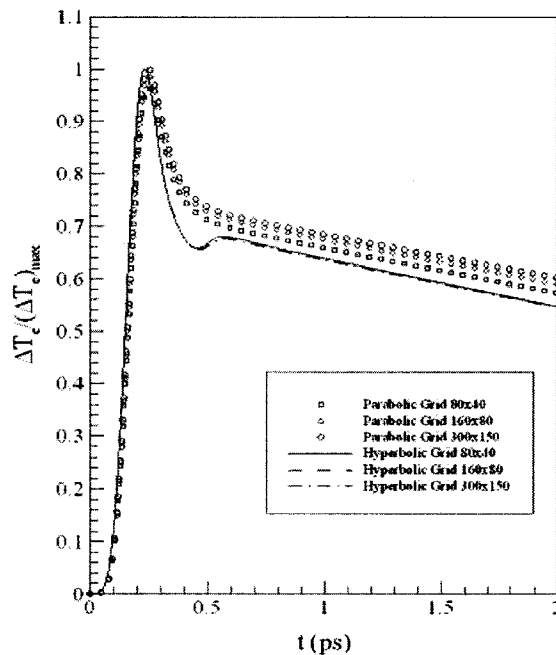


Figure 5.9 Change in electron temperature at $x = 0$ and $y = 0$ versus time for various meshes (80×40 , 160×80 and 300×150) comparing with parabolic model [Wang 2006a].

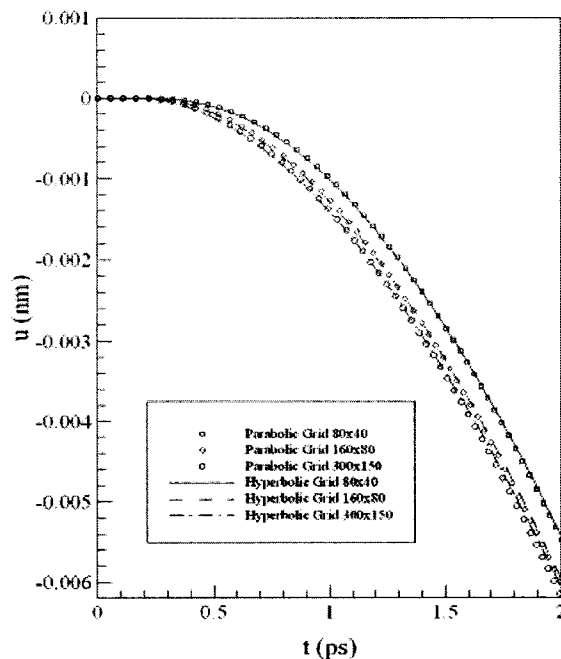


Figure 5.10 Displacement (u) at $x = 0$ and $y = 0$ versus time for various meshes (80×40 , 160×80 and 300×150) with parabolic model [Wang 2006a].

Figure 5.11 is obtained using a mesh of 160×80 and $\Delta t = 0.005 ps$. In Figure 5.11, we compare the normal stress (σ_x) at $y = 0 \mu m$ and $t = 10 ps$ obtained by our hyperbolic two-step model, the parabolic model [Wang 2006a], and Chen et al.'s method [Chen 2002a]. The figure shows that the present method and the method based on the parabolic two-step model avoid non-physical oscillations in the solution.

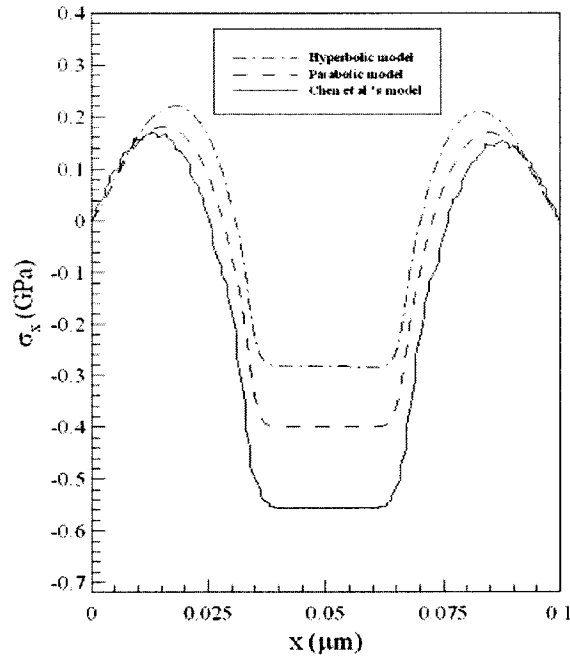
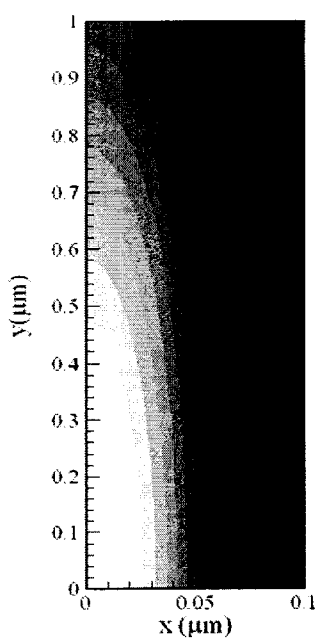
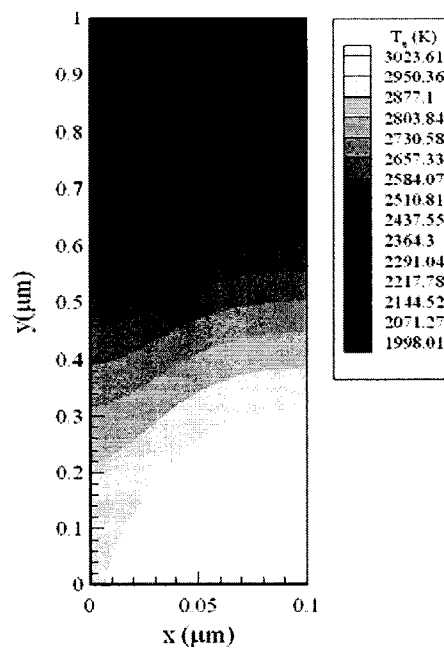


Figure 5.11 Comparison of the hyperbolic model, parabolic model [Wang 2006a] and Chen *et al.*'s method in [Chen 2002a] with regard to the normal stress (σ_x) at $y = 0 \mu\text{m}$ at $t = 10 \text{ps}$.

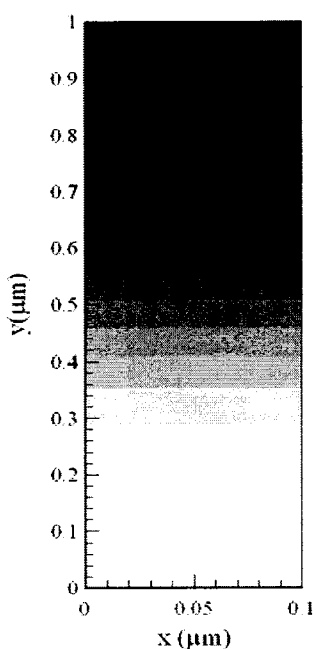
Figure 5.12 and 5.13 are the contour plots showing respectively electron temperature and lattice temperature profiles at different times (a) $t = 0.25 \text{ps}$, (b) $t = 0.5 \text{ps}$, (c) $t = 1 \text{ps}$, (d) $t = 10 \text{ps}$, and (e) $t = 20 \text{ps}$. From Figure 5.12, we can see that the electron temperature rises to its maximum at the beginning and then decreases to a uniform distribution at $t = 20 \text{ps}$ while the lattice temperature rises gradually with time.



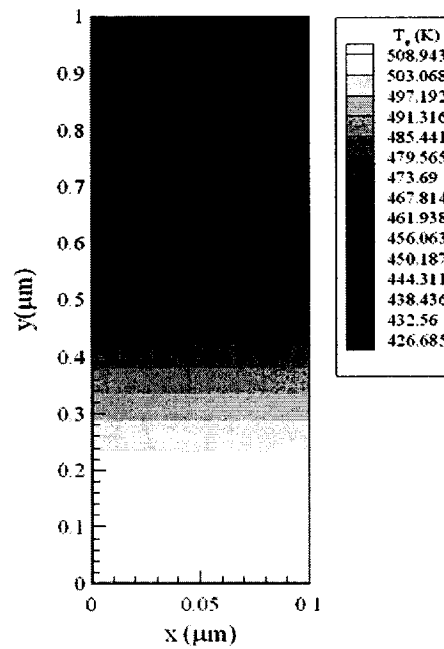
(a)



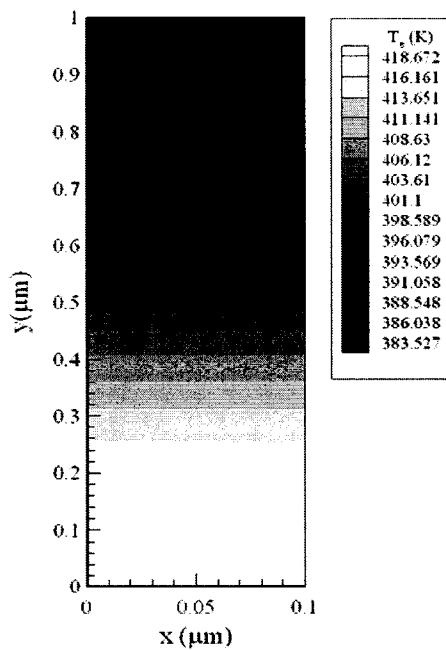
(b)



(c)

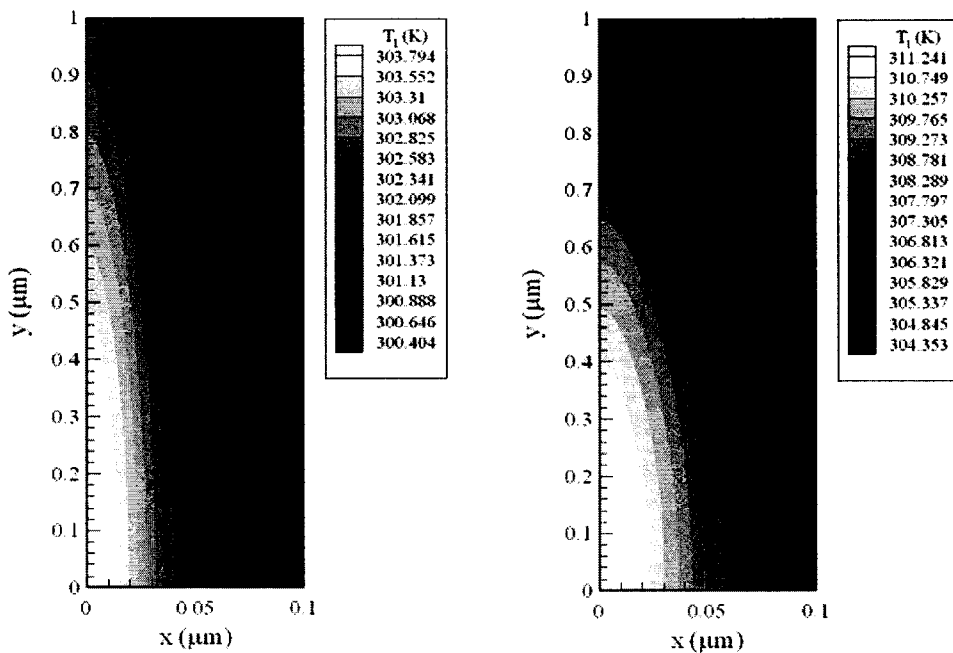


(d)



(e)

Figure 5.12 Contour plots of electron temperature distributions at (a) $t = 0.25 ps$, (b) $t = 0.5 ps$, (c) $t = 1 ps$, (d) $t = 10 ps$, and (e) $t = 20 ps$.



(a)

(b)

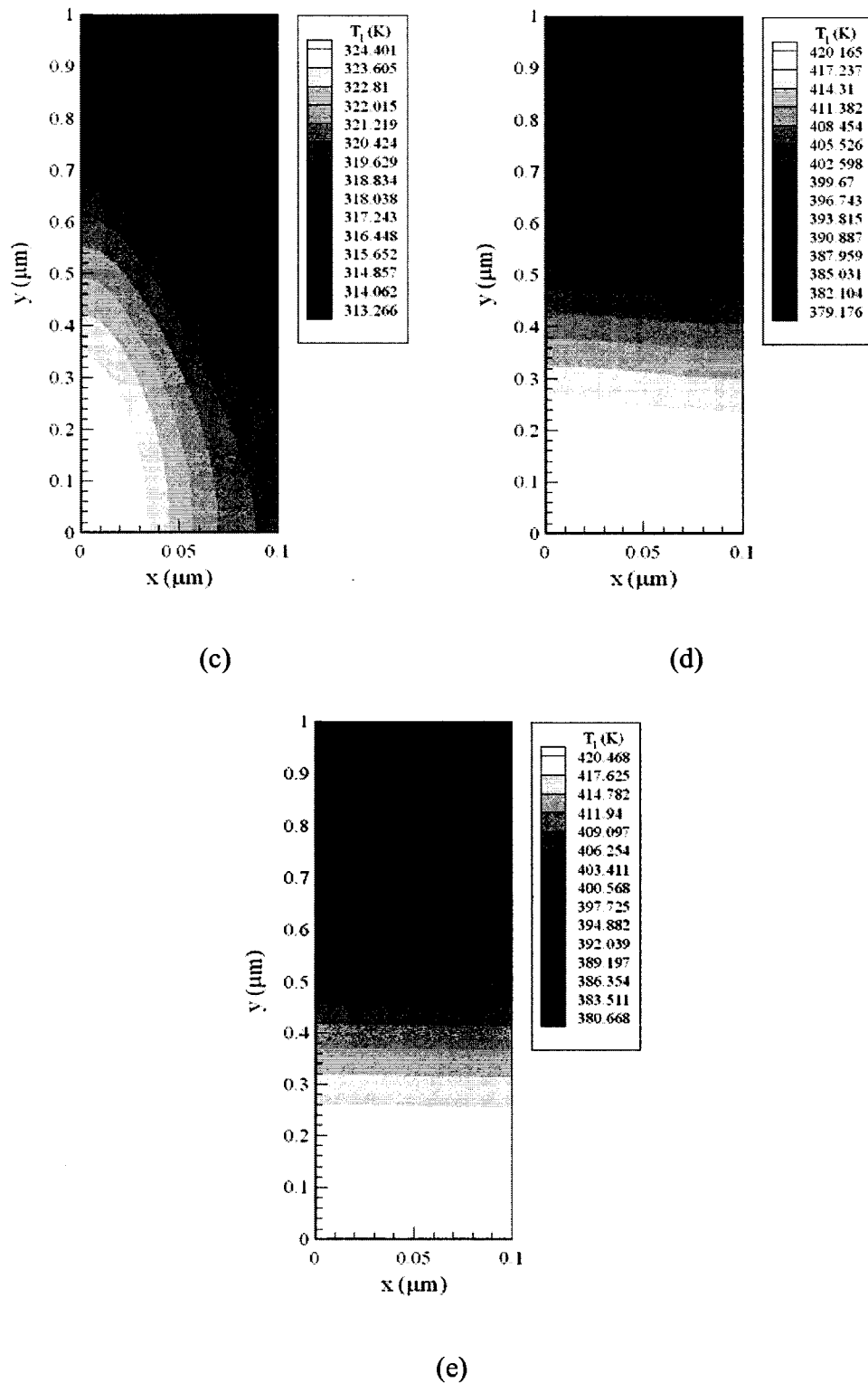
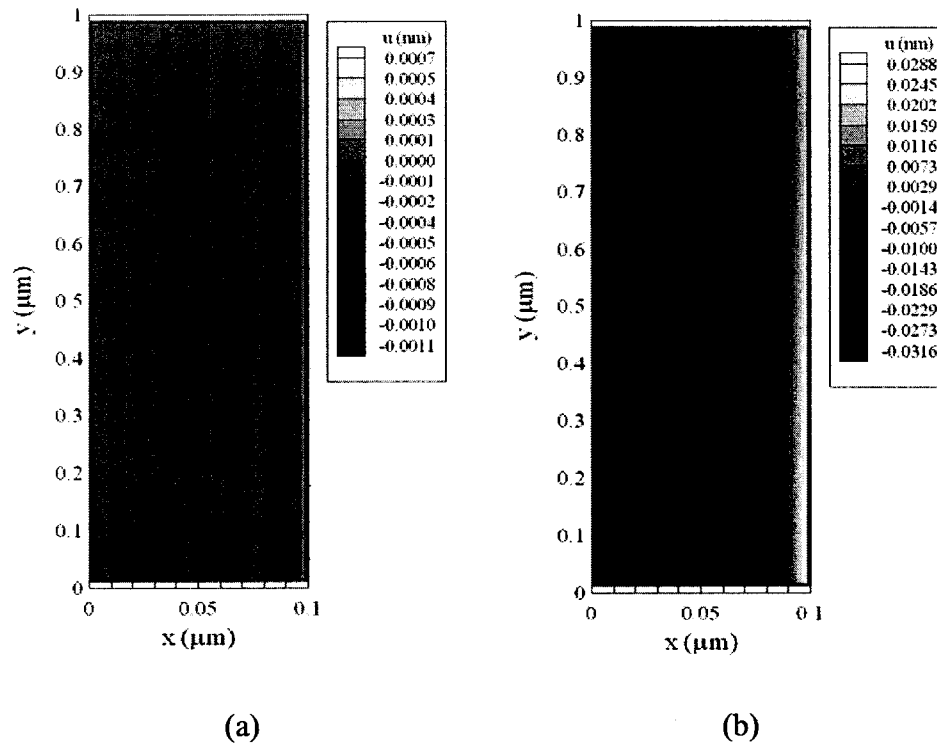


Figure 5.13 Contour plots of lattice temperature distributions at (a) $t = 0.25 \text{ ps}$, (b) $t = 0.5 \text{ ps}$, (c) $t = 1 \text{ ps}$, (d) $t = 10 \text{ ps}$, and (e) $t = 20 \text{ ps}$.

Figure 5.14 and Figure 5.15 are the contour plots of displacement u (thickness direction) and displacement v (length direction) profiles at different times (a) $t = 1ps$, (b) $t = 5ps$, (c) $t = 10ps$, (d) $t = 15ps$, and (e) $t = 20ps$.



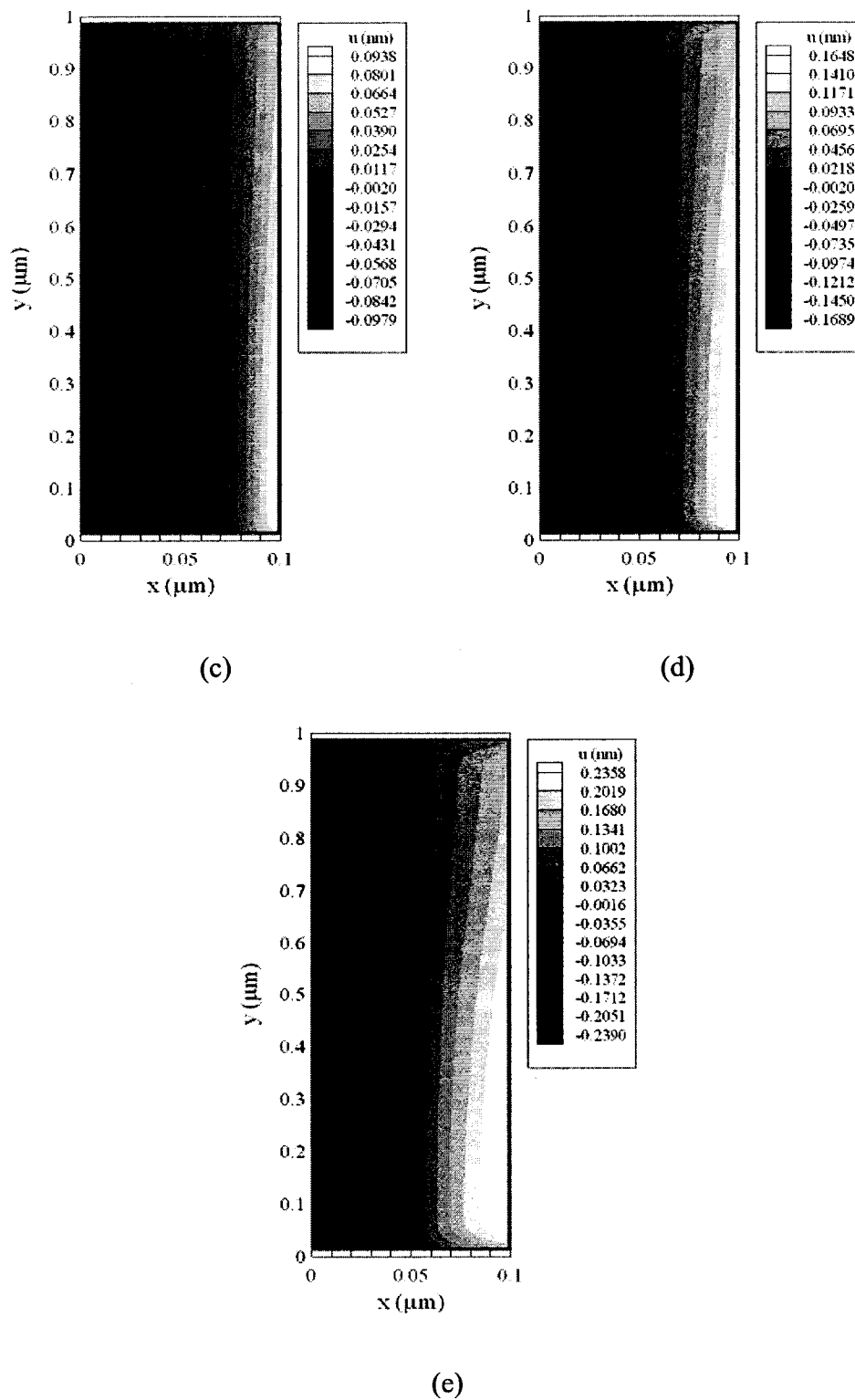
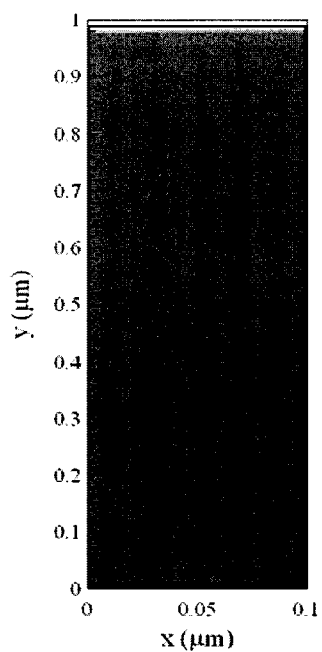
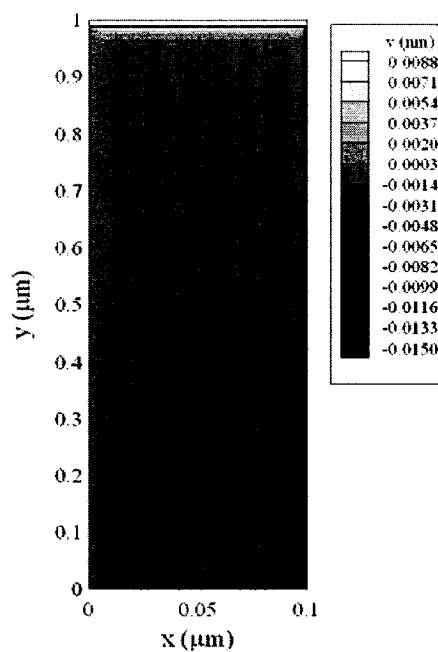


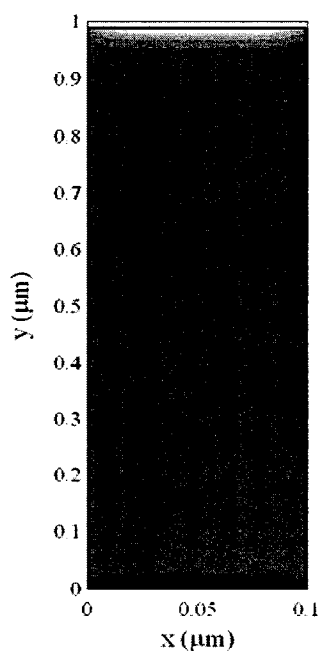
Figure 5.14 Contour plots of displacement (u) distributions at (a) $t = 1 \text{ ps}$, (b) $t = 5 \text{ ps}$, (c) $t = 10 \text{ ps}$, (d) $t = 15 \text{ ps}$, and (e) $t = 20 \text{ ps}$.



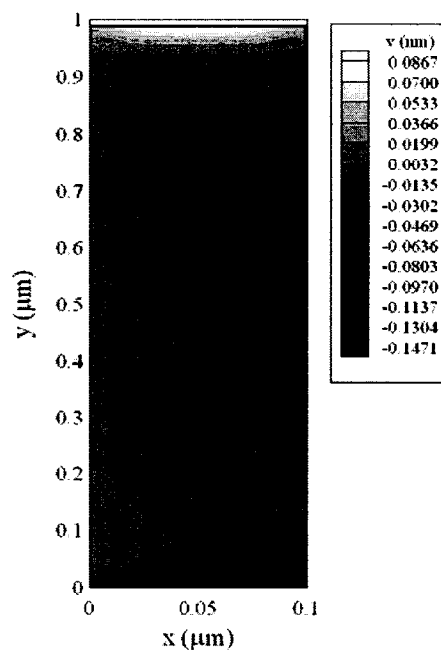
(a)



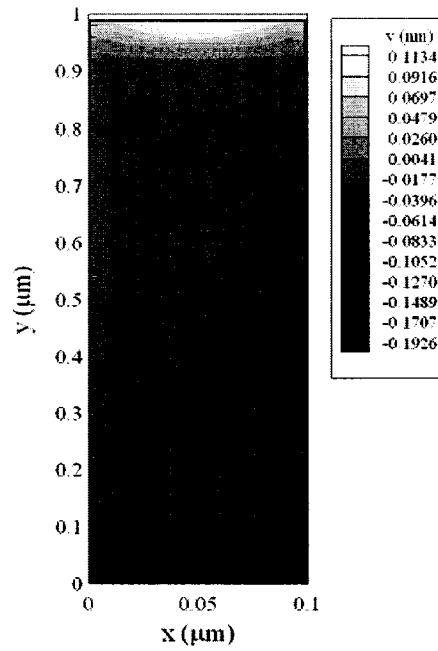
(b)



(c)



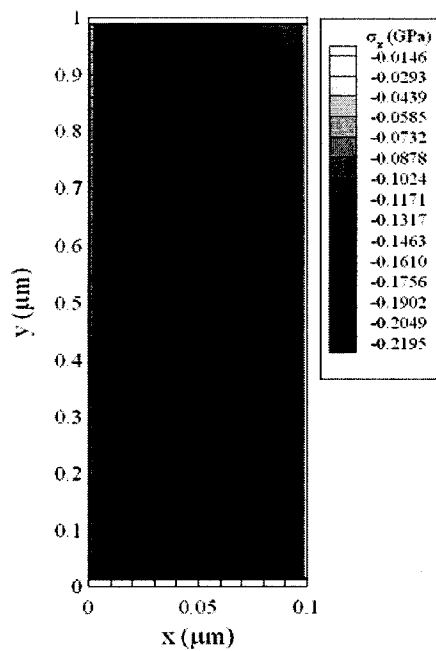
(d)



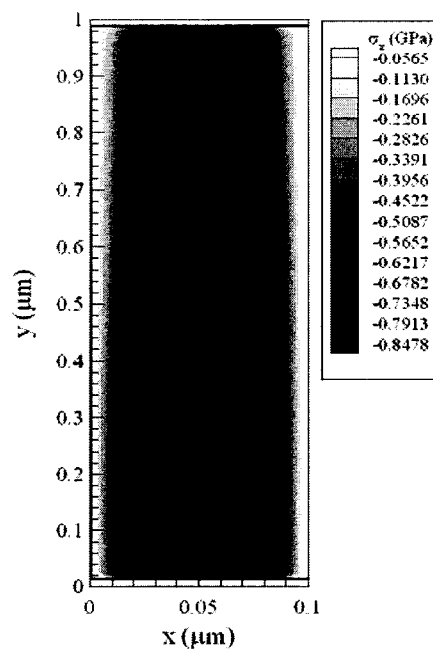
(e)

Figure 5.15 Contour plots of displacement (v) distributions at (a) $t = 1ps$, (b) $t = 5ps$, (c) $t = 10ps$, (d) $t = 15ps$, and (e) $t = 20ps$.

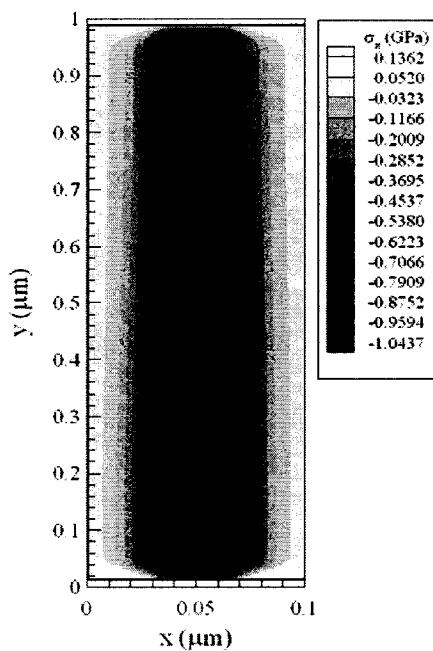
Figure 5.16 and Figure 5.17 are the contour plots of normal stress σ_x (thickness direction) and normal stress σ_y (length direction) profiles at different times (a) $t = 1ps$, (b) $t = 5ps$, (c) $t = 10ps$, (d) $t = 15ps$, and (e) $t = 20ps$.



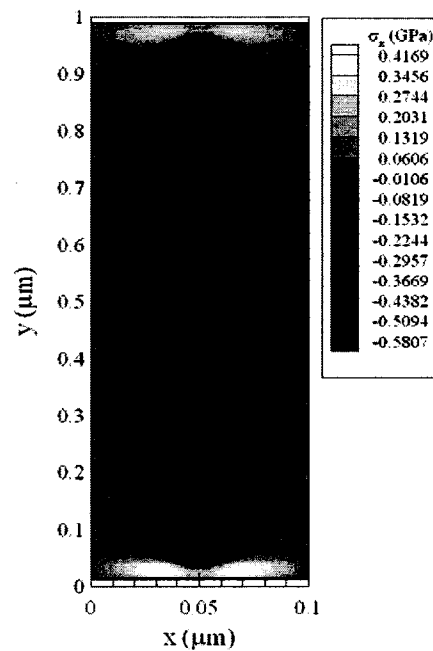
(a)



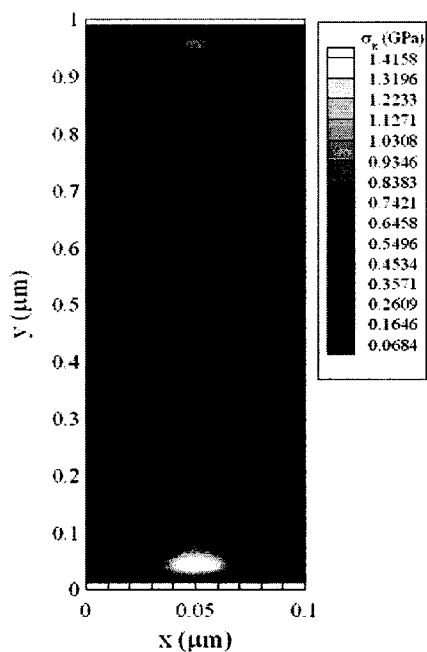
(b)



(c)

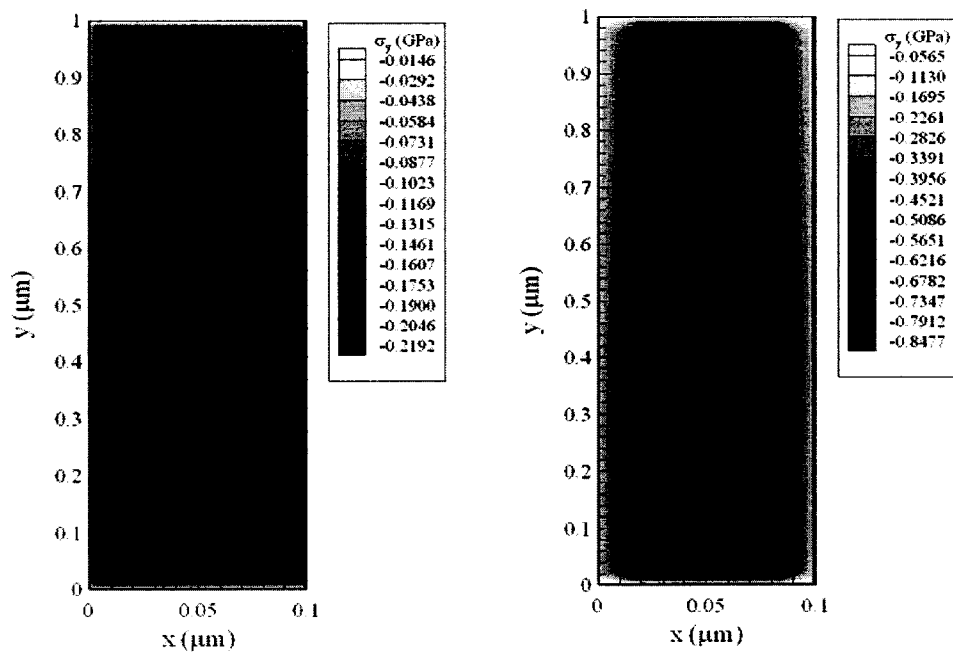


(d)



(e)

Figure 5.16 Contour plots of normal stress (σ_x) distributions at (a) $t = 1$ ps, (b) $t = 5$ ps, (c) $t = 10$ ps, (d) $t = 15$ ps, and (e) $t = 20$ ps.



(a)

(b)

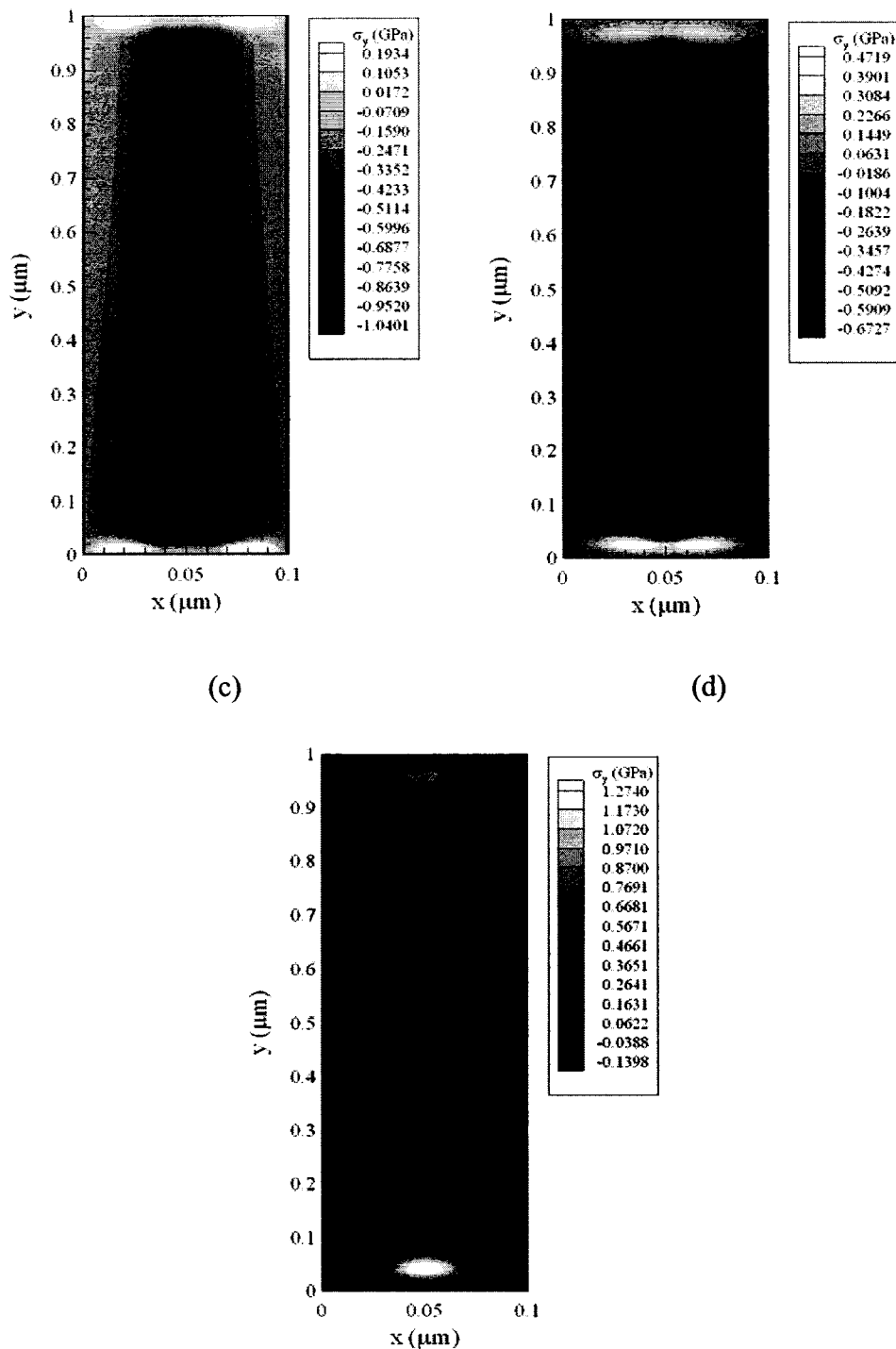


Figure 5.17 Contour plots of normal stress (σ_y) distributions at (a) $t = 1 \text{ ps}$, (b) $t = 5 \text{ ps}$, (c) $t = 10 \text{ ps}$, (d) $t = 15 \text{ ps}$, and (e) $t = 20 \text{ ps}$.

Based on the analysis of displacement and stress waves, we can conclude the significance of the hot-electron-blast effect on the ultrafast deformation mainly along the thickness direction. Furthermore, the proposed methodology allows us to avoid non-physical oscillations of the solution.

5.3 Two-Dimensional Double-Layered Case

5.3.1 Example Description

In order to test the applicability of the numerical scheme developed in section 4.2, Equations (4.67)-(4.82), we consider the temperature rise and deformation in a two-dimensional double-layered thin film, which is a gold layer padding on a chromium layer with the dimensions $0.05\ \mu\text{m}$ (thickness) \times $1\ \mu\text{m}$ (length) for each layer, as shown in Figure 5.18. Here, we assume that the interface of the two layers is perfectly contacted.

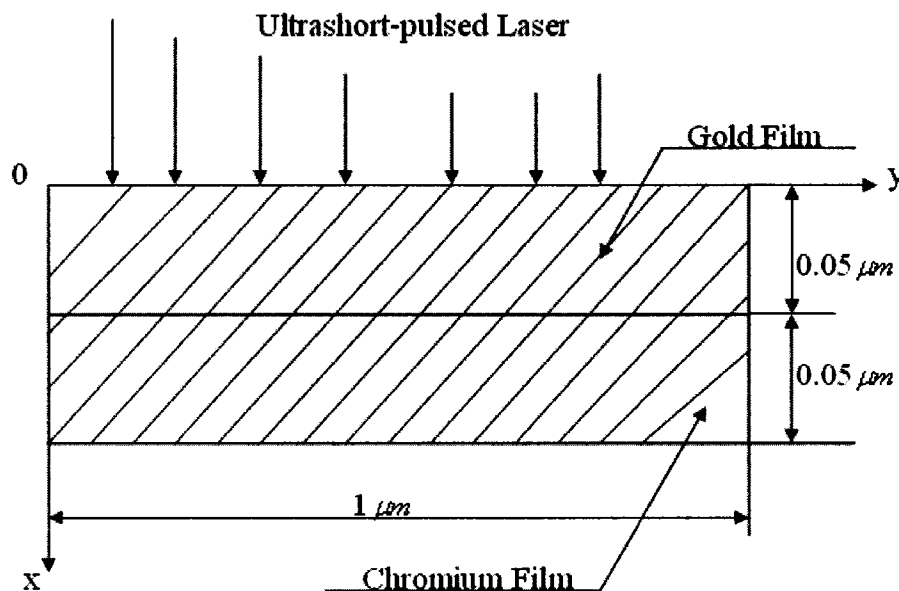


Figure 5.18 Configuration of a 2D double-layered micro thin film.

The electron thermal conductivity ($k_e(T_e, T_l)^{(m)}$) is chosen to be [Chen 2002a, Qiu 1992 and Tzou 2002]

$$(k_e(T_e, T_l))^{(m)} = k_0^{(m)} \cdot \frac{T_e^{(m)}}{T_l^{(m)}}. \quad (5.3)$$

The heat source is given by

$$S(x, y, t) = 0.94J \frac{1-R}{t_p x_s} \exp \left[-\frac{x}{x_s} - \left(\frac{y}{y_s} \right)^2 - 2.77 \left(\frac{t-2t_p}{t_p} \right)^2 \right], \quad (5.4)$$

where $R = 0.93$, $t_p = 0.1 \times 10^{-12} s$, $x_s = 15.3 \times 10^{-9} m$ and $y_s = 1.0 \times 10^{-6} m$.

The thermophysical properties for gold and chromium are listed in Table 5.3 [Touloukian 1970a, b, Chen 2003, Tzou 1996].

Table 5.3 Thermophysical properties of gold and chromium [Touloukian 1970a, b, Chen 2003, Tzou 1996]

Properties	Unit	Gold	Chromium
ρ	kg/m^3	19300	7190
Λ	$J/m^3 K^2$	70	193.3
λ	Pa	199.0×10^9	83.3×10^9
μ	Pa	27×10^9	115.0×10^9
α_T	K^{-1}	14.2×10^{-6}	4.9×10^{-6}
A_e	$J/m^3 K^2$	70	193.3
C_l	$J/m^3 K$	2.5×10^6	3.3×10^6
G	$W/m^3 K$	2.6×10^{16}	42×10^{16}

τ_e	ps	0.04	0.0068
τ_l	ps	0.8	0.136
$k_0(k_l)$	W/mK	315	94

In this example, we choose three different meshes of 80×40 , 160×80 and 200×100 to test the convergence of the scheme. The time increment is $0.005 ps$. The initial temperature T_0 is set to be 300 K. In order to study the hot-electron blast force, we use three different values of laser influences $J = 500 J/m^2$, $1000 J/m^2$ and $2000 J/m^2$.

5.3.2 Results and Analysis

Figure 5.19 shows the change in electron temperature $(\Delta T_e / (\Delta T_e)_{\max})$ at $x = 0$ and $y = 0$ versus time for various meshes (80×40 , 160×80 and 200×100) with laser influence $J = 500 J/m^2$. The maximum temperature rise of T_e , which is $(\Delta T_e)_{\max}$, is about 3930 K, which is close to that obtained by Qiu and Tien [Qiu 1994]. Meanwhile, by comparing our results with that of the parabolic model [Wang 2006b] in Figure 5.19, we can see a slight difference between the parabolic model and our hyperbolic model, which indicates the effect of relaxation time τ_e and τ_l . Figure 5.20 shows the displacement (u) at $x = 0$ and $y = 0$ versus time for various meshes (80×40 , 160×80 and 200×100). Both figures show that the mesh size has no significant effect on the solution, implying the solution is convergent.

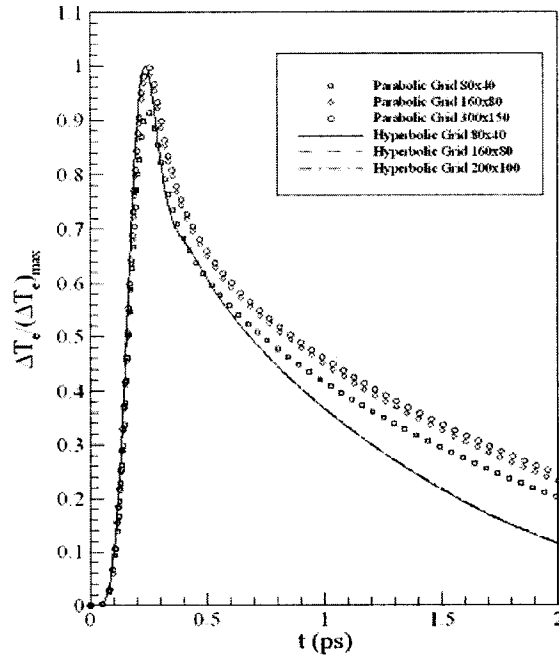


Figure 5.19 Change in electron temperature at $x = 0$ and $y = 0$ versus time for various meshes (80×40 , 160×80 and 200×100) with $J = 500 J/m^2$ comparing with parabolic model [Wang 2006b].

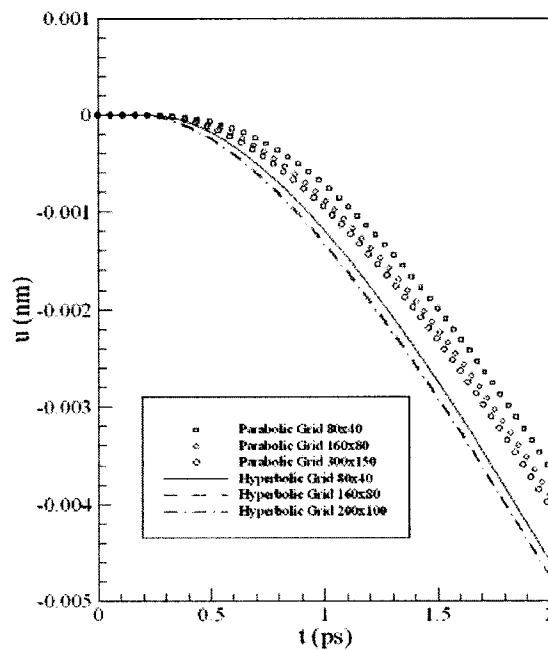
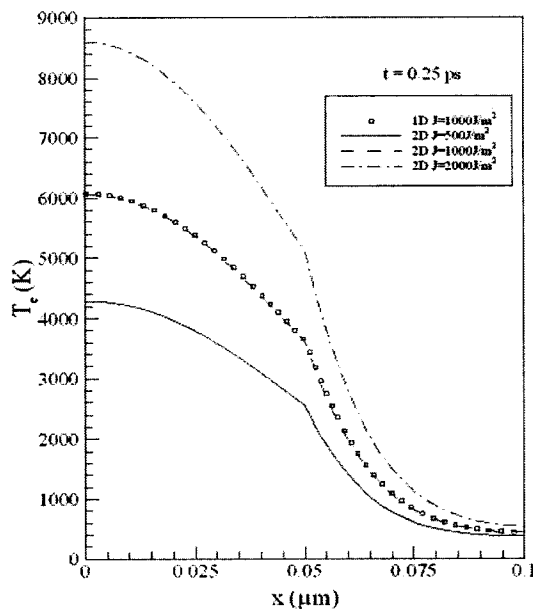
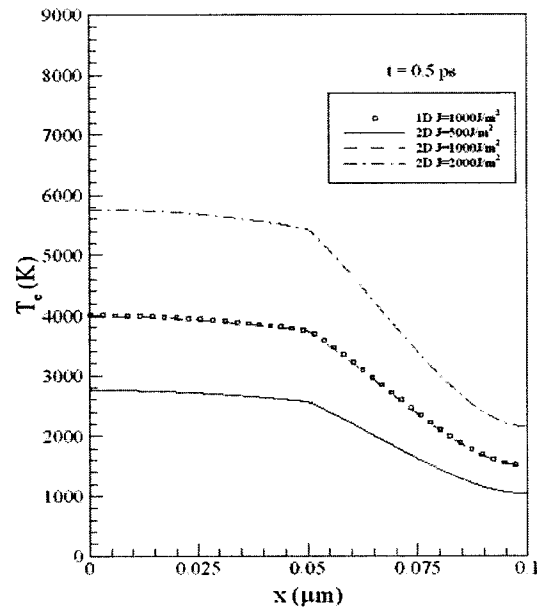


Figure 5.20 Displacement (u) at $x = 0$ and $y = 0$ versus time for various meshes (80×40 , 160×80 and 200×100) with $J = 500 J/m^2$ comparing with parabolic model [Wang 2006b].

Figure 5.21 and Figure 5.22 show respectively the comparison of electron temperature (T_e) and lattice temperature (T_l) versus x at $y = 0 \mu\text{m}$ with three different laser fluences ($J = 500 \text{ J/m}^2$, 1000 J/m^2 and 2000 J/m^2) at various times (a) $t = 0.25 \text{ ps}$, (b) $t = 0.5 \text{ ps}$, (c) $t = 1 \text{ ps}$, (d) $t = 10 \text{ ps}$, and (e) $t = 20 \text{ ps}$. It can be seen that the electron temperature reaches its maximum at the beginning and then decreases, whereas the lattice temperature increases gradually with time. Furthermore, the heat is transferred from the gold layer to the chromium layer.



(a)



(b)

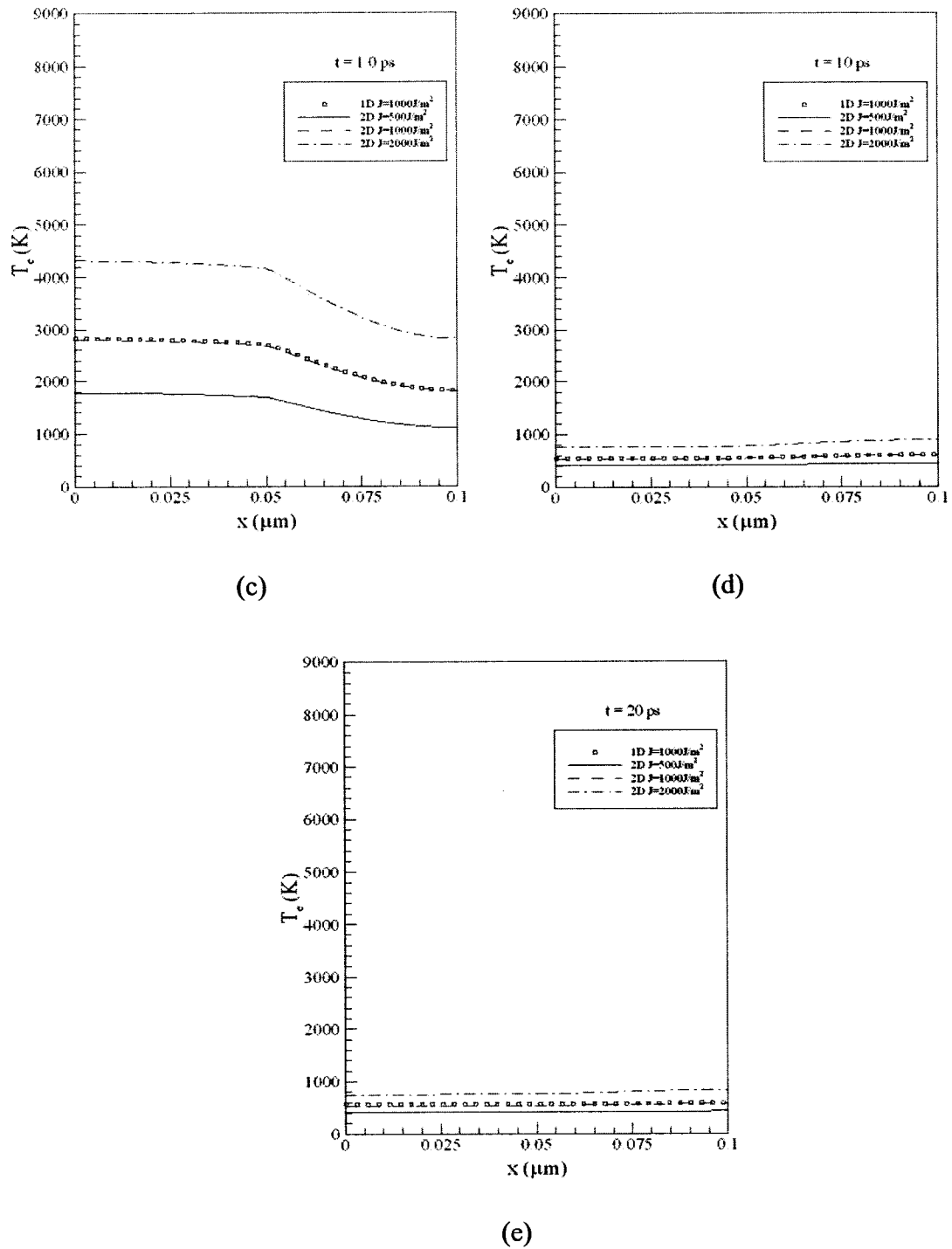
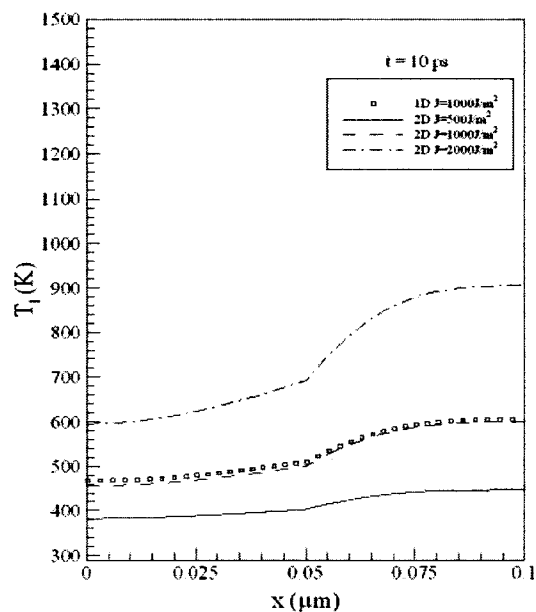
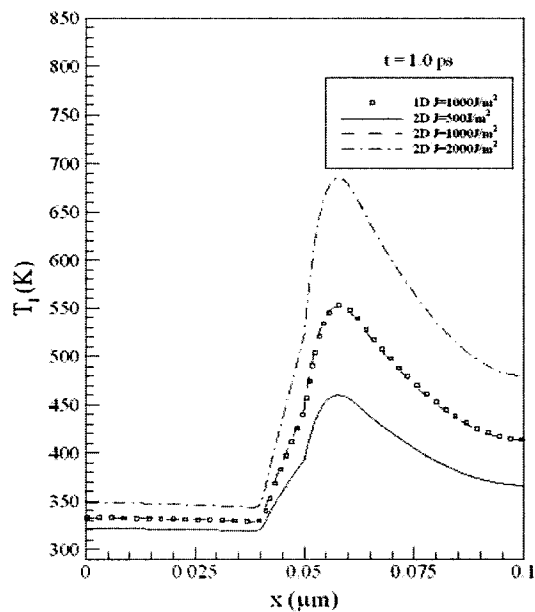
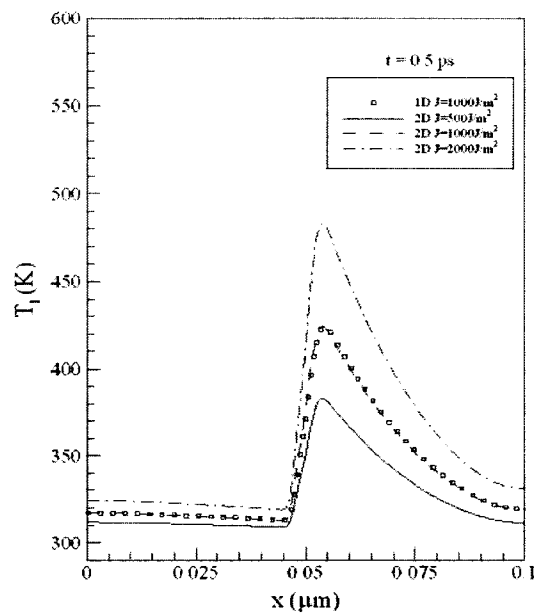
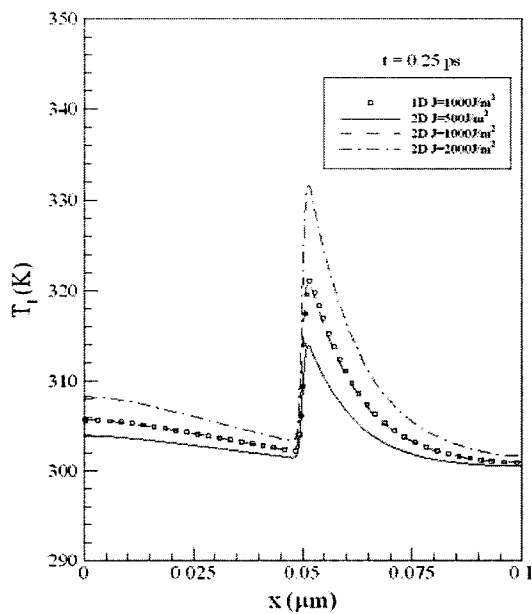
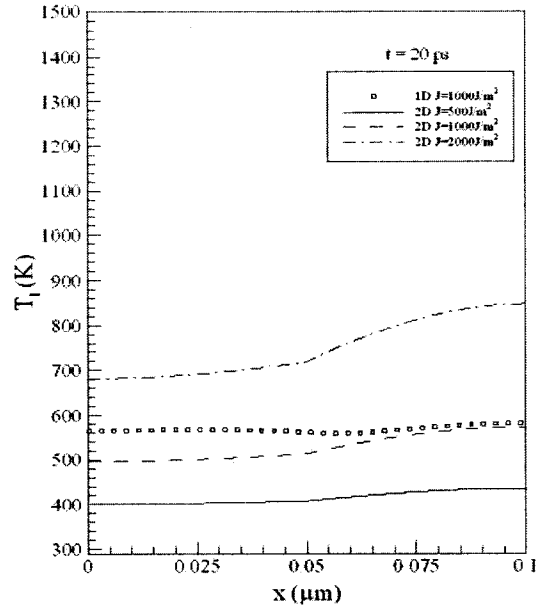


Figure 5.21 Comparison of electron temperature (T_e) at $y = 0 \mu\text{m}$ at (a) $t = 0.25 \text{ ps}$, (b) $t = 0.5 \text{ ps}$, (c) $t = 1 \text{ ps}$, (d) $t = 10 \text{ ps}$, and (e) $t = 20 \text{ ps}$ with $J = 500 \text{ J/m}^2$, 1000 J/m^2 and 2000 J/m^2 .





(e)

Figure 5.22 Comparison of lattice temperature (T_l) at $y = 0 \mu m$ at (a) $t = 0.25 ps$, (b) $t = 0.5 ps$, (c) $t = 1 ps$, (d) $t = 10 ps$, and (e) $t = 20 ps$ with $J = 500 J/m^2$, $1000 J/m^2$ and $2000 J/m^2$.

Figure 5.23 and Figure 5.24 show the comparison of displacement u (thickness direction) and v (length direction) along x at $y = 0 \mu m$ with three different laser fluences ($J = 500 J/m^2$, $1000 J/m^2$ and $2000 J/m^2$) at various times (a) $t = 5 ps$, (b) $t = 10 ps$, (c) $t = 15 ps$, and (d) $t = 20 ps$.

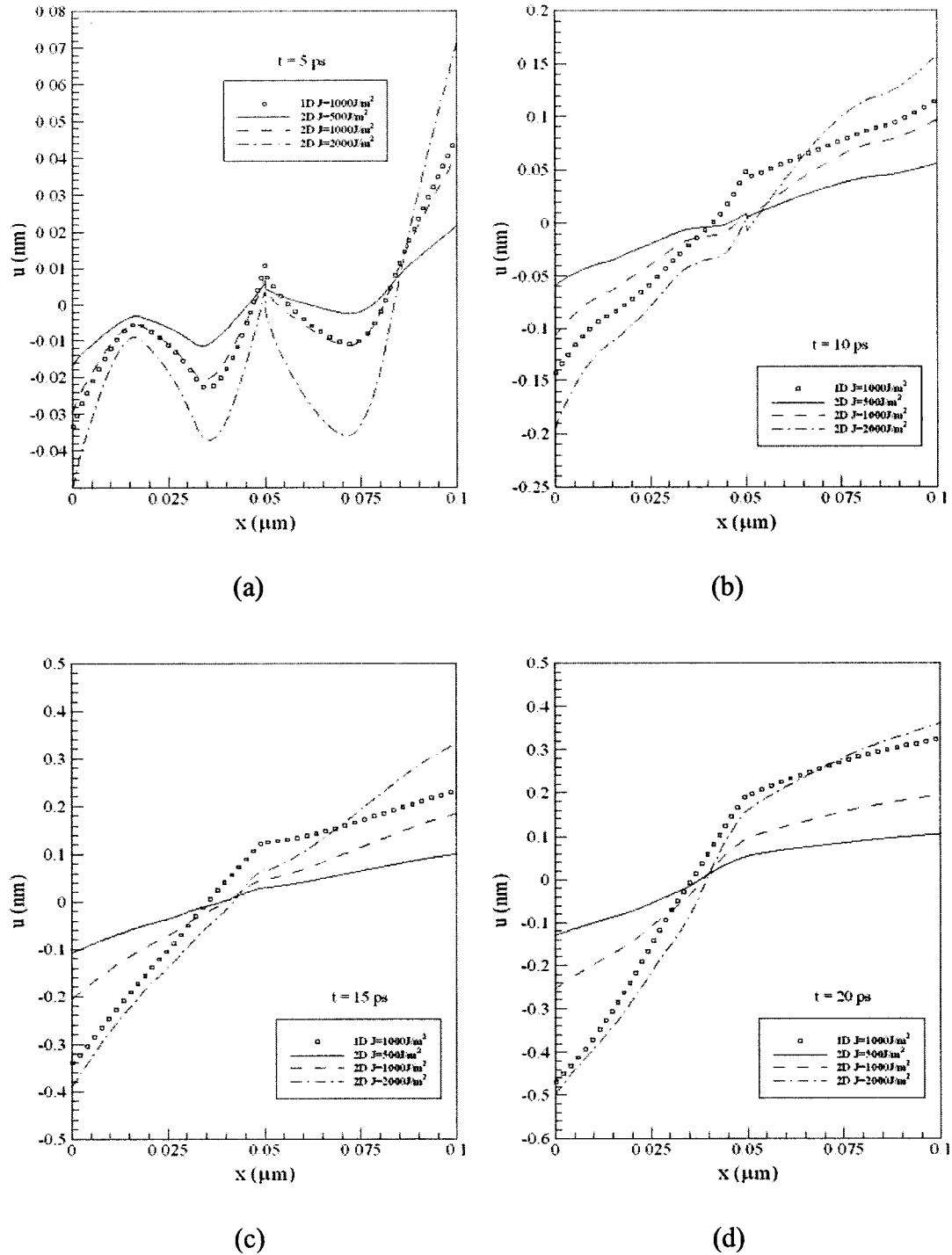


Figure 5.23 Comparison of displacement (u) at $y = 0 \mu\text{m}$ at (a) $t = 5 \text{ ps}$, (b) $t = 10 \text{ ps}$, (c) $t = 15 \text{ ps}$, and (d) $t = 20 \text{ ps}$ with $J = 500 \text{ J/m}^2$, 1000 J/m^2 and 2000 J/m^2 .

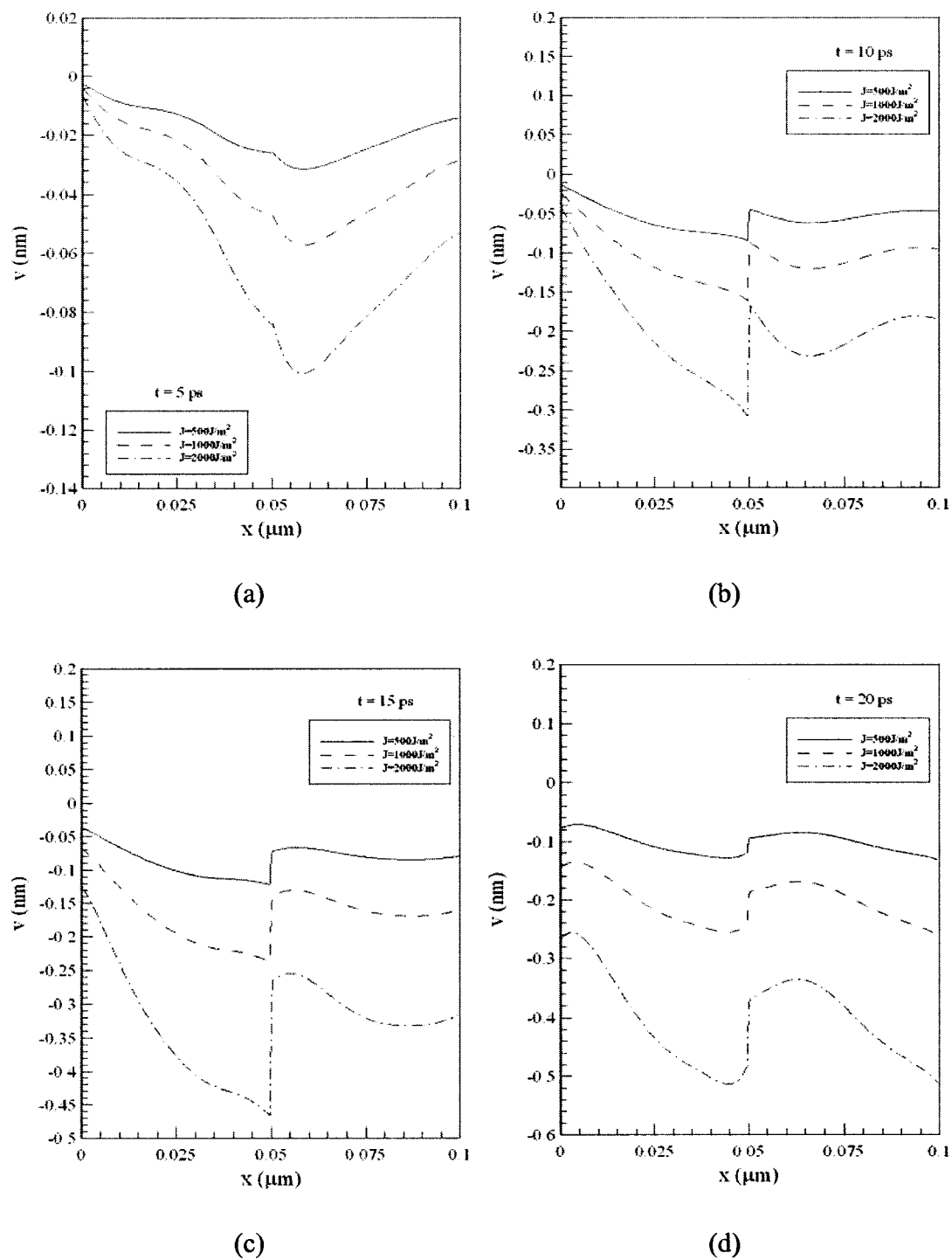
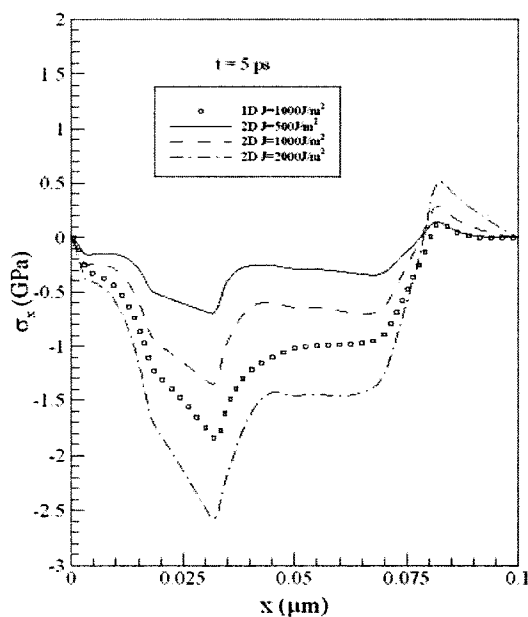
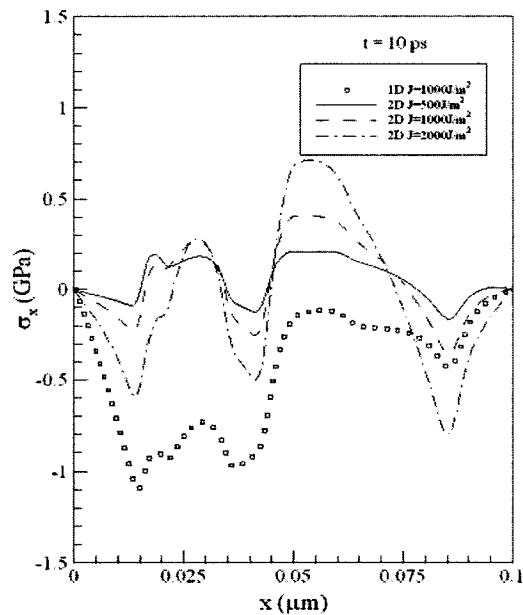


Figure 5.24 Comparison of displacement (v) at $y = 0 \mu\text{m}$ at (a) $t = 5 \text{ ps}$, (b) $t = 10 \text{ ps}$, (c) $t = 15 \text{ ps}$, and (d) $t = 20 \text{ ps}$ with $J = 500 \text{ J/m}^2$, 1000 J/m^2 and 2000 J/m^2 .

Figure 5.25 and Figure 5.26 show the comparison of normal stress σ_x (thickness direction) and σ_y (length direction) along x at $y=0\mu m$ with three different laser fluences ($J = 500 J/m^2$, $1000 J/m^2$ and $2000 J/m^2$) at various times (a) $t = 5 ps$, (b) $t = 10 ps$, (c) $t = 15 ps$, and (d) $t = 20 ps$.



(a)



(b)

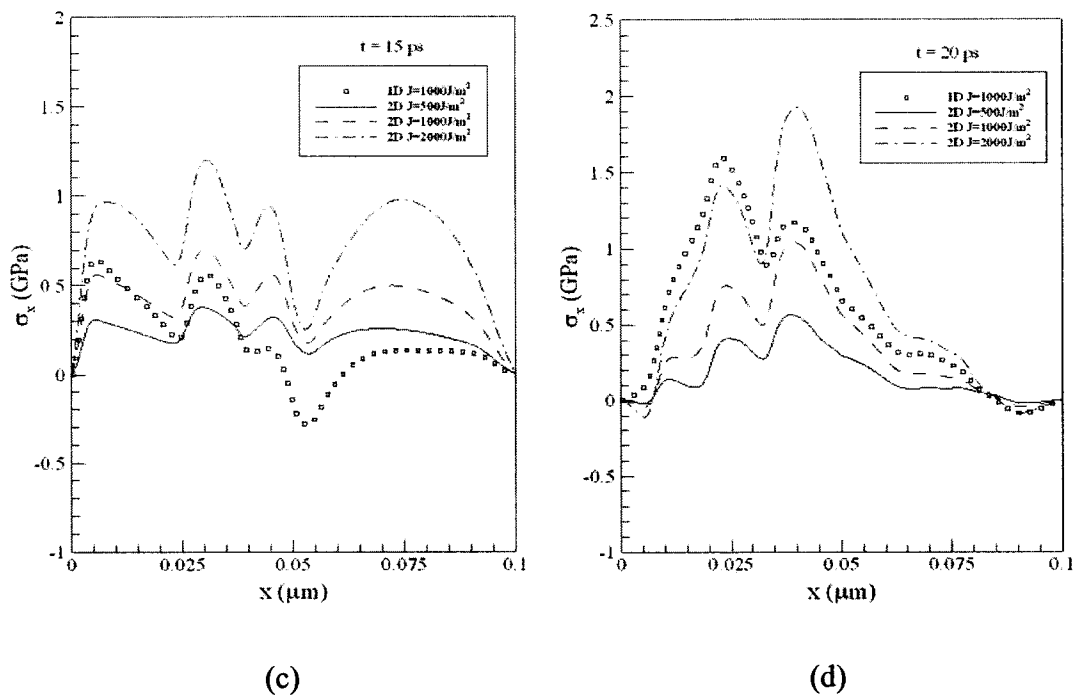
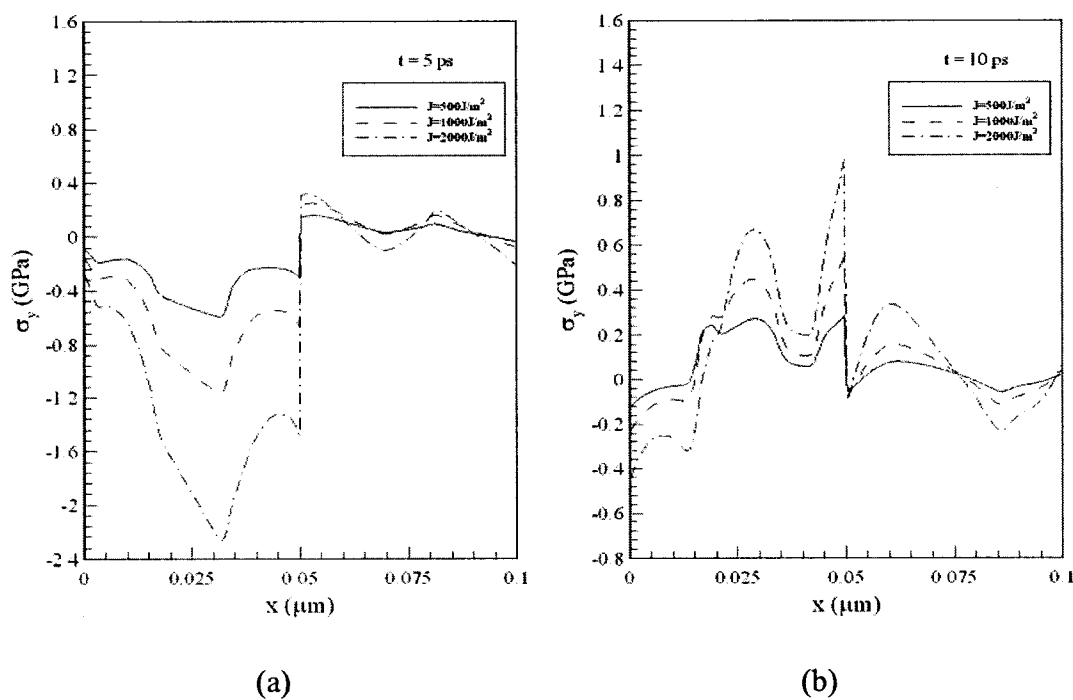


Figure 5.25 Comparison of normal stress (σ_x) at $y = 0 \mu\text{m}$ at (a) $t = 5 \text{ ps}$, (b) $t = 10 \text{ ps}$, (c) $t = 15 \text{ ps}$, and (d) $t = 20 \text{ ps}$ with $J = 500 \text{ J/m}^2$, 1000 J/m^2 and 2000 J/m^2 .



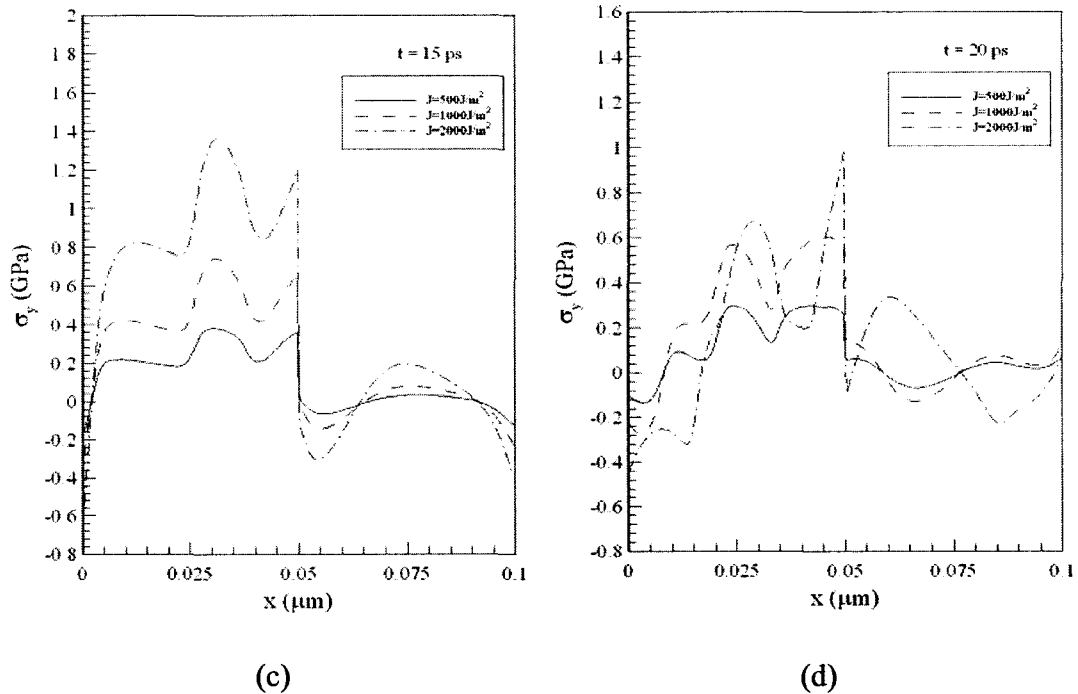


Figure 5.26 Comparison of normal stress (σ_y) at $y = 0 \mu\text{m}$ at (a) $t = 5 \text{ ps}$, (b) $t = 10 \text{ ps}$, (c) $t = 15 \text{ ps}$, and (d) $t = 20 \text{ ps}$ with $J = 500 \text{ J/m}^2$, 1000 J/m^2 and 2000 J/m^2 .

Figure 5.27 and Figure 5.28 show the contour plots of electron temperature (T_e) profile and lattice temperature (T_l) profile with the laser fluence of $J = 1000 \text{ J/m}^2$ at various times (a) $t = 0.25 \text{ ps}$, (b) $t = 0.5 \text{ ps}$, (c) $t = 1 \text{ ps}$ and (d) $t = 10 \text{ ps}$, respectively.

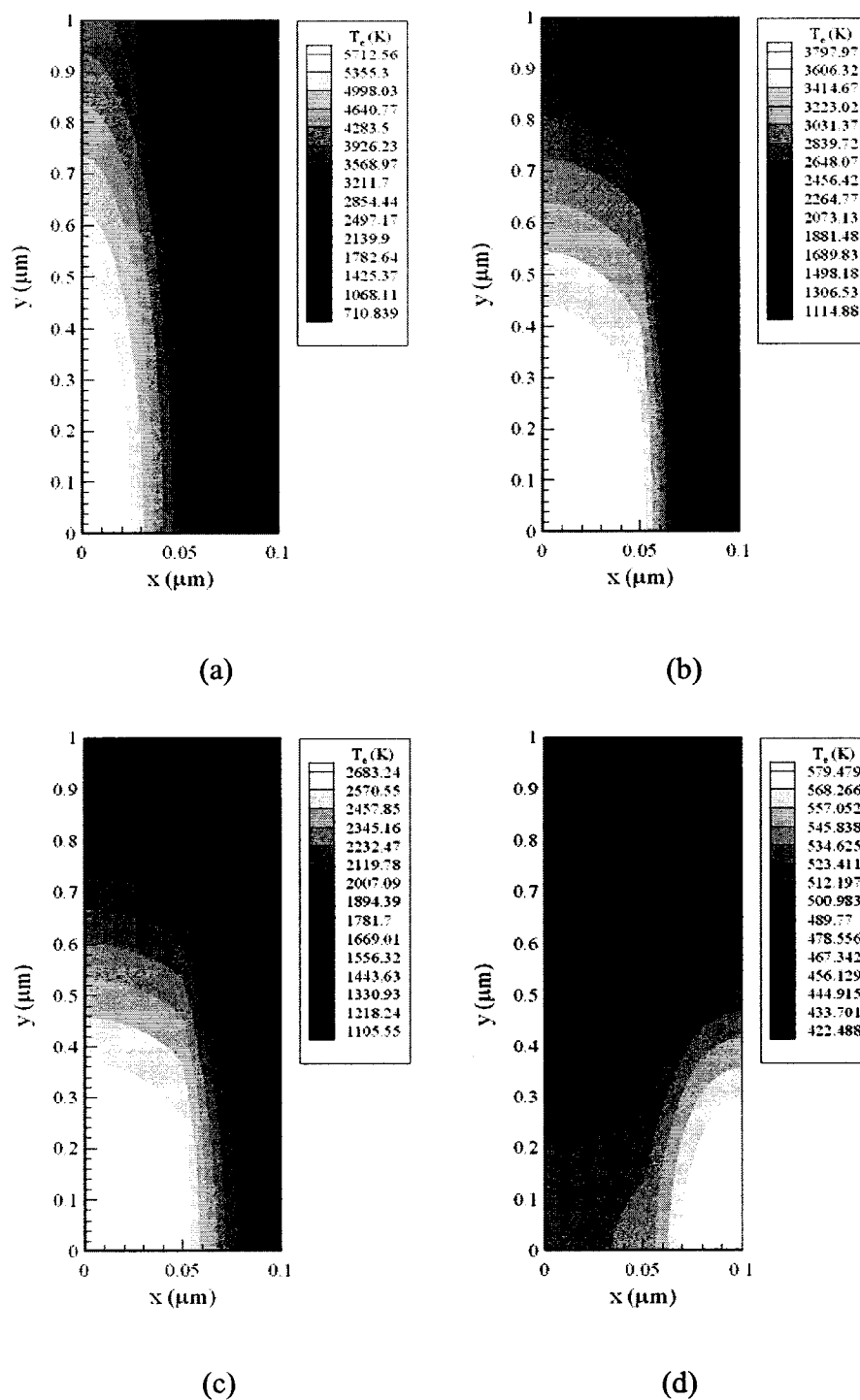


Figure 5.27 Contour plots of electron temperature (T_e) profiles with $J = 1000 J/m^2$ at (a) $t = 0.25 ps$, (b) $t = 0.5 ps$, (c) $t = 1 ps$ and (d) $t = 10 ps$.

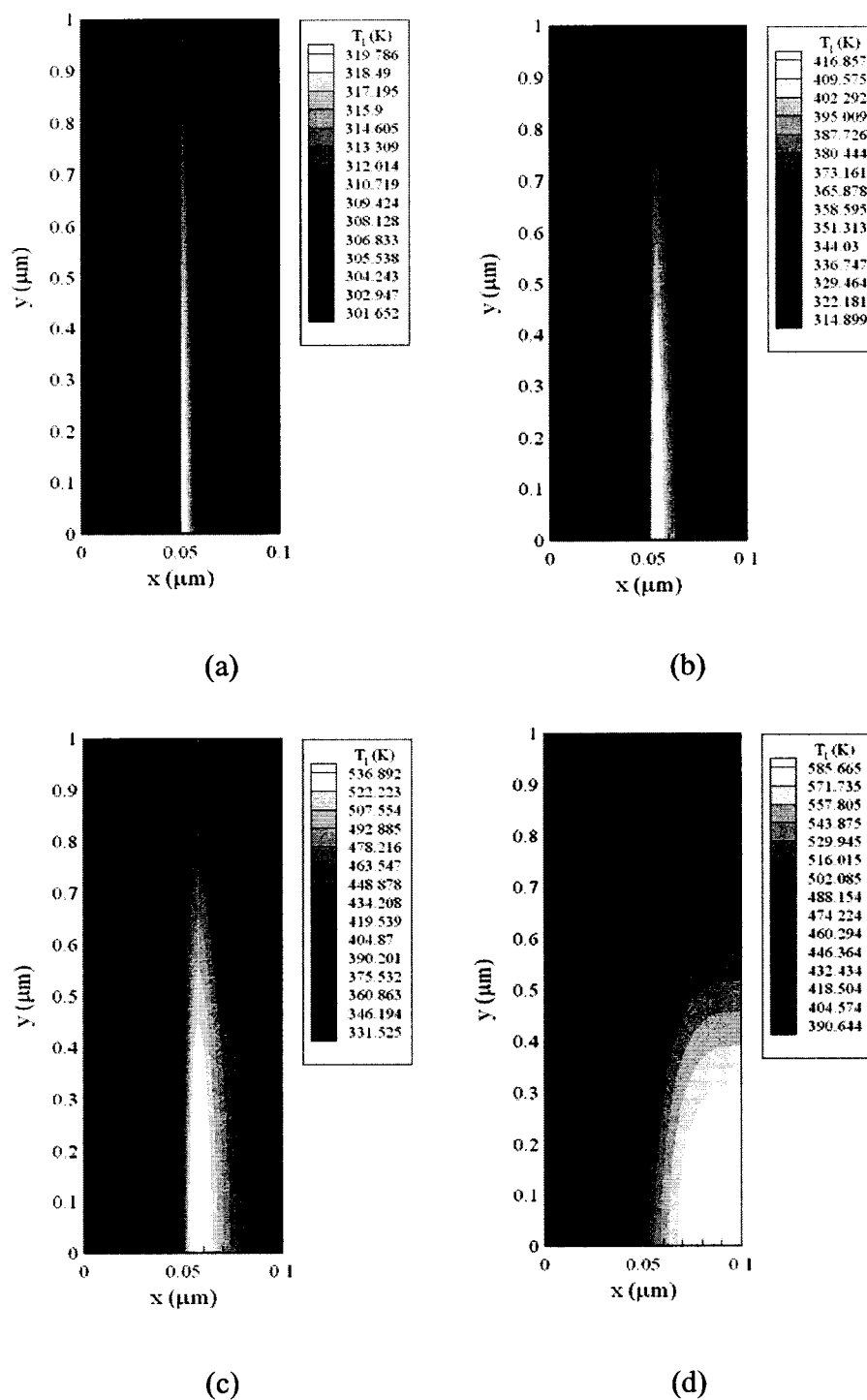
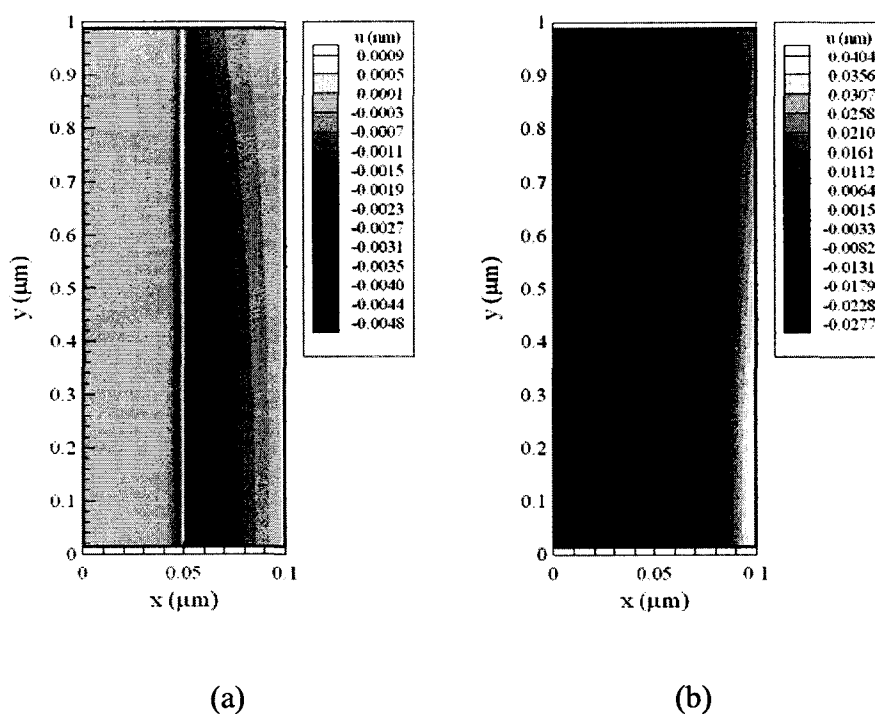


Figure 5.28 Contour plots of lattice temperature (T_l) profiles with $J = 1000 J/m^2$ at (a) $t = 0.25 ps$, (b) $t = 0.5 ps$, (c) $t = 1 ps$ and (d) $t = 10 ps$.

Figures 5.29-5.32 show the contour plots of displacement u (thickness direction) profile, displacement v (length direction) profile, normal stress σ_x (thickness direction) profile and σ_y (length direction) profile with the laser fluence of $J = 1000 J/m^2$ at various times (a) $t = 1 ps$, (b) $t = 5 ps$, (c) $t = 10 ps$, and (d) $t = 20 ps$, respectively. Again, it can be seen that the heat is transferred from the gold layer to the chromium layer. It can be seen from Figure 5.29 and Figure 5.30 (especially, $t = 10 ps$ and $t = 20 ps$) that the film is expanding because of the displacement changes from negative to positive along the x and y directions, respectively.



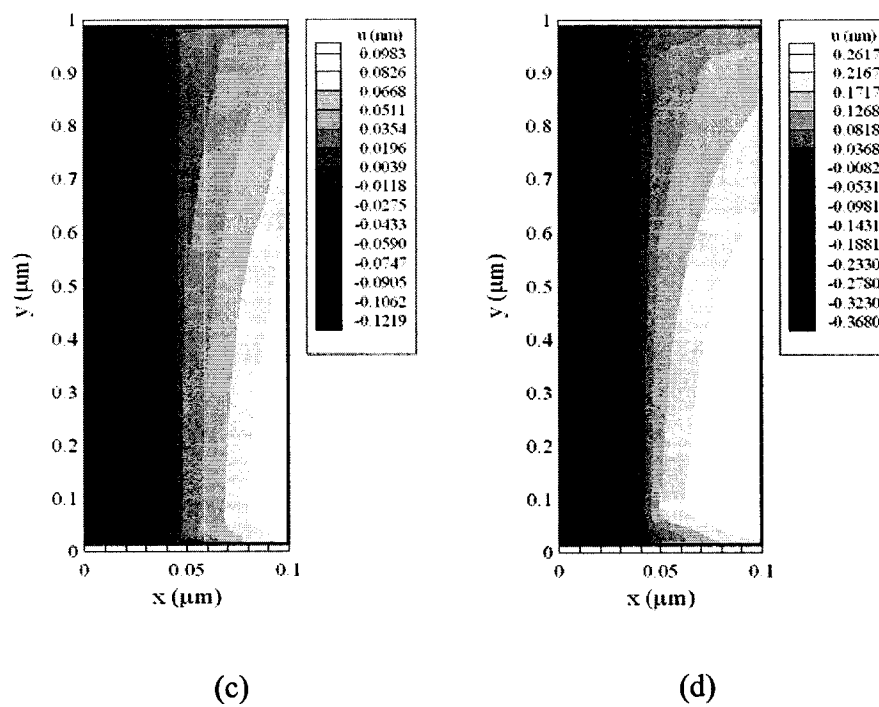


Figure 5.29 Contour plots of displacement u profile with $J = 1000 \text{ J/m}^2$ at (a) $t = 1 \text{ ps}$, (b) $t = 5 \text{ ps}$, (c) $t = 10 \text{ ps}$, and (d) $t = 20 \text{ ps}$.

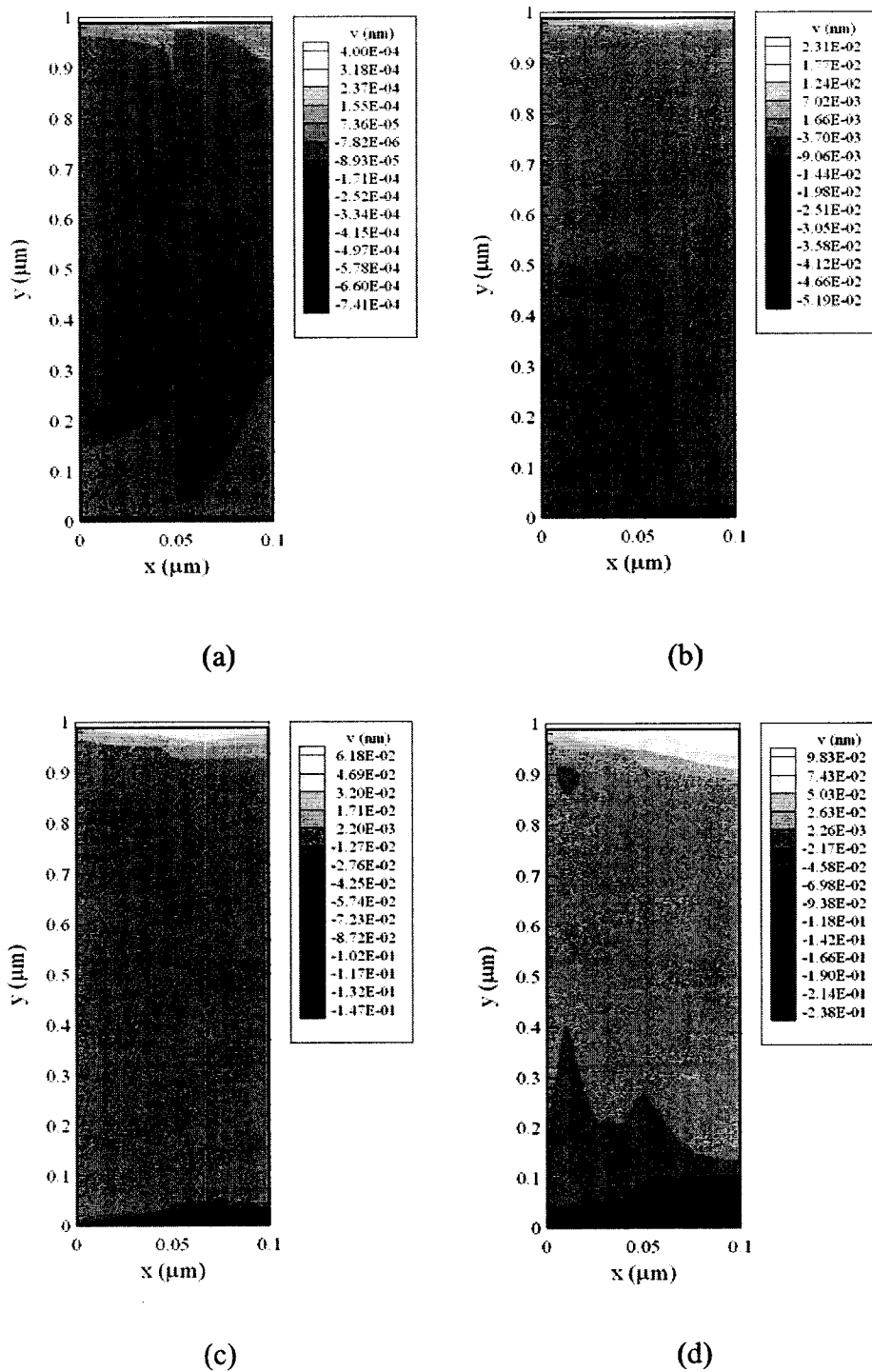


Figure 5.30 Contour plots of displacement v profile with $J = 1000 \text{ J/m}^2$ at (a) $t = 1 \text{ ps}$, (b) $t = 5 \text{ ps}$, (c) $t = 10 \text{ ps}$, and (d) $t = 20 \text{ ps}$.

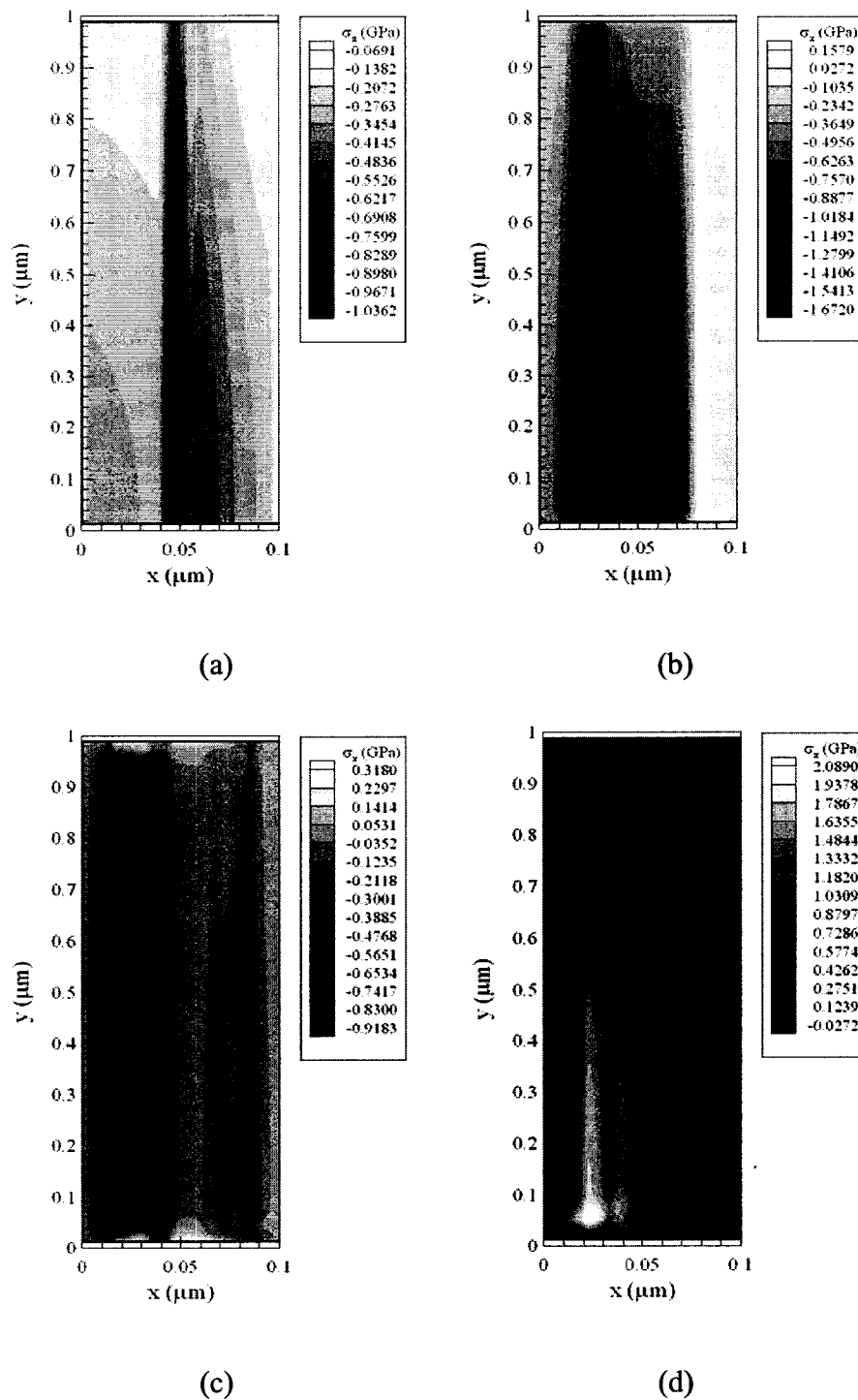


Figure 5.31 Contour plots of normal stress σ_x profiles with $J = 1000 J/m^2$ at (a) $t = 1 ps$, (b) $t = 5 ps$, (c) $t = 10 ps$, and (d) $t = 20 ps$.

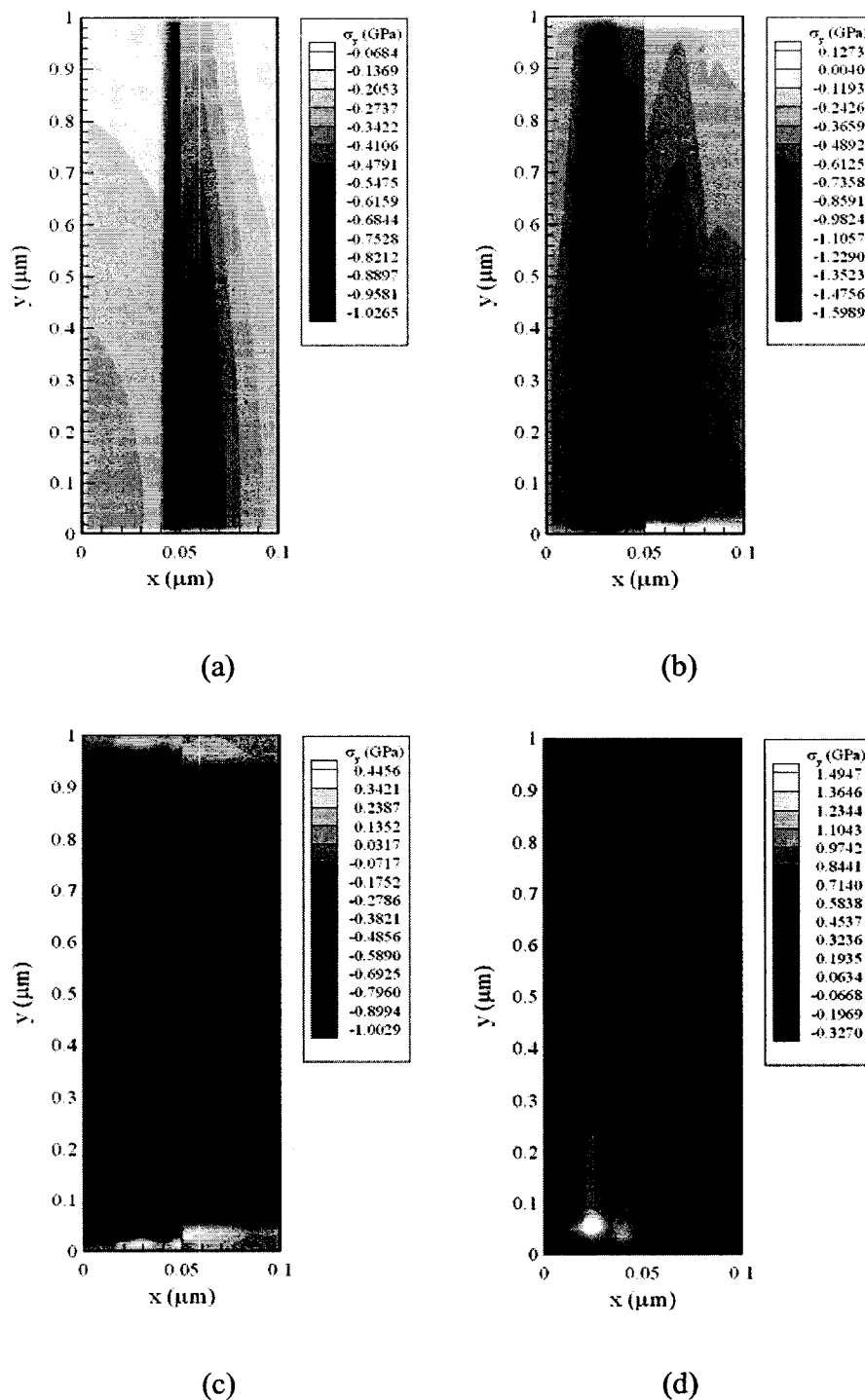


Figure 5.32 Contour plots of normal stress σ_y profiles with $J = 1000 J/m^2$ at (a) $t = 1 ps$, (b) $t = 5 ps$, (c) $t = 10 ps$, and (d) $t = 20 ps$.

CHAPTER 6

CONCLUSION AND FUTURE WORK

It was pointed out in the literature that the hyperbolic two-step model is more accurate than the parabolic model when the laser pulse duration is much shorter than the electron-lattice thermal relaxation time. However, it has not been seen in the literature employing the hyperbolic two-step model for studying thermal deformation in a micro thin film exposed to ultrashort-pulsed lasers, which is important for enhancing our understanding of micro heat transfer in a micro thin film exposed to ultrashort-pulsed lasers.

In this dissertation, we develop a finite difference scheme for solving the generalized hyperbolic two-step model with temperature-dependent thermal properties in a one-dimensional double-layered thin film exposed to ultrashort-pulsed lasers. The scheme is obtained based on an energy estimate for the hyperbolic two-step system. We then apply the finite difference scheme to studying thermal deformation in two-dimensional single-layered and double-layered thin films exposed to ultrashort-pulsed lasers, by coupling with the dynamic equations of motions. The method accounts for the coupling effect between lattice temperature and strain rate, as well as for the hot-electron-blast effect in momentum transfer. In order to avoid non-physical oscillations in the

solution, we replace the displacement components in the dynamic equations of motion with the velocity components and design staggered grids.

To test applicability of the scheme, we consider three cases including a one-dimensional thin film of a gold layer on a chromium layer with perfectly contacted interface, a two-dimensional thin film of gold and a two-dimensional thin film of a gold layer on a chromium layer with perfectly contacted interface. Numerical results show that the method allows avoidance of non-physical oscillations in the solution and there are some differences between the hyperbolic two-step model and the parabolic model. Particularly, one may see the differences regarding the change in electron temperature ($\Delta T_e / (\Delta T_e)_{\max}$) (see Figures 5.9 and 5.19) and the displacement (u) in x direction (see Figures 5.10 and 5.20).

The future research may focus on a two-dimensional double-layered micro thin film with nonlinear interfacial conditions, which means the interface is imperfectly contacted and a three-dimensional double-layered micro thin film, where the model and computation may be much more complicated.

APPENDIX A

**SOURCE CODE FOR 1D
DOUBLE-LAYERED CASE**

C This is the program for solving nonlinear two-step equations

```

      DIMENSION sa(0:802,0:3),sb(0:802,0:3)
      DIMENSION sm(0:802,0:3),sp(0:802,0:3)
      DIMENSION TEM(1000),tke(0:802,0:3)
      DIMENSION
sd(0:802),se(0:802),sf(0:802)
      DIMENSION S(0:802),RHS(0:802)
      DIMENSION beta(0:802),v(0:802)
      DIMENSION
TE(0:802,0:3),TL(0:802,0:3)
      DIMENSION qe(0:802,0:3),ql(0:802,0:3)
      DIMENSION
tk0(0:3),Cl(0:3),G(0:3),Ae(0:3)
      DIMENSION taue(0:3),taul(0:3)

```

C Type

```

double precision sa,sb,sm,sp,TEM,sd,se
double precision sf,S, RHS,beta,v,TE,TL
double precision qe,ql,tk0,Cl,G,Ae,dx,dt
double precision SJ,tp,delta,R,taue,taul
double precision ss,temp1,temp2,temp3,max

```

C Data

```

integer flag
tk0(1)=3.15D-13
tk0(2)=9.4D-14
Cl(1)=2.5D-3
Cl(2)=3.3D-3
G(1)=2.6D-5
G(2)=4.2D-4
Ae(1)=7.0D-8
Ae(2)=1.933D-7
timestep=1200
dx=1.250D-7
dt=5.0D-3
N=400
T0=300.0
SJ=50.00D-5
tp=0.1
delta=1.53D-5
R=0.93
taue(1)=0.04
taul(1)=0.8
taue(2)=6.8D-3
taul(2)=0.136
ss=0.94*SJ*(1.0-R)/(tp*delta)
max=0.0

```

C Initial condition

```

do i=1,2*N
do j=0,2
TL(i,j)=T0

```

```

TE(i,j)=T0
qe(i,j)=0
ql(i,j)=0
sa(i,j)=0
sb(i,j)=0
sm(i,j)=0
sp(i,j)=0
tke(i,j)=0
enddo
enddo

```

```
do nt=0,timestep
```

```
c print *,nt
```

C Heat Source

```
do j=1,2*N
```

```

c S(j)=ss*exp(-j*dx/delta
c $ -2.77*((nt+0.5)*dt-2.0*tp)*
c $ (((nt+0.5)*dt-2.0*tp)/(tp*tp))
temp1=((nt+0.5)*dt-2.0*tp)/tp
S(j)=ss*exp(-j*dx/delta)*
$ exp(-2.77*temp1**2)
enddo

```

C Gold

```

flag=1
do while(flag.eq.1)
do m=1,2
do j=1,N
if(m.eq.1) then

```

```

temp1=abs((TE(j,1)+TE(j,0))/(TL(j,1)+TL(j,0)))
temp2=abs((TE(j-1,1)+TE(j-1,0))/(TL(j-1,1)+TL(j-1,0)))
else
temp1=abs((TE(j+N-1,1)+TE(j+N-1,0))
& /(TL(j+N-1,1)+TL(j+N-1,0)))
temp2=abs((TE(j+N-2,1)+TE(j+N-2,0))
& /(TL(j+N-2,1)+TL(j+N-2,0)))
end if
tke(j,m) =0.5*tk0(m)*(temp1+temp2)
c tke(j)=tk0;
end do
end do
do m=1,2
do j=2,N
temp1=2*taue(m)+dt
temp2=2*taue(m)-dt
sb(j,m)=-((tke(j,m)/temp1)*(dt/dx)
if(m.eq.1) then
temp3=sb(j,m)*(TE(j,0)-TE(j-1,0))
sa(j,m)=qe(j,0)*temp2/temp1+temp3
else
temp3=sb(j,m)*
& (TE(j+N-1,0)-TE(j+N-2,0))
sa(j,m)=qe(j+N-1,0)*temp2/temp1

```

```

& +temp3
  end if
end do
end do

do m=1,2
do j=1,N
if(m.eq.1) then
temp1=TE(j,1)**2+TE(j,0)**2
$ +TE(j,1)*TE(j,0)
temp2=TE(j,0)+TE(j,1)
sp(j,m)=G(1)*dx*(TE(j,0)-TL(j,2))
$ -TL(j,0))-2*dx*S(j)
else
temp1=TE(j+N-1,1)**2+TE(j+N-1,0)**2
$ +TE(j+N-1,1)*TE(j+N-1,0)
temp2=TE(j+N-1,0)-TE(j+N-1,1)
sp(j,m)=G(m)*dx*(TE(j+N-1,0)-TL(j+N-
1,2))
$ -TL(j+N-1,0))-2*dx*S(j+N-1)
end if
sm(j,m)=-
4.0*(dx/dt)*Ae(m)*temp1/(3.0*temp2)

end do
end do

do j=1,2*N-1
if(j.eq.1) then
sd(j)=0
se(j)=sm(1,1)-G(1)*dx+sb(2,1)
sf(j)=sb(2,1)
RHS(j)=sa(2,1)+sp(1,1)+qe(2,0)+sm(1,1)
*TE(1,0)
else if(j.eq.2*N-1) then
sd(j)=sb(N,2)
se(j)=sm(N,2)-G(2)*dx+sb(N,2);
sf(j)=0
RHS(j)=-sa(N,2)+sp(N,2)-qe(2*N-1,0)
$ +sm(N,2)*TE(2*N-1,0)
else if(j.eq.N) then
sd(j)=sb(N,1)
se(j)=sm(N,1)+sm(1,2)+sb(N,1)
$ -G(1)*dx+sb(2,2)-G(2)*dx
sf(j)=sb(2,2)
RHS(j)=(sm(N,1)+sm(1,2))*TE(N,0)-
sa(N,1)
$ -qe(N,0)+sp(N,1)+sa(2,2)+qe(N+1,0)+sp(1,2)
else if(j.LT.N) then
sd(j)=sb(j,1)
se(j)=sm(j,1)-G(1)*dx+sb(j+1,1)+sb(j,1)
sf(j)=sb(j+1,1)
RHS(j)=sa(j+1,1)-sa(j,1)+sp(j,1)+
$ qe(j+1,0)-qe(j,0)+sm(j,1)*TE(j,0)
else
L=j-N+1
sd(j)=sb(L,2)
se(j)=sm(L,2)-
G(2)*dx+sb(L+1,2)+sb(L,2)
sf(j)=sb(L+1,2)
RHS(j)=sa(L+1,2)-sa(L,2)+sp(L,2)+
$ qe(j+1,0)-qe(j,0)+sm(L,2)*TE(j,0)
end if
end do
beta(0)=0.0;
v(0)=0.0;
do j=1,2*N-1
beta(j)=sf(j)/(se(j)-sd(j)*beta(j-1))
v(j)=(RHS(j)+sd(j)*v(j-1))
$ /(se(j)-sd(j)*beta(j-1))
end do
TE(2*N,2)=0
flag=0

do m=1,2*N-1
j=2*N-m
TE(j,2)=beta(j)*TE(j+1,2)+v(j)
if(abs(TE(j,2)-TE(j,1)).gt.0.000001) then
flag=1
end if
end do

cccccccccccccccccccccccccccccccccccccccccccccccccccccccccccc
do j=1,2*N
if(j.eq.1) then
qe(j,2)=0.0
else if(j.eq.2*N) then
qe(j,2)=0.0
else if(j.LE.N) then
qe(j,2)=sa(j,1)+sb(j,1)*(TE(j,2)-TE(j-1,2))
else
L=j-N+1
qe(j,2)=sa(L,2)+sb(L,2)*(TE(j,2)-TE(j-1,2))
end if
end do
cccccccccccccccccccccccccccccccccccccccccccccccccccccccccccc
c debug.....
if(nt.eq.0) then
print *,qe(220,2)
end if
c debug .....

do m=1,2
do j=2,N
temp1=2*taul(m)*dx+dt*dx
temp2=2*taul(m)*dx-dt*dx
sb(j,m)=-tk0(m)*dt/temp1
if (m.eq.1) then
temp3=sb(j,m)*(TL(j,0)-TL(j-1,0))
sa(j,m)=ql(j,0)*temp2/temp1+temp3

```

```

else
temp3=sb(j,m)*(TL(j+N-1,0)-TL(j+N-
2,0))
sa(j,m)=ql(j+N-1,0)*temp2/temp1+temp3
end if
end do
end do
do m=1,2
do j=1,N
if (m.eq.1) then
sp(j,m)=-G(m)*dx*(TE(j,0)+TE(j,2)-TL(j,0))
else
sp(j,m)=-G(m)*dx*(TE(j+N-1,0)+TE(j+N-
1,2)
$ -TL(j+N-1,0))
end if

sm(j,m)=-2.0*dx*Cl(m)/dt;
end do
end do
do j=1,2*N-1
if(j.eq.1) then
sd(j)=0
se(j)=sm(1,1)-G(1)*dx+sb(2,1)
sf(j)=sb(2,1)
RHS(j)=sa(2,1)+sp(1,1)+ql(2,0)+sm(1,1)
*TL(1,0)
else if(j.eq.2*N-1) then
sd(j)=sb(N,2)
se(j)=sm(N,2)-G(2)*dx+sb(N,2);
sf(j)=0
RHS(j)=-sa(N,2)+sp(N,2)-ql(2*N-1,0)
$ +sm(N,2)*TL(2*N-1,0)
else if(j.eq.N) then
sd(j)=sb(N,1)
se(j)=sm(N,1)+sm(1,2)+sb(N,1)
$ -G(1)*dx+sb(2,2)-G(2)*dx
sf(j)=sb(2,2)
RHS(j)=(sm(N,1)+sm(1,2))*TL(N,0)-
sa(N,1)
$ -ql(N,0)+sp(N,1)+sa(2,2)+ql(N+1,0)+sp(1,2)
else if(j.LT.N) then
sd(j)=sb(j,1)
se(j)=sm(j,1)-G(1)*dx+sb(j+1,1)+sb(j,1)
sf(j)=sb(j+1,1)
RHS(j)=sa(j+1,1)-sa(j,1)+sp(j,1)+
$ ql(j+1,0)-ql(j,0)+sm(j,1)*TL(j,0)
else
L=j-N+1
sd(j)=sb(L,2)
se(j)=sm(L,2)-
G(2)*dx+sb(L+1,2)+sb(L,2)
sf(j)=sb(L+1,2)
RHS(j)=sa(L+1,2)-sa(L,2)+sp(L,2)+
$ ql(j+1,0)-ql(j,0)+sm(L,2)*TL(j,0)
end if

end do
beta(0)=0.0;
v(0)=0.0;
do j=1,2*N-1
beta(j)=sf(j)/(se(j)-sd(j)*beta(j-1))
v(j)=(RHS(j)+sd(j)*v(j-1))
$ /(se(j)-sd(j)*beta(j-1))
end do
TL(2*N,2)=0
flag=0

do m=1,2*N-1
j=2*N-m
TL(j,2)=beta(j)*TL(j+1,2)+v(j)
if(abs(TL(j,2)-TL(j,1)).gt.0.000001) then
flag=1
end if
end do

cccccccccccccccccccccccccccccccccccccccccccccccccccccccccccc
do j=1,2*N
if(j.eq.1) then
ql(j,2)=0.0
else if(j.eq.2*N) then
ql(j,2)=0.0
else if(j.LE.N) then
ql(j,2)=sa(j,1)+sb(j,1)*(TL(j,2)-TL(j-1,2))
else
L=j-N+1
ql(j,2)=sa(L,2)+sb(L,2)*(TL(j,2)-TL(j-1,2))
end if
end do
cccccccccccccccccccccccccccccccccccccccccccccccccccccccccccc

if(flag.eq.1) then
do j=1,2*N
TE(j,1)=TE(j,2)
TL(j,1)=TL(j,2)
qe(j,1)=qe(j,2)
ql(j,1)=ql(j,2)
end do
else
do j=1,2*N
TE(j,0)=TE(j,2)
TL(j,0)=TL(j,2)
qe(j,0)=qe(j,2)
ql(j,0)=ql(j,2)
TE(j,1)=TE(j,2)
TL(j,1)=TL(j,2)
qe(j,1)=qe(j,2)
ql(j,1)=ql(j,2)
end do
end if

end do

```

```

if (max.lt.(TE(1,0)-T0)) then
max=TE(1,0)-T0
end if
TEM(nt)=TE(1,0)-T0

if (nt.eq.40) then
open (unit=9,file='500J/TE02P.dat')
do j=1,2*N-1
write(9,1010) j*dx,TE(j,0)
end do

open (unit=10,file='500J/TL02P.dat')
do j=1,2*N-1
write(10,1010) j*dx,TL(j,0)
end do
endif

C time=0.25ps
if (nt.eq.50) then
open (unit=11,file='500J/TE025P.dat')
do j=1,2*N-1
write(11,1010) j*dx,TE(j,0)
end do

open (unit=12,file='500J/TL025P.dat')
do j=1,2*N-1
write(12,1010) j*dx,TL(j,0)
end do
endif

C time=0.5ps
if (nt.eq.100) then
open (unit=13,file='500J/TE05P.dat')
do j=1,2*N-1
write(13,1010) j*dx,TE(j,0)
end do

open (unit=14,file='500J/TL05P.dat')
do j=1,2*N-1
write(14,1010) j*dx,TL(j,0)
end do
endif

C time=1.0ps
if (nt.eq.200) then
open (unit=15,file='500J/TE1P.dat')
do j=1,2*N-1
write(15,1010) j*dx,TE(j,0)
end do

open (unit=16,file='500J/TL1P.dat')
do j=1,2*N-1
write(16,1010) j*dx,TL(j,0)
end do
endif

C time=6.0ps
if (nt.eq.1200) then
open (unit=17,file='500J/TE6P.dat')
do j=1,2*N-1
write(17,1010) j*dx,TE(j,0)
end do

open (unit=18,file='500J/TL6P.dat')
do j=1,2*N-1
write(18,1010) j*dx,TL(j,0)
end do
endif

1010 format(e15.6,2e15.6)

end do

C open(unit=6,file='ratio.dat')
C print *, "zone"
C do j=0,TIMESTEP
C print *,(j)*dt,TEM(j)/max
C end do
c do j=1,2*N-1
c print *,j*dx,TL(j,0)
c end do

end

```


APPENDIX B

SOURCE CODE FOR 2D SINGLE-LAYERED CASE

```

c Program main
  implicit double precision (a-h,l,o-z)
  dimension t(4001),t1(4001),x(400),y(200)
  dimension
TEo(400,200),TEold(400,200),TLo(400,200),TLold(400,200),
  $          qexo(400,200),qlxo(400,200),
qeyo(400,200),qlyo(400,200),
  $          qex(400,200),qlx(400,200),
qey(400,200),qly(400,200),
  $          TEm(4001),TLm(4001),
u1m(4001),u2m(4001), v1m(4001),v2m(4001),
  $ xsao(401,201),ysao(401,201),ssao(401,201),
  $
xsao(401,201),ysao(401,201),ssao(401,201),
  $ xsan(401,201),ysan(401,201),ssan(401,201),
  $ xseo(401,201),yseo(401,201),sseo(401,201),
  $ xsen(401,201),ysen(401,201),ssen(401,201),
  $
v1o(401,201),v2o(401,201),v1n(401,201),v2n(401,201),
  $
u1o(401,201),u2o(401,201),u1n(401,201),u2n(401,201)
C          $
u1xt(401,2001),xsxt(401,2001),u2xt(401,2001),y
sxt(401,2001),
C $ u1xt1(401,2001),xsxt1(401,1000),
C $ u2xt1(401,1000),ysxt1(401,1000)

integer p, counter

C-----Constants-----
C Lamé constant
  lemta=199.0d+9
C Shear modulus
  cmiu=27.0d+9
C Thermal expansion coefficient
  alphas=14.2d-6
C Density
  rou=1.93d+4
  theta=1.0

lx=1.0D-7
ly=1.0D-6
n=80
m=40
dx=lx/n
dy=ly/m
p=400
dt=0.005d-12

counter=0
t(1)=0.0
x(1)=0.0
y(1)=0.0

T0=300.0

do j=2,m+1
  y(j)=y(j-1)+dy
end do

do i=2,n+1
  x(i)=x(i-1)+dx
end do

C-----Initial conditions when k=1-----
C TEo: TE at the previous time point
C TEold: TE at the right now time point, but at
iteration i
C qexo: qex at the previous time point
C qex: qex at the right now time point
k=1
do j=1,m+1
  do i=1,n+1
    TEo(i,j)=T0
    TLo(i,j)=T0
    TEold(i,j)=T0
    TLold(i,j)=T0
    xsan(i,j)=0.0
    ysan(i,j)=0.0
    xsao(i,j)=0.0
    ysao(i,j)=0.0
    ssao(i,j)=0.0
    xsao(i,j)=0.0
    ysao(i,j)=0.0
    ssao(i,j)=0.0
    xseo(i,j)=0.0
    yseo(i,j)=0.0
    sseo(i,j)=0.0
    v1o(i,j)=0.0
    v2o(i,j)=0.0
    u1o(i,j)=0.0
    u2o(i,j)=0.0
  end do
end do

do j=2,m
  do i=1,n
    qexo(i,j)=0.0
    qlxo(i,j)=0.0
    qex(i,j)=0.0
    qlx(i,j)=0.0
  enddo
enddo

```

```

do j=1,m
  do i=2,n
    qeyo(i,j)=0.0
    qlyo(i,j)=0.0
    qey(i,j)=0.0
    qly(i,j)=0.0
  enddo
enddo

TEm(k)=0.0
TLm(k)=0.0

big=0.0

write(*,*) 'start'
C-----Initial Conditions Defined-----
C*****
C----Start the Time Step Loop from 2 to p+1-----
do k=2,p+1
  t(k)=(k-1)*dt
  t1(k)=(k-0.5)*dt

  call
temp(n,m,dx,dy,x,y,t1(k),dt,TL0,TLold,TE0,TEold,
$
xsan,ysan,xsao,ysao,qexo,qeyo,qlxo,qlyo,
$ qex,qey,qlx,qly)
C-----Debug-----
C if(k.eq.100) then
C print *, TEold(14,20)
C endif
C-----Debug-----

do j=1,m+1
do i=1,n+1
  xsan(i,j)=xsao(i,j)
  ysan(i,j)=ysao(i,j)
enddo
enddo

tol=1d-16
detuvmax=tol+1d-5

do while (detuvmax.gt.tol)
  detuvmax=0.0
C Compute stress
do j=1,m+1
  xsen(1,j)=0.0
  xsen(n+1,j)=0.0
end do

do i=1,n+1
  ysen(i,1)=0.0
  ysen(i,m+1)=0.0
end do

do j=2,m
  do i=2,n
    xsen(i,j)=(lemta+2.0*cmiu)*xsan(i,j)+lemta*ysan(
i,j)
$
(3.0*lemta+2.0*cmiu)*alphan*(TLold(i,j)-300.0)
  end do
end do
c
do j=1,m
  ssen(1,j)=0.0
  ssen(n,j)=0.0
end do

do i=2,n-1
  ssen(i,1)=0.0
  ssen(i,m)=0.0
end do

do j=2,m-1
do i=2,n-1
  ssen(i,j)=cmiu*ssan(i,j)
end do
end do

C Calculate velocity

call
velocity(n,m,dx,dy,dt,TE0,TEold,xseo,yseo,sseo,
$
xsen,ysen,ssen,v1o,v2o,v1n,v2n,u1o,u2o,
u1n,u2n)

C Calculate strain

do j=2,m
do i=2,n
  xsan(i,j)=((theta*(v1n(i,j)-v1n(i-1,j))
+ (1.0-theta)*(v1o(i,j)-
v1o(i-1,j)))/dx)
$
*dt+xsao(i,j)
c
  ysan(i,j)=((theta*(v2n(i,j)-v2n(i,j-1))
+ (1.0-theta)*(v2o(i,j)-
v2o(i,j-1)))/dy)

```

```

$          *dt+ysao(i,j)          xseo(i,j)=xsen(i,j)
      end do          yseo(i,j)=ysen(i,j)
      end do          sseo(i,j)=ssen(i,j)
c          v1o(i,j)=v1n(i,j)
c Shear strain      v2o(i,j)=v2n(i,j)
c          u1o(i,j)=u1n(i,j)
      do j=2,m-1          u2o(i,j)=u2n(i,j)
      do i=2,n-1          end do
          ssan(i,j)=((theta*(v1n(i,j+1)-v1n(i,j))
$              +(1.0-
theta*(v1o(i,j+1)-v1o(i,j)))/dy          end do
$              +(theta*(v2n(i+1,j)-
v2n(i,j))          end do
$              +(1.0-
theta*(v2o(i+1,j)-v2o(i,j)))/dx          do j=2,m
$              *dt+ssao(i,j)          do i=1,n
          end do          qexo(i,j)=qex(i,j)
          end do          qlxo(i,j)=qlx(i,j)
          enddo
c          do j=1,m
c Completion of calculation of strain      do i=2,n
c          qeyo(i,j)=qey(i,j)
          do j=1,m+1          qlyo(i,j)=qly(i,j)
          do i=1,n+1          enddo
              det1=xsan(i,j)-xsao(i,j)          enddo
              det2=ysan(i,j)-ysao(i,j)
              det3=ssan(i,j)-ssao(i,j)
              det=max(abs(det1),abs(det2),abs(det3))
          if( abs(det).gt.detuvmax) then
              detuvmax=abs(det)
          endif
          end do
          end do
c          counter=counter+1
          write(*,*) counter
          do j=1,m+1
          do i=1,n+1
              xsao(i,j)=xsan(i,j)
              ysao(i,j)=ysan(i,j)
              ssao(i,j)=ssan(i,j)
          end do
          end do
c          C end of time loop k=2,p+1
          end do
c          C Outputs
          write(*,*) 'detuvmax=', detuvmax
          C open(unit=6,file='TE02.dat')
          C print *, "zoneTE"
          C do i=1,n+1
          C print *, x(i), TEold(i,j)
          C enddo
c          C open(unit=6,file='TL02.dat')
          C print *, "zoneTL"
          C do i=1,n+1
          C print *, x(i), TLold(i,1)
          C enddo
c          C open(unit=6,file='U1.dat')
          C print *, "zoneU1"
          do j=1,m+1
          do i=1,n+1
              TEo(i,j)=TEold(i,j)
              TLo(i,j)=TLold(i,j)
              xsao(i,j)=xsan(i,j)
              ysao(i,j)=ysan(i,j)
              ssao(i,j)=ssan(i,j)
          end do
          end do

```

```

C do i=1,n+1
C   print *, x(i), u1n(i,2)
C   enddo

C   open(unit=6,file='V1.dat')
C   print *, "zoneV1"
C   do i=1,n+1
C     print *, x(i), v1n(i,2)
C   enddo

C   open(unit=6,file='xse10(Test).dat')
C   print *, "zonexse1"
C   do i=1,n+1
C     print *, (x(i)*1.0D+6), (xseo(i,2)*1.0D-9)
C   enddo

C   open(unit=6,file='yse1.dat')
C   print *, "zoneyse1"
C   do i=1,n+1
C     print *, x(i), ysen(i,2)
C   enddo

C show the temperature TE at x=0 and y=0 versus
time
  open(unit=6,file='etm84H(T).dat')
  print *, "zone"
  do k=1,p+1
    print *, (t(k)*1.0D+12),(TEm(k))
  enddo

C   open(unit=6,file='um84H.dat')
C   print *, "zone"
C   do k=1,p+1
C     print *, (t(k)*1.0D+12),(u1m(k)*1.0D+9)
C   enddo

C   open(unit=45,file='vm3.dat')
C   do k=1,p+1
C     write(45,1020) t(k),v1m(k),v2m(k)
C   enddo

1010  format(401e15.6)
1020  format(e15.6,2e15.6)

  end

  subroutine
temp(n,m,dx,dy,x,y,t,dt,TLo,TLold,TEo,TEold,
$
xsan,ysan,xsao,ysao,qexo,qeyo,qlxo,qlyo,
$   qex,qey,qlx,qly)

  implicit double precision (a-h,l,o-z)
  double precision TEM
  dimension x(400),y(200),TEM(1000)

  dimension
TEo(400,200),TEold(400,200),
$   TLo(400,200),TLold(400,200),
$   TNew(400,200), TLnew(400,200),
$   xsan(401,201),ysan(401,201),
$   xsao(401,201),ysao(401,201),S(401,201),
$   tkex(401,201),tkey(401,201),
$   qexo(400,200),qlxo(400,200),
$   qex(400,200),qlx(400,200),
$   qeyo(400,200),qlyo(400,200),
$   qey(400,200),qly(400,200),
$   dTE(400,200),dTL(400,200)

  integer iteration,flagE,flagL

C-----All the Constants-----
C Lame constant
  lemta=199.0d+9
C Shear modulus
  cmui=27.0d+9
C Thermal expansion coefficient
  alphas=14.2d-6
C Electron heat capacity
  Ae=70.0
C Lattice heat capacity
  cl=2.5d+6
C Electron - lattice coupling factor
  g=2.6d+16
C Electron thermal conductivity
  tk0=315.0
C Laser fluence
  flu=500
C Laser pulse duration
  tp=0.1D-12
C Optical penetration depth
  delta=15.3d-9
C Surface reflectivity
  sur=0.93
C Spatial profile parameters
  rs=1.0d-6
C Electron relaxation time
  taue=0.04D-12
C Lattice relaxation time
  taul=0.8D-12

  iteration=0

  d=dt*dx*dy
  sse=dt/(2.0*taue+dt)
  ssl=dt/(2.0*taul+dt)
  ee=-2.0*dx*dy*(3.0*lemta+2.0*cmui)*alphas
  ffl=2.0*dx*dy*cl

C-----Iteration starts-----
C flagE and flagL indicate whether TE and TL are
precise enough

```

```

C keep on iterating as long as flagE or flagL
equals to 1
2  flagE=1
   flagL=1

   aximumE=0.0

   do j=2,m+1
     do i=2,n+1

temp1=abs((TEold(i,j)+TEo(i,j))/(TLold(i,j)+TLo(
i,j)))
temp2=abs((TEold(i-1,j)+TEo(i-1,j))
/(TLold(i-1,j)+TLo(i-1,j)))
temp3=abs((TEold(i,j-1)+TEo(i,j-1))
/(TLold(i,j-1)+TLo(i,j-1)))

tkex(i,j)=0.5*tk0*(temp1+temp2)
tkey(i,j)=0.5*tk0*(temp1+temp3)
enddo
enddo

do j=2,m
do i=2,n

S(i,j)=0.94*flu*(1.0-sur)/(tp*delta)
$      *exp(-x(i)/delta-y(j)*y(j)/(rs*rs)
$      -2.77*(t-2.0*tp)*(t-
2.0*tp)/(tp*tp))

ffe=4.0*Ae*dx*dy*(TEold(i,j)*TEold(i,j)
$      +TEold(i,j)*TEo(i,j)+TEo(i,j)*TEo(i,j))
$      /(3.0*(TEold(i,j)+TEo(i,j)))

tempx1=dt*dy*tkex(i,j)/dx
tempx2=dt*dy*tkex(i-1,j)/dx

tempy1=dt*dx*tkey(i,j)/dy
tempy2=dt*dx*tkey(i,j-1)/dy

a1=ffe+(tempx1+tempx2+tempy1+tempy2)*sse+g
*d

b1=-4.0*dy*taue*sse*(qexo(i,j)-
qexo(i-1,j))
b2=-4.0*dx*taue*sse*(qeyo(i,j)-
qeyo(i,j-1))

c1=tempx1*sse*(TEold(i+1,j)+TEo(i+1,j)-TEo(i,j))
c2=-tempx2*sse*(TEo(i,j)-TEold(i-
1,j)-TEo(i-1,j))
c3=tempy1*sse*(TEold(i,j+1)+TEo(i,j+1)-TEo(i,j))

c4=-tempy2*sse*(TEo(i,j)-TEold(i,j-
1)-TEo(i,j-1))

d1=-g*d*(TEo(i,j)-TLold(i,j)-TLo(i,j))
d2=2.0*d*S(i,j)
d3=ffe*TEo(i,j)

C TEnew: The new TE at the right now time point
calculated based on the
C old TEs and TEs at the previous time point
TEnew(i,j)=(b1+b2+c1+c2+c3+c4+d1+d2+d3)/a1

C dTE: Difference between the new and the old
TEs at now time point
dTE(i,j)=abs(TEnew(i,j)-TEold(i,j))

C aximumE: The maximum difference between all
the new and the old TEs
if (aximumE.le.dTE(i,j)) then
aximumE=dTE(i,j)
endif
enddo
enddo

C If aximumE is less than 1D-6, which means that
the largest difference
C between the new and old TEs are smaller than
1D-6, make flagE=0 to
C stop the iteration for TE
if(aximumE.lt.1D-6) then
flagE=0
endif

C Since the calculation have no boundary TEs, just
make them equal to
C their neighbours
do j=2,m
TEnew(1,j)=TEnew(2,j)
TEnew(n+1,j)=TEnew(n,j)
end do
do i=1,n+1
TEnew(i,1)=TEnew(i,2)
TEnew(i,m+1)=TEnew(i,m)
end do
C-----TEnew Calculated-----
C*****
C-----Start calculating TLnew-----
aximumL=0.0

do j=2,m
do i=2,n

e1=ffl+2.0*tk0*dt*dy*ssl/dx+2.0*tk0*dt*dx*ssl/d
y+d*g

```

```

1,j))      f1=-4.0*dy*taul*ssl*(qlxo(i,j)-qlxo(i-
1))      f2=-4.0*dx*taul*ssl*(qlyo(i,j)-qlyo(i,j-
1))

          g1=-tk0*dt*dy*ssl*(2.0*TL0(i,j)-
TLold(i-1,j)
          $   -TL0(i-1,j)-TLold(i+1,j)-TL0(i+1,j))/dx
          g2=-tk0*dt*dx*ssl*(2.0*TL0(i,j)-
TLold(i,j-1)
          $   -TL0(i,j-1)-TLold(i,j+1)-TL0(i,j+1))/dy

          h1=-g*d*(TL0(i,j)-TEnew(i,j)-TEo(i,j))
          h2=ee*(xsan(i,j)+ysan(i,j)-xsao(i,j)-
ysao(i,j))
          h3=fll*TL0(i,j)

TLnew(i,j)=(f1+f2+g1+g2+h1+h2+h3)/e1

          dTL(i,j)=abs(TLnew(i,j)-TLold(i,j))

          if(aximumL.lt.dTL(i,j)) then
          aximumL=dTL(i,j)
          endif

          enddo
        enddo

        if(aximumL.lt.1D-6) then
          flagL=0
        endif

        do j=2,m
          TLnew(1,j)=TLnew(2,j)
          TLnew(n+1,j)=TLnew(n,j)
        end do

        do i=1,n+1
          TLnew(i,1)=TLnew(i,2)
          TLnew(i,m+1)=TLnew(i,m)
        end do

C Update all the TEold, TLold with TEnew and TLnew
        do j=1,m+1
          do i=1,n+1
            TEold(i,j)=TEnew(i,j)
            TLold(i,j)=TLnew(i,j)
          enddo
        enddo

C If flagE or flagL is still be 1, then we should go
back to 2
C to do iteration again to calculate new TE and TL
C Use "iteration" to remember the time of
iterations

          if((flagE.eq.1).OR.(flagL.eq.1)) then
            iteration=iteration+1
            goto 2
          else
C-----Compute qex and qey-----
            do j=2,m
              do i=1,n
                qex(i,j)=4.0*taue*sse*qexo(i,j)/dt-
qexo(i,j)
                $   -
tkex(i,j)*sse*(TEold(i+1,j)+TEo(i+1,j)
                $   -TEold(i,j)-TEo(i,j))/dx
              enddo
            enddo

            do j=1,m
              do i=2,n
                qey(i,j)=4.0*taue*sse*qeyo(i,j)/dt-
qeyo(i,j)
                $   -
tkey(i,j)*sse*(TEold(i,j+1)+TEo(i,j+1)
                $   -TEold(i,j)-TEo(i,j))/dy
              enddo
            enddo

C-----Compute qlx and qly-----
            do j=2,m
              do i=1,n
                qlx(i,j)=4.0*taul*ssl*qlxo(i,j)/dt-
qlxo(i,j)
                $   -
tk0*ssl*(TLold(i+1,j)+TL0(i+1,j)
                $   -TLold(i,j)-TL0(i,j))/dx
              enddo
            enddo

            do j=1,m
              do i=2,n
                qly(i,j)=4.0*taul*ssl*qlyo(i,j)/dt-
qlyo(i,j)
                $   -
tk0*ssl*(TLold(i,j+1)+TL0(i,j+1)
                $   -TLold(i,j)-TL0(i,j))/dy
              enddo
            enddo
          endif

          write (*,*) "iteration=", iteration
C-----Iterations Done-----

          END
C   end of subroutine temp()

          subroutine
          velocity(n,m,dx,dy,dt,TEo,TEold,xseo,yseo,sseo,

```

```

$
xsen,ysen,ssen,v1o,v2o,v1n,v2n,u1o,u2o,u1n,u2n)
implicit double precision (a-h,l,o-z)
c
dimension TEO(400,200),TEold(400,200),
$ xseo(401,201),yseo(401,201),sseo(401,201),
$ xsen(401,201),ysen(401,201),ssen(401,201),
$
v1o(401,201),v2o(401,201),v1n(401,201),v2n(401
,201),
$
u1o(401,201),u2o(401,201),u1n(401,201),u2n(401
,201)
c
c Density
lou=1.93d+4
c Electron - blast coefficient
tri=70
theta=1.0
c
do j=2,m
do i=1,n
v1n(i,j)=((theta*(xsen(i+1,j)-xsen(i,j))
$ +(1.0-theta)*(xseo(i+1,j)-
xseo(i,j)))/(dx)
$ +(theta*(ssen(i,j)-ssen(i,j-1))
$ +(1.0-theta)*(sseo(i,j)-sseo(i,j-
1)))/(dy)
$
+tri*theta*(TEold(i+1,j)*TEold(i+1,j)-TEold(i,j)
$ *TEold(i,j))/(dx)
$ +tri*(1.0-
theta)*(TEo(i+1,j)*TEo(i+1,j)
$ -TEo(i,j)*TEo(i,j))
$ /(dx))*dt/lou+v1o(i,j)
c
u1n(i,j)=(theta*v1n(i,j)+(1.0-
theta)*v1o(i,j))*dt+u1o(i,j)
end do
end do
c
do j=1,m
do i=2,n
v2n(i,j)=((theta*(ssen(i,j)-ssen(i-1,j))
$ +(1.0-theta)*(sseo(i,j)-sseo(i-
1,j)))/(dx)
$ +(theta*(ysen(i,j+1)-ysen(i,j))
$ +(1.0-theta)*(yseo(i,j+1)-
yseo(i,j)))/(dy)
$
+tri*theta*(TEold(i,j+1)*TEold(i,j+1)-
TEold(i,j)
$ *TEold(i,j))/(dy)
$ +tri*(1.0-
theta)*(TEo(i,j+1)*TEo(i,j+1)
$ -TEo(i,j)*TEo(i,j))
$ /(dy))*dt/lou+v2o(i,j)
c
u2n(i,j)=(theta*v2n(i,j)+(1.0-
theta)*v2o(i,j))*dt+u2o(i,j)
end do
end do
return
END

```


APPENDIX C

SOURCE CODE FOR 2D DOUBLE-LAYERED CASE

```

c Program main
  implicit double precision (a-h,l,o-z)
  dimension t(4001),t1(4001),x(401),y(201)
  dimension
TEo(401,201),TEold(401,201),TLo(401,201),TLold(401,201),
  $
  TEm(4001),TLm(4001),
u1m(4001),u2m(4001), v1m(4001),v2m(4001),
  $
  qexo(400,200),qlxo(400,200),
qeyo(400,200),qlyo(400,200),
  $
  qex(400,200),qlx(400,200),
qey(400,200),qly(400,200),
  $ xsao(401,201),ysao(401,201),ssao(401,201),
  $
  xsao(401,201),ysao(401,201),ssao(401,201),
  $ xsan(401,201),ysan(401,201),ssan(401,201),
  $ xseo(401,201),yseo(401,201),sseo(401,201),
  $ xsen(401,201),ysen(401,201),ssen(401,201),
  $
v1o(401,201),v2o(401,201),v1n(401,201),v2n(401,201),
  $
u1o(401,201),u2o(401,201),u1n(401,201),u2n(401,201)

  integer p, counter

C Gold lame constant
  lemta1=199.0d+9
C Gold shear modulus
  cmiu1=27.0d+9
C Gold thermal expansion coefficient
  alphas1=14.2d-6
C Gold density
  lou1=1.93d+4

C Chromium lame constant
  lemta2=83.3d+9
C Chromium shear modulus
  cmiu2=115.0d+9
C Chromium thermal expansion coefficient
  alphas2=4.9d-6
C Chromium density
  lou2=7.19d+3

lx=0.5D-7
ly=1.0D-6
n=80
m=40
dx=lx/n
dy=ly/m
p=4000
dt=0.005d-12
counter=0
t(1)=0
x(1)=0

y(1)=0
T0=300.0
do j=2,m+1
  y(j)=y(j-1)+dy
end do
do i=2,2*n+1
  x(i)=x(i-1)+dx
end do

C initial condition
k=1
do j=1,m+1
  do i=1,2*n+1
    TEo(i,j)=T0
    TLo(i,j)=T0
    TEold(i,j)=T0
    TLold(i,j)=T0
C   xsan(i,j)=0.0
C   ysan(i,j)=0.0
    xsao(i,j)=0.0
    ysao(i,j)=0.0
    ssao(i,j)=0.0
    xsao(i,j)=0.0
    ysao(i,j)=0.0
    ssao(i,j)=0.0
    xseo(i,j)=0.0
    yseo(i,j)=0.0
    sseo(i,j)=0.0
    v1o(i,j)=0.0
    v2o(i,j)=0.0
    u1o(i,j)=0.0
    u2o(i,j)=0.0
  end do
end do

do j=2,m
  do i=1,2*n
    qexo(i,j)=0.0
    qlxo(i,j)=0.0
    qex(i,j)=0.0
    qlx(i,j)=0.0
  enddo
enddo

do j=1,m
  do i=2,2*n
    qeyo(i,j)=0.0
    qlyo(i,j)=0.0
    qey(i,j)=0.0
    qly(i,j)=0.0
  enddo
enddo

```

```

TEm(k)=0.0
TLm(k)=T0

big=0.0

write(*,*) 'start'

do k=2,p+1

t(k)=t(k-1)+dt
t1(k)=t(k-1)+dt/2.0

call
temp(n,m,dx,dy,x,y,t1(k),dt,TLo,TLold,TEo,TEold,
$
xsan,ysan,xsao,ysao,qexo,qeyo,qlxo,qlyo,
$ qex,qey,qlx,qly)

do j=1,m+1
do i=1,2*n+1
xsan(i,j)=xsao(i,j)
ysan(i,j)=ysao(i,j)
enddo
enddo

do j=1,m
do i=1,2*n
ssan(i,j)=ssao(i,j)
end do
end do

tol=1d-14
detuvmax=tol+1d-5
do while (detuvmax.gt.tol)
detuvmax=0.0

C Compute stress
do j=1,m+1
xsan(1,j)=0.0
xsan(2*n+1,j)=0.0
end do

do i=1,2*n+1
ysan(i,1)=0.0
ysan(i,m+1)=0.0
end do

do j=2,m

C The thin film of gold

do i=2,n+1

xsan(i,j)=(lemta1+2.0*cmiu1)*xsan(i,j)+lemta1*y
san(i,j)

$
(3.0*lemta1+2.0*cmiu1)*alphi1*(TLold(i,j)-
300.0)

ysen(i,j)=lemta1*xsan(i,j)+(lemta1+2.0*cmiu1)*y
san(i,j)
$
(3.0*lemta1+2.0*cmiu1)*alphi1*(TLold(i,j)-
300.0)
end do

C The thin film of chromium

do i=n+2,2*n

xsen(i,j)=(lemta2+2.0*cmiu2)*xsan(i,j)+lemta2*y
san(i,j)
$
(3.0*lemta2+2.0*cmiu2)*alphi2*(TLold(i,j)-
300.0)

ysen(i,j)=lemta2*xsan(i,j)+(lemta2+2.0*cmiu2)*y
san(i,j)
$
(3.0*lemta2+2.0*cmiu2)*alphi2*(TLold(i,j)-
300.0)
end do

end do

do j=1,m
ssan(1,j)=0.0
ssan(2*n,j)=0.0
end do

C Gold film
do i=1,n-1
ssan(i,1)=0.0
ssan(i,m)=0.0
end do

C Chromium film
do i=n+2,2*n
ssan(i,1)=0.0
ssan(i,m)=0.0
end do

do j=2,m-1

C The thin film of gold

do i=2,n
ssan(i,j)=cmiu1*ssan(i,j)
end do

C The thin film of chromium

do i=n+1,2*n-1

```

```

    ssen(i,j)=cmiu2*ssan(i,j)
end do

end do

ssen(n,1)=cmiu1*ssan(n,1)
ssen(n,m)=cmiu1*ssan(n,m)
ssen(n+1,1)=cmiu2*ssan(n+1,1)
ssen(n+1,m)=cmiu2*ssan(n+1,m)

C Calculate velocity
  call velocity(n,m,dx,dy,dt,TEold,TLold,
  $
xsen,ysen,ssen,xsao,ysao,ssao,v1o,v2o,v1n,v2n,u1
o,u2o,u1n,u2n)

C Calculate strain
  do j=2,m

C The thin film of gold
  do i=2,n
    xsan(i,j)=((v1n(i,j)-v1n(i-1,j))/dx)
    $      *dt+xsao(i,j)

    ysan(i,j)=((v2n(i,j)-v2n(i,j-1))/dy)
    $      *dt+ysao(i,j)
  end do

C At interface

  xsan(n+1,j)=((v1n(n+1,j)-v1n(n,j))*2.0/dx)
  $      *dt+xsao(i,j)

  ysan(n+1,j)=((v2n(n+1,j)-v2n(n+1,j-1))/dy)
  $      *dt+ysao(i,j)

C The thin film of chromium
  do i=n+2,2*n
    xsan(i,j)=((v1n(i+1,j)-v1n(i,j))/dx)
    $      *dt+xsao(i,j)

    ysan(i,j)=((v2n(i,j)-v2n(i,j-1))/dy)
    $      *dt+ysao(i,j)
  end do

end do

C Shear strain
  do j=2,m-1

C The thin film of gold
  do i=2,n
    ssan(i,j)=((v1n(i,j+1)-v1n(i,j))/dy
    $      +(v2n(i+1,j)-v2n(i,j))/dx)
    $      *dt+ssao(i,j)
  end do

end do

C The thin film of chromium
  do i=n+1,2*n-1
    ssan(i,j)=((v1n(i+1,j+1)-v1n(i+1,j))/dy
    $      +(v2n(i+1,j)-v2n(i,j))/dx)
    $      *dt+ssao(i,j)
  end do

end do

ssan(n,1)=((v1n(n,2)-v1n(n,1))/dy
$      +(v2n(n+1,1)-v2n(n,1))/dx)
$      *dt+ssao(n,1)
ssan(n,m)=((v1n(n,m+1)-v1n(n,m))/dy
$      +(v2n(n+1,m)-v2n(n,m))/dx)
$      *dt+ssao(n,m)
ssan(n+1,1)=((v1n(n+2,2)-v1n(n+2,1))/dy
$      +(v2n(n+2,1)-v2n(n+1,1))/dx)
$      *dt+ssao(n+1,1)
ssan(n+1,m)=((v1n(n+2,m+1)-v1n(n+2,m))/dy
$      +(v2n(n+2,m)-v2n(n+1,m))/dx)
$      *dt+ssao(n+1,m)

C Completion of calculation of strain
  do j=1,m+1
    do i=1,2*n+1
      det1=xsan(i,j)-xsao(i,j)
      det2=ysan(i,j)-ysao(i,j)
      det3=ssan(i,j)-ssao(i,j)
      det=max(abs(det1),abs(det2),abs(det3))
      if (abs(det).gt.detuvmax) then
        detuvmax=abs(det)
      endif
    end do
  end do

  do j=1,m+1
    do i=1,2*n+1
      xsao(i,j)=xsan(i,j)
      ysao(i,j)=ysan(i,j)
      ssao(i,j)=ssan(i,j)
    end do
  end do

C write(*,*) 'detuvmax=', detuvmax

C End do with detmax
end do

C-----
  do j=1,m+1
    do i=1,2*n+1

```

```

TEo(i,j)=TEold(i,j)
TLo(i,j)=TLold(i,j)
xsao(i,j)=xsan(i,j)
ysao(i,j)=ysan(i,j)
ssao(i,j)=ssan(i,j)
xseo(i,j)=xsen(i,j)
yseo(i,j)=ysen(i,j)
sseo(i,j)=ssen(i,j)
v1o(i,j)=v1n(i,j)
v2o(i,j)=v2n(i,j)
u1o(i,j)=u1n(i,j)
u2o(i,j)=u2n(i,j)
end do
end do

do j=2,m
do i=1,2*n
qexo(i,j)=qex(i,j)
qlxo(i,j)=qlx(i,j)
enddo
enddo

do j=1,m
do i=2,2*n
qeyo(i,j)=qey(i,j)
qlyo(i,j)=qly(i,j)
enddo
enddo

if (big.lt.(TEold(1,1)-T0)) then
big=TEold(1,1)-T0
end if

TEm(k)=TEold(1,1)-T0
TLM(k)=TLold(1,1)
u1m(k)=u1n(1,2)
u2m(k)=u2n(2,1)
v1m(k)=v1n(1,2)
v2m(k)=v2n(2,1)

counter=counter+1
write(*,*) counter

C Output intermediate result

if (k.eq.50) then

C The result at time t=0.25ps

open(unit=9,file='Te025(y=0).dat')
do i=1,2*n+1
write(9,1010) x(i),TEold(i,1)
enddo

open(unit=10,file='Tl025(y=0).dat')
do i=1,2*n+1

write(10,1010) x(i),TLold(i,1)
enddo

if (k.eq.100) then

C The result at time t=0.5ps

open(unit=11,file='Te05(y=0).dat')
do i=1,2*n+1
write(11,1010) x(i), TEold(i,1)
enddo

open(unit=12,file='Tl05(y=0).dat')
do i=1,2*n+1
write(12,1010) x(i),TLold(i,1)
enddo
end if

if (k.eq.200) then

C The result at time t=1ps

open(unit=13,file='Te1(y=0).dat')
do i=1,2*n+1
write(13,1010) x(i),TEold(i,1)
enddo

open(unit=14,file='Tl1(y=0).dat')
do i=1,2*n+1
write(14,1010) x(i),TLold(i,1)
enddo

open(unit=15,file='u1(y=0).dat')
do i=1,2*n+1
write(15,1010) x(i),u1n(i,2)
enddo

open(unit=16,file='v1(y=0).dat')
do i=2,2*n
write(16,1010) x(i),u2n(i,1)
enddo

open(unit=17,file='sigmax1(y=0).dat')
do i=1,2*n+1
write(17,1010) x(i),xsen(i,2)
enddo

open(unit=18,file='sigmay1(y=0).dat')
do i=2,2*n
write(18,1010) x(i),ysen(i,2)
enddo
end if

if (k.eq.1000) then

```

C The result at time $t=5\text{ps}$

```

open(unit=19,file='Te5(y=0).dat')
do i=1,2*n+1
write(19,1010) x(i),TEold(i,1)
enddo

open(unit=20,file='Tl5(y=0).dat')
do i=1,2*n+1
write(20,1010) x(i),TLold(i,1)
enddo

open(unit=21,file='u5(y=0).dat')
do i=1,2*n+1
write(21,1010) x(i),u1n(i,2)
enddo

open(unit=22,file='v5(y=0).dat')
do i=2,2*n
write(22,1010) x(i),u2n(i,1)
enddo

open(unit=23,file='sigmax5(y=0).dat')
do i=1,2*n+1
write(23,1010) x(i),xsen(i,2)
enddo

open(unit=24,file='sigmay5(y=0).dat')
do i=2,2*n
write(24,1010) x(i),ysen(i,2)
enddo

end if

```

C the result at time $t=10\text{ps}$

```

if (k.eq.2000) then
open(unit=25,file='Te10(y=0).dat')
do i=1,2*n+1
write(25,1010) x(i),TEold(i,1)
enddo

open(unit=26,file='Tl10(y=0).dat')
do i=1,2*n+1
write(26,1010) x(i),TLold(i,1)
enddo

open(unit=27,file='u10(y=0).dat')
do i=1,2*n+1
write(27,1010) x(i),u1n(i,2)
enddo

open(unit=28,file='v10(y=0).dat')
do i=2,2*n
write(28,1010) x(i),u2n(i,1)

```

enddo

```

open(unit=29,file='sigmax10(y=0).dat')
do i=1,2*n+1
write(29,1010) x(i),xsen(i,2)
enddo

```

```

open(unit=30,file='sigmay10(y=0).dat')
do i=2,2*n
write(30,1010) x(i),ysen(i,2)
enddo
end if

```

C the result at time $t=15\text{ps}$

```

if (k.eq.3000) then
open(unit=31,file='u15(y=0).dat')
do i=1,2*n+1
write(31,1010) x(i),u1n(i,2)
enddo

```

```

open(unit=32,file='v15(y=0).dat')
do i=2,2*n
write(32,1010) x(i),u2n(i,1)
enddo

```

```

open(unit=33,file='sigmax15(y=0).dat')
do i=1,2*n+1
write(33,1010) x(i),xsen(i,2)
enddo

```

```

open(unit=34,file='sigmay15(y=0).dat')
do i=2,2*n
write(34,1010) x(i),ysen(i,2)
enddo
end if

```

C the result at time $t=20\text{ps}$

```

if (k.eq.4000) then
open(unit=35,file='Te20(y=0).dat')
do i=1,2*n+1
write(35,1010) x(i),TEold(i,1)
enddo

```

```

open(unit=36,file='Tl20(y=0).dat')
do i=1,2*n+1
write(36,1010) x(i),TLold(i,1)
enddo

```

```

open(unit=37,file='u20(y=0).dat')
do i=1,2*n+1
write(37,1010) x(i),u1n(i,2)
enddo

```

```

open(unit=38,file='v20(y=0).dat')
do i=2,2*n
write(38,1010) x(i),u2n(i,1)

```

```

enddo

open(unit=39,file='sigmax20(y=0).dat')
do i=1,2*n+1
write(39,1010) x(i),xsen(i,2)
enddo

open(unit=40,file='sigmay20(y=0).dat')
do i=2,2*n
write(40,1010) x(i), ysen(i,2)
enddo
end if

C end of time loop k=2,p+1
end do

C Outputs

C open(unit=6,file='xse10(Test).dat')
C print *, "zonexse1"
C do i=1,n+1
C print *, (x(i)*1.0D+6), (xseo(i,2)*1.0D-9)
C enddo

C open(unit=6,file='yse1.dat')
C print *, "zoneyse1"
C do i=1,n+1
C print *, x(i), ysen(i,2)
C enddo

C show the temperature TE at x=0 and y=0 versus
time
C open(unit=6,file='etm84(T).dat')
C print *, "zone"
C do k=1,p+1
C print *, (t(k)*1.0D+12),(TEm(k)/big)
C enddo

C show the temperature u at x=0 and y=0 versus
time
C open(unit=6,file='um315.dat')
C print *, "zone"
C do k=1,p+1
C print *, (t(k)*1.0D+12),(u1m(k)*1.0D+9)
C enddo

1010 format(401e15.6)
1020 format(e15.6,2e15.6)

end

subroutine
temp(n,m,dx,dy,x,y,t,dt,TLo,TLold,TEo,TEold,
$
xsan,ysan,xsao,ysao,qexo,qeyo,qlxo,qlyo,

```

```

$ qex,qey,qlx,qly)

implicit double precision (a-h,l,o-z)
double precision TEM
dimension x(401),y(201),TEM(1000)
dimension
TEo(401,201),TEold(401,201),
$ TLo(401,201),TLold(401,201),
$ TNew(401,201), TLnew(401,201),
$ xsan(401,201),ysan(401,201),
$ xsao(401,201),ysao(401,201),S(401,201),
$ tkex(401,201),tkey(401,201),
$ qexo(400,200),qlxo(400,200),
$ qex(400,200),qlx(400,200),
$ qeyo(400,200),qlyo(400,200),
$ qey(400,200),qly(400,200),
$ dTE(400,200),dTl(400,200)

```

```
integer iteration,flagE,flagL
```

```
C-----All the Constants-----
```

```

C Gold lame constant
lemta1=199.0d+9
C Gold shear modulus
cmiu1=27.0d+9
C Gold thermal expansion coefficient
alphan1=14.2d-6
C Gold electron heat capacity
Ae1=70.0
C Gold latic heat capacity
cl1=2.5d+6
C Gold electron - latic coupling factor
g1=2.6d+16
C Gold electron thermal conductivity
tk01=315.0
C Gold electron relaxation time
taue1=0.04D-12
C Gold lattice relaxation time
taul1=0.8D-12

C Chromium lame constant
lemta2=83.3d+9
C Chromium shear modulus
cmiu2=115.0d+9
C Chromium thermal expansion coefficient
alphan2=4.9d-6
C Chromium electron heat capacity
Ae2=193.3
C Chromium latic heat capacity
cl2=3.3d+6
C Chromium electron - latic coupling factor
g2=4.2d+17
C Chromium electron thermal conductivity
tk02=94.0
C Chromium electron relaxation time
taue2=6.8D-15

```

```

C Chromium lattice relaxation time
  tauL2=1.36D-13
                                enddo
                                enddo

C Laser fluence
  flu=500.0
                                do j=2,m
                                do i=2,n

C Laser pulse duration
  tp=0.1d-12
                                temp1=abs((TEold(i,j)+TEo(i,j))/(TLold(i,j)+TL0(
C Optical penetration depth
  delta=15.3d-9
                                i,j)))
                                temp3=abs((TEold(i,j-1)+TEo(i,j-1))
C Surface reflectivity
  sur=0.93
                                $      /(TLold(i,j-1)+TL0(i,j-1)))

C Spatial profile parameters
  rs=1d-6
                                tkey(i,j)=0.5*tk01*(temp1+temp3)
                                enddo
                                do i=n+1,2*n

                                temp1=abs((TEold(i,j)+TEo(i,j))/(TLold(i,j)+TL0(
                                i,j)))
                                temp3=abs((TEold(i,j-1)+TEo(i,j-1))
                                $      /(TLold(i,j-1)+TL0(i,j-1)))

                                tkey(i,j)=0.5*tk02*(temp1+temp3)
                                enddo
                                enddo

C Calculate TNew for Gold and Chromium layers
and the interface
  do j=2,m
C Gold layer
  do i=2,2*n
    if (i.le.n) then
      S(i,j)=0.94*flu*(1.0-sur)/(tp*delta)
    $      *exp(-x(i)/delta-y(j)*y(j)/(rs*rs)
    $      -2.77*(t-2.0*tp)*(t-
    2.0*tp)/(tp*tp))

    ffe1=4.0*Ae1*dx*dy*(TEold(i,j)*TEold(i,j)
    $      +TEold(i,j)*TEo(i,j)+TEo(i,j)*TEo(i,j))
    $      /(3.0*(TEold(i,j)+TEo(i,j)))

    tempx1=dt*dy*tkex(i,j)/dx
    tempx2=dt*dy*tkex(i-1,j)/dx

    tempy1=dt*dx*tkey(i,j)/dy
    tempy2=dt*dx*tkey(i,j-1)/dy

    a11=ffe1+(tempx1+tempx2+tempy1+tempy2)*sse
    1+g1*d

    b11=ffe1*TEo(i,j)
    b21=-4.0*dy*taue1*sse1*(qexo(i,j)-qexo(i-
    1,j))

    b31=tempx1*sse1*(TEold(i+1,j)+TEo(i+1,j))-
    TEo(i,j)

C-----Iteration starts-----
C flagE and flagL indicate whether TE and TL are
precise enough
C keep on iterating as long as flagE or flagL
equals to 1
2  flagE=1
  flagL=1

  aximumE=0.0

C Define tkex(i,j)
  do j=2,m
  do i=2,n

temp1=abs((TEold(i,j)+TEo(i,j))/(TLold(i,j)+TL0(
i,j)))
  temp2=abs((TEold(i-1,j)+TEo(i-1,j))
  $      /(TLold(i-1,j)+TL0(i-1,j)))

  tkex(i,j)=0.5*tk01*(temp1+temp2)
  enddo
  do i=n+1,2*n

temp1=abs((TEold(i,j)+TEo(i,j))/(TLold(i,j)+TL0(
i,j)))
  temp2=abs((TEold(i-1,j)+TEo(i-1,j))
  $      /(TLold(i-1,j)+TL0(i-1,j)))

  tkex(i,j)=0.5*tk02*(temp1+temp2)

```



```

        b41=-tempx2*sse1*(TEo(i,j)-TEold(i-
1,j)-TEo(i-1,j))
        b51=-4.0*dx*taue1*sse1*(qeyo(i,j)-
qeyo(i,j-1))

b61=tempy1*sse1*(TEold(i,j+1)+TEo(i,j+1)-
TEo(i,j))
        b71=-tempy2*sse1*(TEo(i,j)-
TEold(i,j-1)-TEo(i,j-1))
        b81=-g1*d*(TEo(i,j)-TLold(i,j)-
TLo(i,j))
        b91=2.0*d*S(i,j)

C TNew: The new TE at the right now time point
calculated based on the
C   old TEs and TEs at the previous time point

TNew(i,j)=(b11+b21+b31+b41+b51+b61+b71+b
81+b91)/a11

C dTE: Difference between the new and the old
TEs at now time point
        dTE(i,j)=abs(TNew(i,j)-TEold(i,j))

C Interface at i=n+1
        else if (i.eq.n+1) then
                ai=-
                (tkex(n,j)*sse1+tkex(n+1,j)*sse2)/dx
                bi1=-4.0*taue1*sse1*qexo(n,j)/dt
                bi2=tkex(n,j)*sse1*(TEo(n+1,j)-
TEold(n,j))
                $
                -TEo(n,j))/dx
                bi3=4.0*taue2*sse2*qexo(i,j)/dt
                bi4=-
                tkex(n+1,j)*sse2*(TEold(n+2,j)+TEo(n+2,j)
                $
                -TEo(n+1,j))/dx

                TNew(i,j)=(bi1+bi2+bi3+bi4)/ai

                dTE(i,j)=abs(TNew(i,j)-TEold(i,j))

        else
C Chromium Layer

                S(i,j)=0.94*flu*(1.0-sur)/(tp*delta)
                $
                *exp(-x(i)/delta-y(j)*y(j)/(rs*rs)
                $
                -2.77*(t-2.0*tp)*(t-
                2.0*tp)/(tp*tp))

                ffe2=4.0*Ae2*dx*dy*(TEold(i,j)*TEold(i,j)
                $
                +TEold(i,j)*TEo(i,j)+TEo(i,j)*TEo(i,j))
                $
                /(3.0*(TEold(i,j)+TEo(i,j)))

                tempx1=dt*dy*tkex(i,j)/dx
                tempx2=dt*dy*tkex(i-1,j)/dx

                tempy1=dt*dx*tkey(i,j)/dy
                tempy2=dt*dx*tkey(i,j-1)/dy

a12=ffe2+(tempx1+tempx2+tempy1+tempy2)*sse
2+g2*d

        b12=ffe2*TEo(i,j)
        b22=-4.0*dy*taue2*sse2*(qexo(i,j)-qexo(i-
1,j))

b32=tempx1*sse2*(TEold(i+1,j)+TEo(i+1,j)-
TEo(i,j))
        b42=-tempx2*sse2*(TEo(i,j)-TEold(i-1,j)-
TEo(i-1,j))
        b52=-4.0*dx*taue2*sse2*(qeyo(i,j)-
qeyo(i,j-1))

b62=tempy1*sse2*(TEold(i,j+1)+TEo(i,j+1)-
TEo(i,j))
        b72=-tempy2*sse2*(TEo(i,j)-TEold(i,j-1)-
TEo(i,j-1))
        b82=-g2*d*(TEo(i,j)-TLold(i,j)-TLo(i,j))
        b92=2.0*d*S(i,j)

C TNew: The new TE at the right now time point
calculated based on the
C   old TEs and TEs at the previous time point

TNew(i,j)=(b12+b22+b32+b42+b52+b62+b72+b
82+b92)/a12

C dTE: Difference between the new and the old
TEs at now time point
        dTE(i,j)=abs(TNew(i,j)-TEold(i,j))
        endif
        enddo
        enddo

        do j=2,m
                do i=2,2*n
C aximumE: The maximum difference between all
the new and the old TEs
                        if (aximumE.le.dTE(i,j)) then
                                aximumE=dTE(i,j)
                        endif
                enddo
        enddo

C If aximumE is less than 1D-6, which means that
the largest difference
C between the new and old TEs are smaller than
1D-6, make flagE=0 to
C stop the iteration for TE
        if(aximumE.lt.1D-6) then
                flagE=0

```

```

endif
do j=2,m
  TEnew(1,j)=TEnew(2,j)
  TEnew(2*n+1,j)=TEnew(2*n,j)
end do
do i=1,2*n+1
  TEnew(i,1)=TEnew(i,2)
  TEnew(i,m+1)=TEnew(i,m)
end do
C-----TEnew Calculated-----
C*****
C-----Start calculating TLnew-----
aximumL=0.0

tempx1=tk01*dt*dy/dx
tempx2=tk02*dt*dy/dx
tempy1=tk01*dt*dx/dy
tempy2=tk02*dt*dx/dy

do j=2,m
  do i=2,2*n
C Gold Layer
  if (i.le.n) then
c11=ffl1+2.0*(tempx1+tempy1)*ssl1+d*g1

    d11=ffl1*TLo(i,j)
    d21=-4.0*dy*taul1*ssl1*(qlxo(i,j)-qlxo(i-1,j))
d31=tempx1*ssl1*(TLold(i+1,j)+TLo(i+1,j)-TLo(i,j))
    d41=-tempx1*ssl1*(TLo(i,j)-TLold(i-1,j)-TLo(i-1,j))
    d51=-4.0*dx*taul1*ssl1*(qlyo(i,j)-qlyo(i,j-1))
d61=tempy1*ssl1*(TLold(i,j+1)+TLo(i,j+1)-TLo(i,j))
    d71=-tempy1*ssl1*(TLo(i,j)-TLold(i,j-1)-TLo(i,j-1))
    d81=-g1*d*(TLo(i,j)-TEold(i,j)-TEo(i,j))
    d91=ee1*(xsan(i,j)+ysan(i,j)-xsao(i,j)-ysao(i,j))

TLnew(i,j)=(d11+d21+d31+d41+d51+d61+d71+d81+d91)/c11

    dTL(i,j)=abs(TLnew(i,j)-TLold(i,j))

    else if (i.eq.n+1) then
C Interface at i=n+1

```

```

ci=-(tk01*ssl1+tk02*ssl2)/dx
di1=-4.0*taul1*qlxo(n,j)/(2.0*taul1+dt)
di2=tk01*ssl1*(TLo(n+1,j)-TLold(n,j)-TLo(n,j))/dx
$
di3=4.0*taul2*qlxo(n+1,j)/(2.0*taul2+dt)
di4=-
tk02*ssl2*(TLold(n+2,j)+TLo(n+2,j)-TLo(n+1,j))/dx
$
TLnew(i,j)=(di1+di2+di3+di4)/ci
dTL(i,j)=abs(TLnew(i,j)-TLold(i,j))
else
C Gromium Layer
c11=ffl2+2.0*(tempx2+tempy2)*ssl2+d*g2

    d11=ffl2*Tlo(i,j)
    d21=-4.0*dy*taul2*ssl2*(qlxo(i,j)-qlxo(i-1,j))
d31=tempx2*ssl2*(TLold(i+1,j)+TLo(i+1,j)-TLo(i,j))
    d41=-tempx2*ssl2*(TLo(i,j)-TLold(i-1,j)-TLo(i-1,j))
    d51=-4.0*dx*taul2*ssl2*(qlyo(i,j)-qlyo(i,j-1))
d61=tempy2*ssl2*(TLold(i,j+1)+TLo(i,j+1)-TLo(i,j))
    d71=-tempy2*ssl2*(TLo(i,j)-TLold(i,j-1)-TLo(i,j-1))
    d81=-g2*d*(TLo(i,j)-TEnew(i,j)-TEo(i,j))
    d91=ee2*(xsan(i,j)+ysan(i,j)-xsao(i,j)-ysao(i,j))

TLnew(i,j)=(d11+d21+d31+d41+d51+d61+d71+d81+d91)/c11

    dTL(i,j)=abs(TLnew(i,j)-TLold(i,j))
endif
enddo
enddo

do j=2,m
  do i=2,2*n
C aximumL: The maximum difference between all the new and the old TLs
  if (aximumL.le.dTL(i,j)) then
    aximumL=dTL(i,j)
  endif
enddo
enddo

if(aximumL.lt.1D-6) then

```

```

    flagL=0
endif
do j=2,m
    TLnew(1,j)=TLnew(2,j)
    TLnew(2*n+1,j)=TLnew(2*n,j)
end do

do i=1,2*n+1
    TLnew(i,1)=TLnew(i,2)
    TLnew(i,m+1)=TLnew(i,m)
end do

C Update all the TEold, TLold with TEnew and TLnew
do j=1,m+1
    do i=1,2*n+1
        TEold(i,j)=TEnew(i,j)
        TLold(i,j)=TLnew(i,j)
    enddo
enddo

C If flagE or flagL is still be 1, then we should go
back to 2
C to do iteration again to calculate new TE and TL
C Use "iteration" to remember the time of
iterations
    if((flagE.eq.1).OR.(flagL.eq.1)) then
        iteration=iteration+1
    goto 2
    else
C-----Compute qex and qey-----
        do j=2,m
            do i=1,n
                qex(i,j)=(4.0*taue1/(2.0*taue1+dt)-
1.0)*qexo(i,j)
                $
                tkex(i,j)*sse1/dx*(TEold(i+1,j)+TEo(i+1,j)
                $
                -TEold(i,j)-TEo(i,j))
            enddo
C
                qex(n,j)=(4.0*taue1*sse1/dt-
1.0)*qexo(n,j)-tkex(n,j)
C $
                *sse1/dx
C $
                *(TEold(n+1,j)+TEo(n+1,j)-
TEold(n,j)-TEo(n,j))
C
                qex(n+1,j)=qex(n,j)
                do i=n+1,2*n
                    qex(i,j)=(4.0*taue2/(2.0*taue2+dt)-
1.0)*qexo(i,j)
                    $
                    tkex(i,j)*sse2/dx*(TEold(i+1,j)+TEo(i+1,j)
                    $
                    -TEold(i,j)-TEo(i,j))
                enddo
            enddo

                do j=1,m-1
                    do i=2,n
                        qey(i,j)=(4.0*taue1/(2.0*taue1+dt)-
1.0)*qeyo(i,j)
                        $
                        tkey(i,j)*sse1/dy*(TEold(i,j+1)+TEo(i,j+1)
                        $
                        -TEold(i,j)-TEo(i,j))
                    enddo
                    do i=n+1,2*n
                        qey(i,j)=(4.0*taue2/(2.0*taue2+dt)-
1.0)*qeyo(i,j)
                        $
                        tkey(i,j)*sse2/dy*(TEold(i,j+1)+TEo(i,j+1)
                        $
                        -TEold(i,j)-TEo(i,j))
                    enddo
                enddo

C-----Compute qlx and qly-----
                do j=2,m
                    do i=1,n
                        qlx(i,j)=(4.0*taul1/(2.0*taul1+dt)-
1.0)*qlxo(i,j)
                        $
                        tk01*ssl1/dx*(TLold(i+1,j)+TL0(i+1,j)
                        $
                        -TLold(i,j)-TL0(i,j))
                    enddo
C
                        qlx(n,j)=(4.0*taul1*ssl1/dt-
1.0)*qlxo(n,j)-tk01*ssl1/dx
C $
                        *(TLold(n+1,j)+TL0(n+1,j)-TLold(n,j)
                        $
                        -TL0(n,j))
C
                        qlx(n+1,j)=qlx(n,j)

                        do i=n+1,2*n
                            qlx(i,j)=(4.0*taul2/(2.0*taul2+dt)-
1.0)*qlxo(i,j)
                            $
                            tk02*ssl2/dx*(TLold(i+1,j)+TL0(i+1,j)
                            $
                            -TLold(i,j)-TL0(i,j))
                        enddo
                    enddo

                    do j=1,m
                        do i=2,n
                            qly(i,j)=(4.0*taul1/(2.0*taul1+dt)-
1.0)*qlyo(i,j)
                            $
                            tk01*ssl1/dy*(TLold(i,j+1)+TL0(i,j+1)
                            $
                            -TLold(i,j)-TL0(i,j))
                        enddo
                        do i=n+1,2*n
                            qly(i,j)=(4.0*taul2/(2.0*taul2+dt)-
1.0)*qlyo(i,j)
                            $
                            tk02*ssl2/dy*(TLold(i,j+1)+TL0(i,j+1)
                            $
                            -TLold(i,j)-TL0(i,j))
                        enddo
                    enddo
                enddo
            enddo
        enddo
    enddo

```

```

        enddo
        endif

C      write (*,*) "iteration=", iteration
C-----Iterations Done-----

      END
C    end of subroutine temp()

      subroutine velocity(n,m,dx,dy,dt,TEold,TLold,
$
xsen,ysen,ssen,xsao,ysao,ssao,v1o,v2o,v1n,v2n,u1
o,u2o,u1n,u2n)
      implicit double precision (a-h,l,o-z)

      dimension TEold(401,201),TLold(401,201),
$ xsen(401,201),ysen(401,201),ssen(401,201),
$ xsao(401,201),ysao(401,201),ssao(401,201),
$
v1o(401,201),v2o(401,201),v1n(401,201),v2n(401
,201),
$
u1o(401,201),u2o(401,201),u1n(401,201),u2n(401
,201)

C Gold lame constant
      lemta1=199.0d+9
C Gold shear modulus
      cmu1=27.0d+9
C Gold thermal expansion coefficient
      alphas1=14.2d-6
C Gold density
      lou1=1.93d+4
C Gold electron - blast coefficient
      tri1=70

C Chromium lame constant
      lemta2=83.3d+9
C Chromium shear modulus
      cmu2=115.0d+9
C Chromium thermal expansion coefficient
      alphas2=4.9d-6
C Chromium density
      lou2=7.19d+3
C chromium electron - blast coefficient
      tri2=193.3

C Velocity and displacement in the thickness
direction
      do j=2,m

C The thin film of gold
      do i=1,n
        v1n(i,j)=((xsen(i+1,j)-xsen(i,j))/dx
$ +(ssen(i,j)-ssen(i,j-1))/dy
$
+tri1*(TEold(i+1,j)*TEold(i+1,j)-
TEold(i,j)*TEold(i,j))/dx
$ *dt/lou1+v1o(i,j)
        u1n(i,j)=v1n(i,j)*dt+u1o(i,j)
      end do

C The thin film of chromium
      do i=n+2,2*n+1
        v1n(i,j)=((xsen(i,j)-xsen(i-1,j))/dx
$ +(ssen(i-1,j)-ssen(i-1,j-1))/dy
$
+tri2*(TEold(i,j)*TEold(i,j)-TEold(i-
1,j)*TEold(i-1,j))/dx
$ *dt/lou2+v1o(i,j)
        u1n(i,j)=v1n(i,j)*dt+u1o(i,j)
      end do

      v1n(n,2)=((xsen(n+1,2)-xsen(n,2))/dx
$ +ssen(n,2)/dy
$
+tri1*(TEold(n+1,2)*TEold(n+1,2)-
TEold(n,2)*TEold(n,2))/dx
$ *dt/lou1+v1o(n,2)
      u1n(n,2)=v1n(n,2)*dt+u1o(n,2)

C
      v1n(n,m)=((xsen(n+1,m)-xsen(n,m))/dx
$ -ssen(n,m-1)/dy
$
+tri1*(TEold(n+1,m)*TEold(n+1,m)-
TEold(n,m)*TEold(n,m))/dx
$ *dt/lou1+v1o(n,m)
      u1n(n,m)=v1n(n,m)*dt+u1o(n,m)

      v1n(n+2,2)=((xsen(n+2,2)-xsen(n+1,2))/dx
$ +ssen(n+1,2)/dy
$
+tri2*(TEold(n+2,2)*TEold(n+2,2)-
TEold(n+1,2)*TEold(n+1,2))/dx
$ *dt/lou2+v1o(n+2,2)
      u1n(n+2,2)=v1n(n+2,2)*dt+u1o(n+2,2)

      v1n(n+2,m)=((xsen(n+2,m)-xsen(n+1,m))/dx
$ -ssen(n+1,m-1)/dy
$
+tri2*(TEold(n+2,m)*TEold(n+2,m)-
TEold(n+1,m)*TEold(n+1,m))/dx
$ *dt/lou2+v1o(n+2,m)
      u1n(n+2,m)=v1n(n+2,m)*dt+u1o(n+2,m)

      v1n(n,1)=((xsen(n+1,2)-xsen(n,2))/dx
$ +2.0*ssen(n,1)/dy
$
+tri1*(TEold(n+1,1)*TEold(n+1,1)-
TEold(n,1)*TEold(n,1))/dx
$ *dt/lou1+v1o(n,1)
      u1n(n,1)=v1n(n,1)*dt+u1o(n,1)

      v1n(n,m+1)=((xsen(n+1,m)-xsen(n,m))/dx

```

```

$ -2.0*ssen(n,m)/dy
$ +tri1*(TEold(n+1,m+1)*TEold(n+1,m+1)-
TEold(n,m+1)
$ *TEold(n,m+1))/dx)
$ *dt/lou1+v1o(n,m+1)
u1n(n,m+1)=v1n(n,m+1)*dt+u1o(n,m+1)

v1n(n+2,1)=((xsen(n+2,2)-xsen(n+1,2))/dx
$ +2.0*ssen(n+1,1)/dy
$ +tri2*(TEold(n+2,1)*TEold(n+2,1)-
TEold(n+1,1)*TEold(n+1,1))/dx)
$ *dt/lou2+v1o(n+2,1)
u1n(n+2,1)=v1n(n+2,1)*dt+u1o(n+2,1)

v1n(n+2,m+1)=((xsen(n+2,m)-
xsen(n+1,m))/dx
$ -2.0*ssen(n+1,m)/dy
$ +tri2*(TEold(n+2,m+1)*TEold(n+2,m+1)-
TEold(n+1,m+1)
$ *TEold(n+1,m+1))/dx)
$ *dt/lou2+v1o(n+2,m+1)

u1n(n+2,m+1)=v1n(n+2,m+1)*dt+u1o(n+2,m+1)

C Velocity and displacement in the length
direction
do j=1,m

C The thin film of gold
do i=2,n
v2n(i,j)=((ssen(i,j)-ssen(i-1,j))/dx
$ +(ysen(i,j+1)-ysen(i,j))/dy
$ +tri1*(TEold(i,j+1)*TEold(i,j+1)-
TEold(i,j)*TEold(i,j))/dy)
$ *dt/lou1+v2o(i,j)

u2n(i,j)=v2n(i,j)*dt+u2o(i,j)
end do

C The thin film of chromium
do i=n+2,2*n
v2n(i,j)=((ssen(i,j)-ssen(i-1,j))/dx
$ +(ysen(i,j+1)-ysen(i,j))/dy
$ +tri2*(TEold(i,j+1)*TEold(i,j+1)-
TEold(i,j)*TEold(i,j))/dy)
$ *dt/lou2+v2o(i,j)

u2n(i,j)=v2n(i,j)*dt+u2o(i,j)
end do

end do

v2n(n,1)=(ysen(n,2)/dy)*dt/lou1+v2o(n,1)
u2n(n,1)=v2n(n,1)*dt+u2o(n,1)

v2n(n,m)=(-ysen(n,m)/dy)*dt/lou1+v2o(n,m)

u2n(n,m)=v2n(n,m)*dt+u2o(n,m)

v2n(n+2,1)=(ysen(n+2,2)/dy)*dt/lou2+v2o(n+2,1)
u2n(n+2,1)=v2n(n+2,1)*dt+u2o(n+2,1)

v2n(n+2,m)=(-
ysen(n+2,m)/dy)*dt/lou2+v2o(n+2,m)
u2n(n+2,m)=v2n(n+2,m)*dt+u2o(n+2,m)

C The interface between gold and chromium
C Velocity in length direction

do j=1,m
a1=cmiu1*dt/dy
a2=cmiu1*dt/dx
a3=cmiu1*ssao(i,j)
b1=cmiu2*dt/dy
b2=cmiu2*dt/dx
b3=cmiu2*ssao(i,j)

v2n(n+1,j)=(a2*v2n(n,j)+b2*v2n(n+2,j)+b1*(v1n(
n+1,j+1)-v1n(n+1,j))
$ +b3-a1*(v1n(n+1,j+1)-v1n(n+1,j))-
a3)/(a2+b2)

u2n(n+1,j)=v2n(n+1,j)*dt+u2o(n+1,j)

end do

C Velocity in thickness direction
do j=2,m
a1=(lemta1+2.0*cmiu1)*dt*2.0/dx
a2=(lemta1+2.0*cmiu1)*xsao(n+1,j)
a3=lemta1*dt/dy
a4=lemta1*ysao(n+1,j)
a5=(3.0*lemta1+2.0*cmiu1)*alphan1
b1=(lemta2+2.0*cmiu2)*dt*2.0/dx
b2=(lemta2+2.0*cmiu2)*xsao(n+2,j)
b3=lemta2*dt/dy
b4=lemta2*ysao(n+2,j)
b5=(3.0*lemta2+2.0*cmiu2)*alphan2
v1n(n+1,j)=(a1*v1n(n,j)+b1*v1n(n+2,j)+b2
$ +b3*(v2n(n+1,j)-v2n(n+1,j-1))+b4-
b5*(TLold(n+2,j)-300.0)
$ -a2-a3*(v2n(n+1,j)-v2n(n+1,j-1))-
a4+a5*(TLold(n+1,j)-300.0)
$ /(a1+b1)

u1n(n+1,j)=v1n(n+1,j)*dt+u1o(n+1,j)

end do

return
end

```

REFERENCES

- [Al-Nimr 1999] M.A. Al-Nimr and V.S. Arpaci, "Picosecond thermal pulses in thin metal films," *Journal of Applied Physics*, Vol. 85, (1999), pp. 2517-2521.
- [Al-Nimr 2000] M.A. Al-Nimr and V.S. Arpaci, "The thermal behavior of thin metal films in the hyperbolic two-step model," *International Journal of Heat and Mass Transfer*, Vol. 43, (2000), pp. 2021-2028.
- [Al-Nimr 2003] M.A. Al-Nimr, M. Header, and M. Naji, "Use of the microscopic parabolic heat conduction model in place of macroscopic model validation criterion under harmonic boundary heating," *International Journal of Heat and Mass Transfer*, Vol. 46, (2003), pp. 333-339.
- [Al-Odat 2002] M. Al-Odat, M.A. Al-Nimr, and M. Hamdan, "Thermal stability of superconductors under the effect of a two-dimensional hyperbolic heat conduction model," *International Journal of Numerical Methods for Heat & Fluid Flow*, Vol. 12, (2002), pp. 173-177.
- [Anisimov 1974] S.I. Anisimov, B.L. Kapeliovich, and T.L. Perel' man, "Electron emission from metal surface exposed to ultra-short laser pulse," *Soviet Physics Journal of Experimental and Theoretical Physics*, Vol. 39, (1974), pp. 375-377.
- [Antaki 1998] P.J. Antaki, "Solution for non-Fourier dual phase lag heat conduction in a semi-infinite slab with surface heat flux," *International Journal of Heat and Mass Transfer*, Vol. 41, (1998), pp. 2253-2258.
- [Antaki 2002] P.J. Antaki, "Importance of nonequilibrium thermal conductivity during short-pulse laser-induced desorption from metals," *International Journal of Heat and Mass Transfer*, Vol. 45, (2002), pp. 4063-4067.
- [Atkinson 2005] K.E. Atkinson and W. Han, *Theoretical Numerical Analysis: A Function Analysis Framework*, second edition, Texts in Applied Mathematics 39, Springer, (2005).
- [Brorson 1987] S.D. Brorson, J.G. Fujimoto, and E.P. Ippen, "Femtosecond electron heat transfer dynamics in thin gold film," *Physical Review Letters*, Vol. 59, (1987), pp. 1962-1965.

[Cattaneo 1958] C. Cattaneo, "A form of heat conduction equation which eliminates the paradox of instantaneous propagation," *Compte Rendus*, Vol. 247, (1958), pp. 431-433.

[Chen 2001] J.K. Chen and J.E. Beraun, "Numerical study of ultrashort laser pulse interactions with metal films," *Numerical Heat Transfer, Part A*, Vol. 40, (2001), pp. 1-20.

[Chen 2002a] J.K. Chen, J.E. Beraun, and C.L. Tham, "Comparison of one-dimensional and two-dimensional axisymmetric approaches to the thermomechanical response caused by ultrashort laser heating," *Journal of Optics A: Pure Applied Optics*, Vol. 4, (2002), pp. 650-661.

[Chen 2002b] J.K. Chen, W.P. Latham, and J.E. Beraun, "Axisymmetric modeling of femtosecond-pulse laser heating on metal films," *Numerical Heat Transfer, Part B*, Vol. 42, (2002), pp. 1-17.

[Chen 2003] J.K. Chen, J.E. Beraun, and C.L. Tham, "Investigation of thermal response caused by pulse laser heating," *Numerical Heat Transfer, Part A*, Vol. 44, (2003), pp. 705-722.

[Chester 1963] M. Chester, "Second sound in solids," *Physical Review*, Vol. 131, (1963), pp. 2013-2015.

[Chiffell 1994] R.J. Chiffell, *On the wave behavior and rate effect of thermal and thermomechanical waves*, M.S. Thesis, University of New Mexico, Albuquerque, NM, (1994).

[Dai 1999] W. Dai and R. Nassar, "A finite difference method for solving the heat transport equation at microscale," *Numerical Methods for Partial Differential Equations*, Vol. 15, (1999), pp. 697-708.

[Dai 2000] W. Dai and R. Nassar, "A compact finite difference scheme for solving a three-dimensional heat transport equation in a thin film," *Numerical Methods for Partial Differential Equations*, Vol. 16, (2000), pp. 441-458.

[Dai 2001a] W. Dai and R. Nassar, "A finite difference scheme for solving a three-dimensional heat transport equation in a thin film with micro-scale thickness," *International Journal for Numerical Methods in Engineering*, Vol. 50, (2001), pp. 1665-1680.

[Dai 2001b] W. Dai and R. Nassar, "A compact finite difference scheme for solving a one-dimensional heat transport equation at the microscale," *Numerical Heat Transfer, Part A*, Vol. 130, (2001), pp. 431-441.

[Dai 2004] W. Dai and T. Zhu, "A nonlinear finite difference scheme for solving the parabolic two-step model with temperature dependent thermal properties in a double-layered thin film exposed by ultrashort-pulsed lasers," *Computational and Information Science*, Vol. 3314, (2004), pp. 304-309.

[Elliot 1989] D.J. Elliot and B.P. Piwczyk, "Single and multiple pulse ablations of polymetric and high density materials with excimer laser radiation at 193 nm and 248 nm," *Mater. Res. Soc. Symp. Proc.* Vol. 129, (1989), pp. 627-636.

[Evans 1998] L.C. Evans, *Patial Differential Equations*, American Mathematical Society, Providence, Phode Island, (1998).

[Grigoropoulos 1994] C.P. Grigoropoulos, Heat transfer in laser processing of thin films, in: C.L. Tien (Ed), *Annual Review of Heat Transfer*, Vol. 5, Hemisphere, New York, (1994), pp. 77-130.

[Joseph 1989] D.D. Jpseph and L. Preziosi, "Heat waves," *Reviews of Modern Physics*, Vol. 61, (1989), pp. 41-73.

[Joseph 1990] D.D. Jpseph and L. Preziosi, "Addendum to the paper on heat waves," *Reviews of Modern Physics*, Vol. 62, (1990), pp. 375-391.

[Joshi 1993] A.A. Joshi and A. Majumdar, "Transient ballistic and diffusive phonon heat transport in thin films," *Journal of Applied Physics*, Vol. 74, (1993), pp. 31-39.

[Kaye 1973] G.W.C. Kaye, *Tables of Physical and Chemical Constants and some Mathematical Functions*, Longman, London, UK, (1973), pp. 31.

[Kaba 2004] I. Kaba, *A Numerical Method to Solve the Two-Step Parabolic Heat Transport Equations in a Microsphere Subjected to an Ultrafast Laser Pulse*, Ph. D. Dissertation, Louisiana Tech University, LA, (2004).

[Kaba 2005] I. Kaba and W. Dai, "A stable three-level finite difference scheme for solving the parabolic two-step model in a 3-D micro-sphere heated by ultrashort-pulsed lasers," *Journal of Computational and Applied Mathematics*, Vol. 181, (2005), pp. 125-147.

[Kaganov 1957] M.L. Kaganov, I. M. Lifshitz, and M.V. Tanatarov, "Relaxation between electrons and crystalline lattices," *Soviet Physics Journal of Experimental and Theoretical Physics*. Vol. 4, (1957), pp. 173-178.

[Knapp 1990] J.A. Knapp, P. Borgesen, and R.A. Zuhr, "Beam-solid interactions: physical phenomena," *Mater. Res. Soc. Symp. Proc.*, Vol. 157 (1990).

- [Lin 1997] C.K. Lin, C.C. Hwang, and Y.P. Chang, "The unsteady solution of a unified heat conduction equation," *International Journal of Heat and Mass Transfer*, Vol. 40, (1997), pp. 1716-1719.
- [Naji 2003] M. Naji, M.A. Al-Nimr, and M. Hader, "The validity of using the microscopic hyperbolic heat conduction model under as harmonic fluctuating boundary heating source," *International Journal of Thermophysics*, Vol. 24, (2003), pp. 545-557.
- [Narayan 1991] J. Narayan, V.P. Gosbole, and G.W. White, "Laser method for synthesis and processing of continuous diamond films on nondiamond substrates," *Science*, Vol. 52, (1991), pp. 416-418.
- [Opsal 1991] J. Opsal, "The application of thermal wave technology to thickness and grain size of aluminum films, in Metallization," *Performance and Reliability Issues for VLSI and ULSI, SPIE*, Vol. 1596, (1991), pp. 120-131.
- [Ozisik 1994] M.N. Ozisik and D.Y. Tzou, "On the wave theory in heat conduction," *Journal of Heat Transfer*, Vol. 116, (1994), pp. 526-535.
- [Patanka 1980] S.V. Patanka, *Numerical Heat Transfer and Fluid Flow, Chapter 5*, McGraw-Hill, New York, (1980).
- [Qiu 1992] T.Q. Qiu and C.L. Tien, "Short-pulse laser heating on metals," *International Journal of Heat and Mass Transfer*, Vol. 35, (1992), pp. 719-726.
- [Qiu 1993] T.Q. Qiu and C.L. Tien, "Heat transfer mechanisms during short-pulse laser heating of metals," *ASME Journal of Heat Transfer*, Vol. 115, (1993), pp. 835-841.
- [Qiu 1994] T.Q. Qiu, T. Juhasz, C. Suarez, W.E. Bron, and C.L. Tien, "Femtosecond laser heating of multi-layer metals II – experiments," *International Journal of Heat and Mass Transfer*, Vol. 37, (1994), pp. 2789-2808.
- [Tang 1999] D.W. Tang and N. Araki, "Wavy, wavelike, diffusive thermal responses of finite rigid slabs to high-speed heating of laser-pulses," *International Journal of Heat and Mass Transfer*, Vol. 42, (1999), pp. 855-860.
- [Touloukian 1970a] Y.S. Touloukian, R.W. Powell, C.Y. Ho, and P.G. Klemens, "Thermal conductivity," *Thermophysical Properties of Matter*, Vol. 1, IFI/Plenum, New York, (1970), pp. 193.
- [Touloukian 1970b] Y.S. Touloukian and E.H. Buyco, "Specific heat," *Thermophysical Properties of Matter*, Vol. 4, IFI/Plenum, New York, (1970), pp. 204.
- [Tzou 1989a] D.Y. Tzou, "On the thermal shock wave induced by a moving and source," *ASME Journal of Heat Transfer*, Vol. 111, (1989), pp. 232-238.

- [Tzou 1989b] D.Y. Tzou, "Shock wave formation around a moving heat source in a solid with finite speed of heat propagation," *International Journal of Heat and Mass Transfer*, Vol. 32, (1989), pp. 1979-1987.
- [Tzou 1990a] D.Y. Tzou, "Thermal shock waves induced by a moving crack," *ASME Journal of Heat Transfer*, Vol. 112, (1990), pp. 21-27.
- [Tzou 1990b] D.Y. Tzou, "Thermal shock waves induced by a moving crack – a heat flux formulation," *International Journal of Heat and Mass Transfer*, Vol. 33, (1990), pp. 877-885.
- [Tzou 1992] D.Y. Tzou, "Thermal shock phenomena under high-rate response in solids," *Annual Review of Heat Transfer*, Hemisphere Publishing Inc., Washington, D. C., (1992), pp. 111-185.
- [Tzou 1995a] D.Y. Tzou, "A unified field approach for heat conduction from macro- to micro- scales," *Journal of Heat Transfer*, Vol. 117, (1995), pp. 1837-1840.
- [Tzou 1995b] D.Y. Tzou, "The generalized lagging response in small-scale and high-rate heating," *International Journal of Heat and Mass Transfer*, Vol. 38, (1995), pp. 3231-3240.
- [Tzou 1995c] D.Y. Tzou, "Experimental support for the lagging behavior in heat propagation," *Journal of Thermophysics and Heat Transfer*, Vol. 6, (1995), pp. 686-693.
- [Tzou 1995d] D.Y. Tzou and Y.S. Zhang, "An analytic study on the fast-transient process in small scales," *International Journal of Engineering*, Vol. 33, (1995), pp. 1449-1463.
- [Tzou 1996] D.Y. Tzou, *Macro-To Micro Heat Transfer- The Lagging Behavior*, Taylor & Francis, Washington, DC, (1996).
- [Tzou 2001] D.Y. Tzou and K.S. Chiu, "Temperature-dependent thermal lagging in ultrafast laser heating," *International Journal of Heat and Mass Transfer*, Vol. 44, (2001), pp. 1725-1734.
- [Tzou 2002] D.Y. Tzou, J.K. Chen, and J.E. Beraun, "Hot-electron blast induced by ultrashort-pulsed lasers in layered media," *International Journal of Heat and Mass Transfer*, Vol. 45, (2002), pp. 3369-3382.
- [Vernotte 1958] P. Vernotte, "Les paradoxes de la theorie continue de lequation de la chaleur," *Compte Rendus*, Vol. 246, (1958), pp. 3154-3155.
- [Vernotte 1961] P. Vernotte, "Some possible complication in the phenomena of thermal conduction", *Compte Rendus*, Vol. 252, (1961), pp. 2190-2191.

[Wang 2000] L. Wang and X. Zhou, "Dual-Phase-Lagging Heat Conduction," *Shandong University Press*, Jinan, 2000.

[Wang 2001] L. Wang, M. Xu, and X. Zhou, "Well-posedness and solution structure of dual-phase-lagging heat conduction," *International Journal of Heat and Mass Transfer*, Vol. 44, (2001), pp. 1659-1669.

[Wang 2006a] H. Wang, W. Dai, R. Nassar, and R. Melnik, "A finite difference method for studying thermal deformation in a thin film exposed to ultrashort-pulsed lasers," *International Journal of Heat and Mass Transfer*, Vol. 49, (2006), pp. 2712-2723.

[Wang 2006b] H. Wang, W. Dai, R. Nassar, and R. Melnik, "A finite difference method for studying thermal deformation in a double-layered thin film exposed to ultrashort-pulsed lasers," *International Journal of Thermal Sciences*, Vol. 45, (2006), pp. 1179-1196.

[Wang 2007] H. Wang, "A Finite Difference Method for Studying Thermal Deformation in Two-Dimensional Micro Scale Metal Thin Films Exposed to Ultrashort Pulsed Lasers," Ph. D. Dissertation, Louisiana Tech University, LA, 2007.